Development and Implementation of a Kinetic Quantitative Analysis of Novel Small Molecule Ice Recrystallization Inhibitors

Stephanie Abraham

Thesis submitted to the
Faculty of Graduate and Postdoctoral Studies
in partial fulfillment of the requirements for the
MSc degree in Chemistry

Department of Chemistry and Biomolecular Sciences
Faculty of Science
University of Ottawa

Candidate	Supervisor
Stephanie Abraham	Professor Robert N. Ben

Abstract

The effects of ice recrystallization are well recognized throughout the literature. This phenomenon is the major cause of cellular damage during freezing and thawing of cells, ultimately reducing post-thaw viability and function. Herein, we describe a method for quantifying the inhibitory effect on ice recrystallization of novel small molecules that are cryoprotectants for red blood cells. The method is ideally suited to the splat-cooling assay, where ice high ice volume fractions are present. Using our method, we have derived first order rate constants for the increase of average crystal size based upon a "binning" approach of ice crystals as a function of size and time. Using this reliable metric, dose-response curves were constructed to obtain IC_{50} values. Two very effective inhibitors of ice recrystallization, PMP-Glc and pBrPh-Glc, were shown to have low IC_{50} values while Glc, a known ineffective inhibitor of ice recrystallization, did not. Furthermore, this kinetic approach was adapted to suit a condensed and simplified assay for the screening of new compounds for their ice recrystallization inhibition activity. This was accomplished through studying the initial rates from the binning approach and constructing dose-response curves that led to very comparable IC_{50} values when the full kinetic profile was assessed. This work therefore presents the quantification of ice recrystallization inhibition and the adaptation to a condensed screening assay for use in our laboratory.

Acknowledgements

There are so many people who have helped me along this journey, and I am indebted to each and every one of them. Without them, none of this work would have been possible, and I wish to extend my heartfelt gratitude.

First and foremost, to my supervisor, Dr. Robert Ben, for taking a chance on me and accepting me into his research group off-cycle. I deeply appreciate all of his patience in teaching me to be a better researcher and critical thinker. I am also grateful for the support and guidance he has given me even during the most difficult of times.

I wish to thank everyone who assisted in the development of this research project. To Chantelle Capicciotti not only for her constant advice when I started in this lab, but to her and her former undergraduate student, Evan Perley-Robertson, for laying the groundwork of the kinetics project for me to follow. To Melody Afagh, for being an amazing sport and for spending a few weeks with me circling ice crystals seemingly without end. Special thanks goes out to Dr. Jeff Keillor for his constant aid in developing the kinetics project, and for numerous insightful conversations in his office (that somehow occasionally turned into hockey talk). This project would not have been possible without him. Last but certainly not least, I wholeheartedly wish to thank Kerkeslin Keillor not only for being a model undergraduate student, but for truly helping me get this project off the ground and for all of the wonderful conversations in the tiny third floor lab.

I have been fortunate enough to have been surrounded by some truly amazing labmates and coworkers. To Anna Balcerzak, for setting me up in her bay, for teaching me the ropes, for her endless patience and support, and for having an amazing taste in music. To Malay Doshi, for forcing me to solve problems on the board and always keeping me on my toes, and for all the fun life conversations. To Jennie Briard, for always being so kind and helpful, and for the walks home together. Special thanks goes out to Vanessa Musca for her help in editing this thesis. To all other past and present members of the Ben and Durst labs: Thomas Charlton, Kyle McClymont, Jessica Poisson, Madeleine Adam, Julia Meyer, Matt Alteen, Amanda Saikaley, and Vik Raina – thank you for all of the fun memories. *Merci à Bob Nadon au laboratoire de premier cycle pour tout son aide durant mon travail de TA, surtout pour tous les toasts au beurre de peanut quand j'ai oublié de manger et le thé chaud quand j'étais malade.*

I am so grateful to have been surrounded by wonderful friends without whose support I would not be here today. To Kim, for taking this journey with me, for letting me sleep on her couch when I first moved to Ottawa, and for all the fun baking nights. To Cedric, for all the life lessons and fond memories, and for looking out for me even from across the sea. Most importantly, to Jasmine, for always believing in me and telling me I can when I thought I couldn't. A huge thank you goes out to my Montreal crew, my ringette team, my writing buddies, and my Internet pen-pals.

Finally, I would like to thank my entire family for their constant love and belief in whatever I set out to do. Special thanks go out to my parents, who have instilled in me the value of hard work, determination, and a good education. This would not have been possible without them.

I have grown so much in these past two and a half years, and I will carry the lessons I've learned here for the rest of my life. Thank you all for having been a part of it.

Table of Contents

List of Figures

List of Tables

List of Equations

List of Abbreviations

AFGPs	Antifreeze glycoproteins
AFPs	Antifreeze proteins
BAs	Biological antifreezes
DOMAN	Domain Recognition Software
DSC	Differential scanning calorimetry
FOV	Field of view
IC_{50}	Half maximal inhibitory concentration
IRI	Ice recrystallization inhibition
LSW	Lifshitz Slyozov Wagner
MGS	Mean grain size
PBS	Phosphate-buffered saline
PMP	*para*-methoxyphenyl
QLL	Quasi-liquid layer
WAXS	Wide-angle X-ray scattering

Chapter 1: Introduction

1.1 Recrystallization

Recrystallization is a known phenomenon that has been extensively studied in the fields of geology and metallurgy.[1,2] In metallurgy, it is defined as the nucleation and growth of non-deformed grains in the place of deformed ones, completely replacing the original grains. Differently oriented grains meet at an interface known as the grain boundary, which contains poorly aligned atoms that result in a less ordered structure and less efficient packing. This increases the amount of stored energy as well as increases grain strain in the crystalline structure.[3-5] Recrystallization therefore results in a more ordered system, which reduces the amount of energy. This phenomenon also occurs in ice, where it is defined as the growth of large ice crystals (or ice grains) at the expense of smaller ones. As such, recrystallization can be defined as a thermodynamically driven process that results in an overall reduction of free energy in the system.

1.2 The structure of ice

Ice exists in many different polymorphic forms where individual water molecules can adopt different three-dimensional arrangements depending on temperature and pressure. Most commonly found below 0°C and atmospheric pressure is the hexagonal ice I_h lattice unit.[6,7] It possesses a regular crystalline structure in which a single oxygen atom is hydrogen-bonded to two hydrogen atoms. The hexagonal ice I_h lattice unit has four axes, a_1, a_2, a_3, and c, and the surface of the hexagonal unit has eight faces. The properties and phases of ice are influenced by

the arrangement of intermolecular hydrogen bonds. At 0°C and atmospheric pressure, ice grows most rapidly along the *a*-axis, resulting in hexagonal shaped crystals that grow as sheets.[6-9]

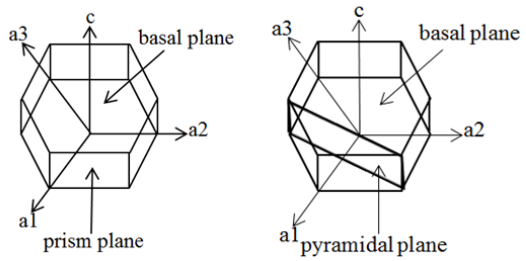

Figure 1.1 Schematic representation of the ice I_h lattice unit illustrating the a_1, a_2, a_3, and c axes and the basal, prism, and pyramidal planes.[10]

Studies have indicated that the interface between the ice lattice and bulk water is not an abrupt transition when ice is in an aqueous solution. There exists a semi-ordered layer called the quasi-liquid layer (QLL) between the highly ordered ice lattice and the less ordered bulk water that surrounds ice crystals.[11-20] The exact molecular nature and thickness of the QLL interface has been debated throughout the literature, and it has been studied with a wide variety of techniques.[18-32] Ellipsometric studies, measuring the refractive index on the basal and prism faces of ice, suggest that the interface is more like water than ice in nature.[16-19,28,29] However, other studies suggest that the orientation and motion of water molecules in the QLL closely resembles that of ice.[20,22,31] The thickness of the QLL between ice lattice and bulk water is approximately 10-15 Å thick, though this has been shown to be temperature-dependent.[14,15,24,28,33] At temperatures approaching the melting point of ice (-0.03 °C), the thickness is 15 nm, which corresponds to approximately 40 monolayers of water.[21] However, below -10 °C, the thickness is less than 0.3 nm, approximately one monolayer of water. These effects also vary depending on which face of ice from which they are calculated. Studies have

suggested that the QLL is thicker on the basal and prism faces than on the pyramidal and secondary prism faces.[11,16,18] Light scattering techniques have shown that ice crystals grow into the QLL, which becomes thicker during growth, and not into the bulk water layer.[34,35]

1.3 Recrystallization in ice

In ice, recrystallization is thought to occur through either grain boundary migration or Ostwald ripening.[36-43] Grain boundary migration in ice, similarly to grain boundary migration in metals and alloys, is a process through which large ice grains grow at the expense of smaller ones.[1,2,36] Grain boundaries are the interfaces between differently oriented ice grains.[37,38] Individual grain boundaries tend to be curved, with the degree of curvature proportional to the size of the grain. Small ice crystals have a higher degree of curvature, and thus more convex grain boundaries, which results in a higher amount of surface energy, while large ice crystals have more concave grain boundaries and lower amounts of surface energy.[37] Grain boundary migration therefore occurs from the transfer of individual molecules from grains with convex boundaries (higher in energy) to grains with more concave boundaries (lower in energy). Grain boundaries migrate towards their centre of curvature in order to decrease the overall degree of grain boundary curvature which in turn decreases the energy of the system.[39,40] This reduction in grain boundary curvature and energy is thus the driving force of grain boundary migration in ice.

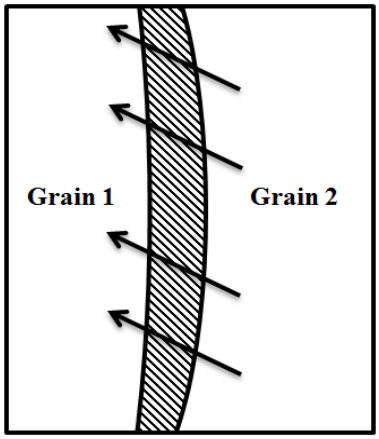

Figure 1.2 Depiction of a liquid layer (shaded) in a curved boundary between two grains. Large grains with concave boundaries (grain 2) grow larger while smaller grains with convex boundaries (grain 1) decrease in size, reducing the overall degree of grain boundary curvature. The direction of grain boundary migration is indicated by the arrows.[10]

Grain boundary migration in polycrystalline ice works under the assumption that water molecules transfer from the shrinking grain to the growing grain directly, therefore neglecting the presence of bulk-water or the QLL in between individual ice grains.[39] However, Ostwald ripening of polycrystalline ice in aqueous solution accounts for the presence of bulk-water and the QLL by considering the entire ice crystal/water system. In ice, Ostwald ripening is a thermodynamically driven process whereby large ice crystals grow larger at the expense of smaller crystals, resulting in an overall reduction in energy of the ice crystal/bulk-water interface.[41-43] This has been shown to occur in ice slurries, where there is a high liquid volume fraction within the system, though it has not yet been determined that Ostwald ripening theory holds true in completely frozen samples. In a slurry system, smaller ice crystals have a higher surface area to volume ratio than larger ice crystals, resulting in a higher surface free energy since water molecules along the surface are less stable than the water molecules within the crystal.[41,42] A constant ice volume is maintained throughout the Ostwald ripening process. During this process, water molecules transfer from the surface of smaller ice crystals to bulk-

water and then to the surface of larger ice crystals. The net result is an increase in average ice crystal size and a decrease in the total number of ice crystals, thereby reducing the free energy of the system.[43]

1.4 Impact of ice recrystallization

Ice recrystallization is a well-known problem in the fields of frozen foods and cryopreservation. Frozen food products have a finite shelf life due to the fact that ice recrystallization and ice morphology directly affect texture, taste, and overall quality of the frozen product.[44,45] Similarly, ice recrystallization has a negative impact in the field of medicine, where cryostorage is an important method for the preservation of biological materials, stem cells, and red blood cells, and is a significant cause of cellular injury and death.[46,47]

1.5 Inhibiting ice recrystallization

Ice recrystallization inhibition (IRI) is a type of antifreeze activity exhibited by certain types of compounds that results in very small ice crystals within a frozen sample, thus inhibiting their growth during recrystallization.

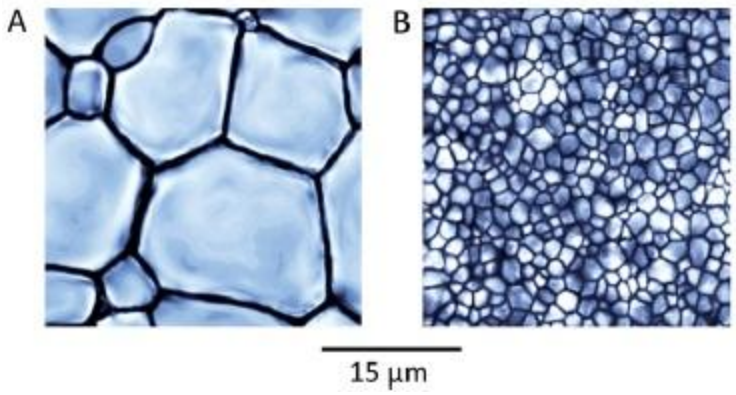

Figure 1.3 Photographs of annealed ice crystals from a splat-cooling assay, where A) depicts no inhibition of ice recrystallization and B) depicts inhibition of ice recrystallization, maintaining small ice crystal sizes within the frozen sample.[48]

The first compounds discovered to show this activity were biological antifreezes (BAs), a class of molecules comprised of antifreeze proteins (AFPs) and antifreeze glycoproteins (AFGPs).[9,49-55] Compounds exhibiting IRI activity are highly desirable for medical, commercial, and industrial applications, particularly in the field of cryopreservation.[56-59]

1.6 Assays used to assess IRI activity

Methods of assessing ice recrystallization inhibition activity include the capillary method assay, wide-angle X-ray scattering (WAXS), differential scanning calorimetry (DSC), or the splat-cooling assay.[60-65] The capillary method assay has the advantage that it allows for direct comparison of samples while the assay is performed, as several samples can be run at once. However, it does not provide any quantification of IRI activity. Instead, it simply provides an indication of whether or not IRI activity is present.[61,62] WAXS and DSC provide evidence of freezing point depression in the presence of antifreezes, as well as consider the morphology of ice crystals, which again is a qualitative rather than quantitative assessment of IRI activity.[63-65]

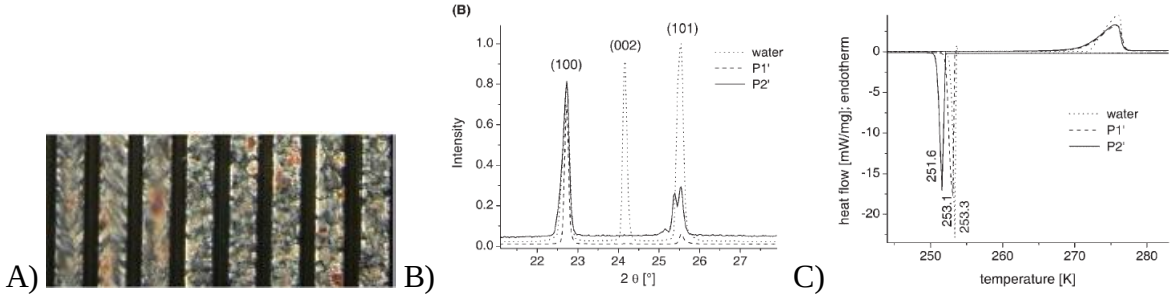

Figure 1.4 A) Capillary method assay results in which capillaries containing varying concentrations of inhibitor can be frozen and compared side-by-side to deduce the presence of IRI activity.[61] B) WAXS diffraction patterns of pure water versus a solution of antifreeze polymers. "Missing" or reduced peaks indicate blockage of directional growth along a specific axis of an ice crystal.[63] C) DSC thermograms of water crystallizations. The presence of antifreezes results in a slight shift in crystallization temperature as well as a broadening of the melting process.[63]

The splat-cooling assay is the most commonly used method for assessing IRI. In this assay, recrystallization is observed by monitoring the change in size of individual ice crystals, where smaller ice crystals indicate a greater degree of activity (Figure 1.3).[66] An aliquot of sample solution is dropped from a height of approximately 2 metres onto a precooled (-80°C) polished aluminum block, freezing as a thin circular wafer.[60] Alternatively, the solution can be pressed between two coverslips and frozen.[67] The samples are then annealed at a temperature below 0°C and ice crystal size is observed under a microscope after a given time.

Ice crystal size can be quantified by measuring the mean largest ice grain dimension along any axis or by measuring mean ice grain area.[43,66,68,69] Analytes are generally assayed in a salt solution (NaCl, $CaCl_2$ or phosphate buffered saline (PBS)) or a 30-45% sucrose solution.[38,60,67] These solutions are used without analyte as positive controls for comparison. The presence of other solutes ensures that the solution is liquid at the annealing temperature and that the eutectic point is below this temperature. Liquid is therefore present between ice crystal boundaries and liquid inclusions can be formed, where inhibitors become concentrated. Furthermore, salt solutions negate non-specific IRI effects observed in pure water.[38]

When first developed by Knight *et al*., the splat-cooling assay was initially subjective and semi-qualitative in nature.[60] Horwath *et al*. have since modified the assay to make it more quantitative, though their method of analysis is quite time-consuming.[70] Our laboratory employs a further optimized method of the splat-cooling assay as a standard method in the assessment of small molecule ice recrystallization inhibitors.[66] Assays are run in triplicate, with pictures of ice crystals taken after an annealing period of 30 minutes and three images per drop are analyzed. An algorithm has been developed to display a number of x/y locations at random so as to eliminate user bias. Statistical analysis has demonstrated that measuring 12 ice crystal sizes per image is sufficient for accurate representation of the sample.[66] The cross-sectional areas of these chosen ice crystals are then measured and thus the mean grain size can be calculated. IRI activity can then be quantified as the relative mean grain size compared to a positive control, where a smaller relative size indicates higher levels of activity.

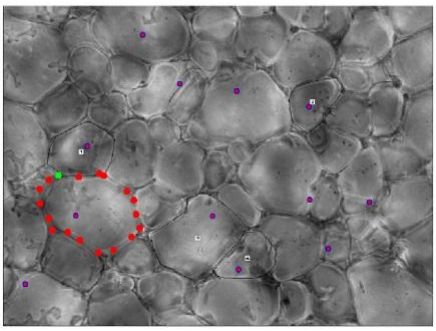

Figure 1.5 Example of an image of annealed ice crystals from a splat-cooling assay being analyzed with DOMAN. The purple dots represent the 12 randomly generated x/y locations. Crystals surrounding these locations are then circled (outlined in red dots) and their area is recorded.[66]

There are some limitations to the current IRI splat-cooling assay that impede its ability to properly quantify the activity of an inhibitor. Firstly, mean grain size at a given time point does not provide an accurate picture of what is truly happening within the sample. Even though on

average, crystals grow larger, there can still be an abundance of small ice crystals at later times. The heterogeneity of ice crystal sizes in a sample therefore suggests a broad population distribution that is generally neglected in IRI analysis. Furthermore, assessing IRI activity at 30 minutes neglects important changes that occur over time, particularly within the first 15 minutes of annealing, where there is a rapid rate of recrystallization. Therefore, a case can be made that inhibitors that slow the initial rate of recrystallization the most could prove to be the most active inhibitors. By only looking at a snapshot of crystal size at a 30 minute time point, it is impossible to obtain this sort of information. Finally, the currently accepted assay does not constitute a fully quantitative measure of a compound's ability to inhibit ice recrystallization, as it relies on one relative measure compared to a control.

1.7 IRI kinetics

As a consequence of the assay limitations discussed above, the need has risen for a more quantifiable means of assessing IRI activity. Interest has thus risen in studying the kinetics of IRI, where rates of recrystallization can be calculated. These rates are dependent on temperature and are most prevalent at temperatures just below 0°C, consistent with the standard annealing temperatures in most IRI assays.[41-43,71,72] They are also dependent on concentration of inhibitor present.[42,43,72-76]

The kinetics of ice recrystallization inhibition have been approximated using Lifshitz Slyozov Wagner (LSW) theory of Ostwald ripening.[41-43,72,74,75,77,78] LSW theory states that, for systems with low ice volume fractions, the increase in ice crystal radius (r) at constant temperature should follow equation 1 where r_0 is the initial mean radius when time (t) equals

zero and k_d is the observed rate of recrystallization. k_d can be obtained from the slope of plotting r^3 (cubed mean radius) versus time.

$$r^3(t) = r_0{}^3 + k_d t$$

Equation 1.1 Rate of recrystallization based on LSW theory.

LSW theory of Ostwald ripening approximates recrystallization kinetics as diffusional growth. Diffusional growth is the diffusion of water molecules from smaller to larger ice crystals. These molecules must travel through an intermediate liquid layer, such as the QLL. However, there must be a low total ice volume fraction during recrystallization as the ice crystals cannot be in direct contact with each other, indicating a large total liquid volume fraction.[41,43,72] LSW theory has been applied to approximate IRI kinetics in sucrose-based assays as high concentrations of sucrose (30-45% w/v) result in large liquid volumes between ice crystals.[41,43,67,72,79]

Koop *et al*. have examined the IRI activity of AFPs and AFGPs by using LSW theory to derive rate constants. This was the first time IRI activity and kinetics were able to be quantified. In these studies, the concentration dependence of these rate constants were plotted and the efficiency was determined as the concentration at which the rate constant is half that of the sucrose control solution (see Figure 1.6).[43,75,80] This method provides a comprehensive quantitative comparison of IRI activity, applicable across a wide range of AF(G)P inhibitors and concentration ranges of 6 orders of magnitude.

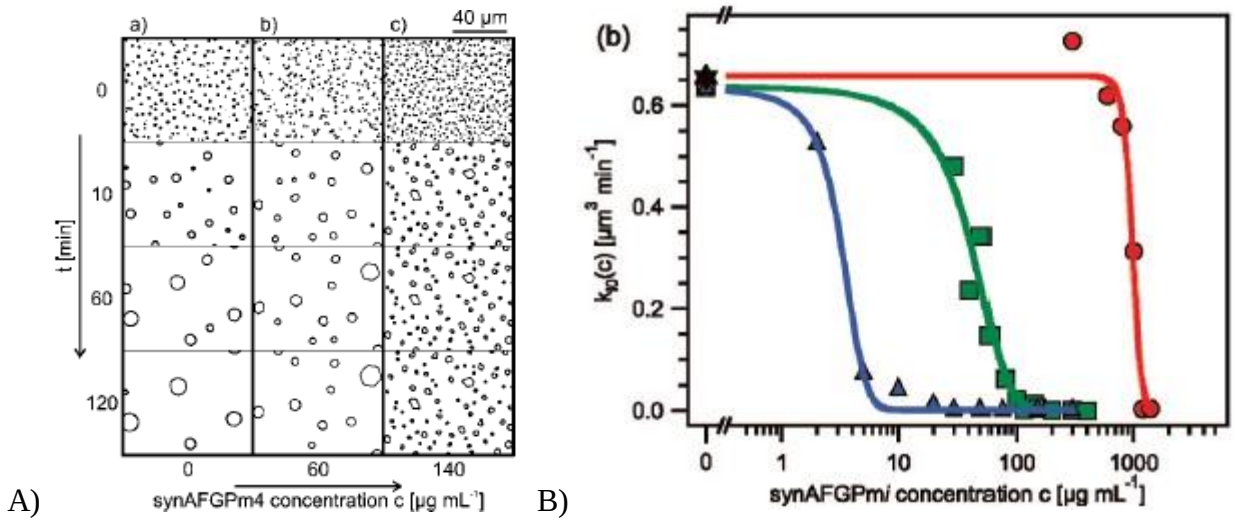

Figure 1.6 A) Images of ice crystals in a sucrose assay during the annealing process, at varying time points and concentrations of inhibitor. B) Rate versus concentration plots of different inhibitors. The blue curve has an inflection point at the lowest concentration compared to the green and the red curves, and thus represents the most effective inhibitor.[43]

Unfortunately, this method may not be applicable to the assay used in our laboratory. Our assay utilizes PBS as a solvent rather than a sucrose solution, and results in a large ice crystal volume fraction where crystals are in close proximity to one another and there is very little liquid volume. As such, our method does not fit the diffusional growth model previously mentioned and LSW theory may not provide an accurate representation of IRI kinetics using a PBS splat-cooling assay. This is due to the fact that the diffusional growth model appears to require small ice volume fractions whereas the splat-cooling assay results in high ice volume fractions. Furthermore, constant high ice volume fractions are representative of those seen in cryopreservation. Since the goal of designing our ice recrystallization inhibitors in our laboratory is to use them as cryoprotectants, PBS is likely the best control in our assay. However, at this time there is no appropriate model for IRI kinetics with a large ice crystal volume as small total liquid volume such as is present in our assay.

Until recently, efficient inhibitors of ice recrystallization were limited to biological antifreezes or synthetic C-linked AFGP analogues. Our laboratory was the first to report that low molecular weight carbohydrate derivatives can inhibit ice recrystallization.[81] This was the first instance of small molecule inhibitors of ice recrystallization, and led to the determination of important structural attributes necessary for IRI activity. It was postulated that the degree of activity was directly related to the degree of carbohydrate hydration, based upon their ability to alter the structure of bulk water.[82-85] The most active monosaccharide was found to be D-galactose, which incidentally possesses the highest hydration number (8.7).[83] From here, using a carbohydrate scaffold, structural features necessary for potent IRI activity were assessed, leading to the discovery of a class of IRI active phenolic glycosides.[86] The first phenolic glycosides to demonstrate IRI activity contained β-linked paramethoxyphenyl (PMP) moieties.

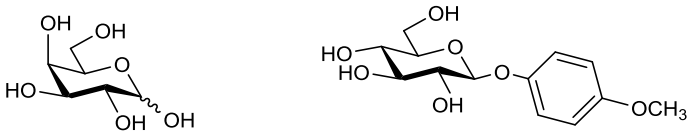

Figure 1.7 Structures of D-galactose and β-PMP-Glc, an IRI active phenolic glycoside.

As mentioned previously, there currently exists no appropriate kinetic model to fit with the IRI activity of our compounds utilizing the splat-cooling assay in which there is a constant high ice volume fraction. With this in mind, a former Ph.D student in the Ben group, Chantelle Capicciotti, with her undergraduate student at the time, Evan Perley-Robertson, endeavoured to explore the time and inhibitor concentration dependence of ice crystal size.[86] Our assay assesses a compound's ability to inhibit ice recrystallization by observing the mean ice crystal area at a singular time point and concentration (usually 22 mM), an approach that ignores both the effects

of time and concentration on IRI. As such, the mean ice crystal area of a PBS control was measured over a range of time increments from 0 min to 120 min (every 5 minutes for the first 30 minutes and then at 15-minute intervals), and then repeated with two different inhibitors, D-galactose with moderate activity at 22 mM and β-PMP-Glc with potent activity at 22 mM. This experiment would provide information on the time dependence of IRI activity. Furthermore, the concentration dependence was studied by repeating this experiment at varying inhibitor concentrations. Due to its moderate activity at 22 mM, galactose was tested at higher concentrations of 55, 110, and 220 mM. Meanwhile, PMP-Glc, being a very active inhibitor, was tested at lower concentrations of 5.5 and 11 mM. For all of these concentrations, mean ice crystal area was plotted against time (see Figure 1.8).

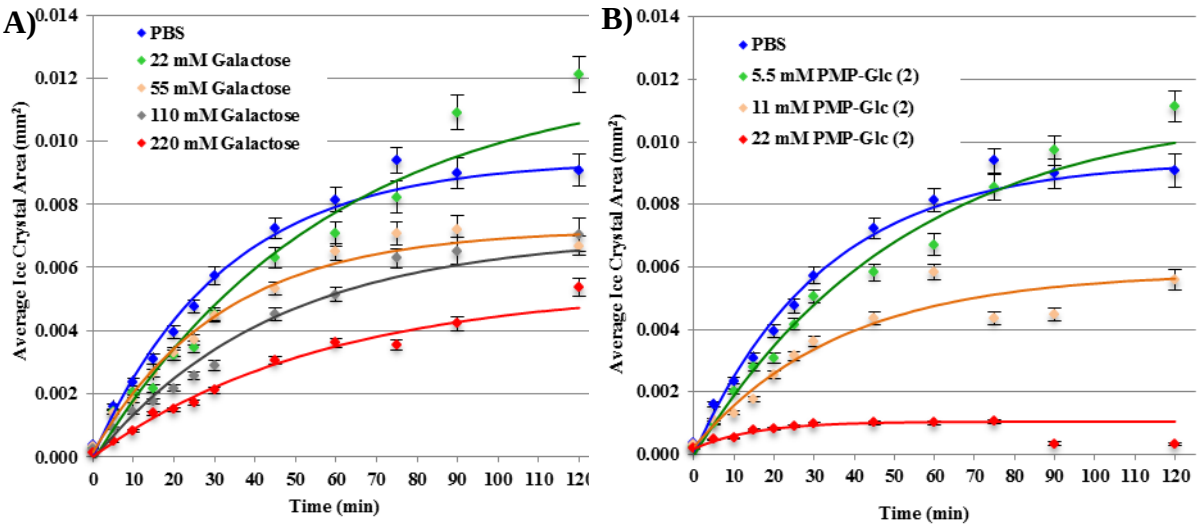

Figure 1.8 Time dependence of ice crystal sizes at varying concentrations compared to a PBS control of A) galactose, a moderate inhibitor, and B) PMP-Glc, a potent inhibitor. The more concentrated the inhibitor solution, the smaller the average ice crystal size. This work was carried out by Chantelle Capicciotti.[86]

From these results, we can determine that there are three major findings: first, that simply considering a compound's inhibition endpoint does not provide an accurate depiction of its

ability to inhibit ice recrystallization; second, the rate at which a compound reaches its endpoint varies; and third, that there is a definite concentration effect on both endpoint and rate. The observations leading to these conclusions are discussed below.

The crystal growth plots in Figure 1.8 indicate that even past the 30 min annealing time point used in our laboratory's assay, in most cases ice crystal size continues to increase. It first appears that for the PBS control solution, the ice crystal size increases in an inverse exponential fashion before eventually beginning to remain constant, once past 75 min. It is interesting to note that at 22 mM, the mean ice crystal size of galactose is smaller than that of PBS, but past 60 min the mean ice crystal areas are similar to or actually larger than PBS. As such, this leads to the observation that a compound that demonstrates IRI activity at the standard tested 30 min time point may not continue to inhibit ice recrystallization as time goes on, and may only slow ice recrystallization for a certain period of time before ultimately failing. Conversely, ice crystals in 22 mM PMP-Glc essentially stop growing past 30 min, and remain much smaller than PBS.

The concentration profiles of these inhibitors were then examined. For galactose, ice crystals appear to grow at an inverse exponential rate before becoming more or less constant in size from 75 min onwards. However, the end point ice crystal size varies depending on the concentration of inhibitor used. For example, the mean ice crystal area of 220 mM galactose at 120 min is about half that of the PBS control, whereas 22 mM galactose has an average ice crystal area slightly higher than PBS. At 30 min, however, the relative difference in ice crystal size between PBS and 220 mM galactose is even greater. These observations therefore demonstrate that there is indeed a pronounced effect on concentration of inhibitor with regards to IRI activity, as well as a definitive time dependence of recrystallization end point and ice crystal size.

Similar results were obtained in the concentration-dependence study of PMP-Glc. While the end point of recrystallization at 22 mM was found at 30 min, ice crystals sizes for 11 mM only began to remain constant past 60 min, and kept growing still for 5.5 mM. Furthermore, there was a drastic difference in end point mean ice crystal area. The time dependence curve of 5.5 mM showed remarkable similarity to that of the PBS curve, indicating that at low enough concentrations, inhibition will not occur. Therefore, it can be deduced that there exists an effective concentration for inhibitors, at which point not only will ice crystal growth be slower than that of a PBS control solution, but ice crystal size will reach an end point lower than that of PBS.

Overall, these results suggest that there is indeed a concentration effect on ice recrystallization inhibition, which proves that testing only one concentration in our standard IRI assay may not be sufficient to determine whether or not a compound is a potent inhibitor of ice recrystallization. Furthermore, this study demonstrates that there are noticeable differences in end point and rate of recrystallization, as evidenced for example by the fact that 22 mM galactose shows activity at 30 min but then does not possess activity relative to PBS at higher time points. With the currently accepted splat-cooling assay method, it is impossible to know whether or not an inhibitor has reached its endpoint through a single snapshot after a set annealing period. Moreover, a rate cannot be determined without observing recrystallization effects at multiple time points. In summary, these findings indicate that our assay does not provide enough information or quantification of a compound's IRI activity, and thus presents the need for the development of a more comprehensive assay.

1.8 References

(1) Doherty, R. D.; Hughes, D. A.; Humphreys, F. J.; Jonas, J. J.; Jensen, D. J.; Kassner, M. E.; King, W. E.; McNelley, T. R.; McQueen, H. J.; Rollett, A. D. *Mater. Sci. Eng., A* **1997**, *A238*, 219-274.
(2) Rios, P. R.; Siciliano, F., Jr.; Sandim, H. R. Z.; Plaut, R. L.; Padilha, A. F. *Mater. Res. (Sao Carlos, Braz.)* **2005**, *8*, 225-238.
(3) Humphreys, F. J.; Hatherly, M. In *Recrystallization and Related Annealing Phenomena (Second Edition)*; Hatherly, F. J. H., Ed.; Elsevier: Oxford, 2004, p 91-119.
(4) Berdichevsky, V. L. *Int. J. Eng. Sci.* **2012**, *57*, 50-78.
(5) Gil Sevillano, J.; van Houtte, P.; Aernoudt, E. *Prog. Mater. Sci.* **1980**, *25*, 69-134.
(6) Fletcher, N. H.; Fletcher, N. H. *Structure and energy of ordinary ice: The Chemical Physics of Ice*; Cambridge University Press, 1970.
(7) Devries, A. L.; Lin, Y. *Biochim. Biophys. Acta, Protein Struct.* **1977**, *495*, 388-392.
(8) Harding, M. M.; Ward, L. G.; Haymet, A. D. J. *Eur. J. Biochem.* **1999**, *264*, 653-665.
(9) Harding, M. M.; Anderberg, P. I.; Haymet, A. D. J. *Eur. J. Biochem.* **2003**, *270*, 1381-1392.
(10) Capicciotti, C. J.; Doshi, M.; Ben, R. N. Ice Recrystallization Inhibitors: From Biological Antifreezes to Small Molecules. In: P. Wilson, editor. Recent Developments in the Study of Recrystallization. New York: InTech; 2013. p177-224.
(11) Hayward, J. A.; Haymet, A. D. J. *J. Chem. Phys.* **2001**, *114*, 3713-3726.
(12) Fletcher, N. H. *Philos. Mag. (1798-1977)* **1962**, *7*, 255-269.
(13) Fletcher, N. H. *Phil. Mag.* **1968**, *18*, 1287-1300.
(14) Karim, O. A.; Haymet, A. D. J. *Chem. Phys. Lett.* **1987**, *138*, 531-534.
(15) Karim, O. A.; Haymet, A. D. J. *J. Chem. Phys.* **1988**, *89*, 6889-6896.
(16) Furukawa, Y.; Yamamoto, M.; Kuroda, T. *J. Cryst. Growth* **1987**, *82*, 665-677.
(17) Furukawa, Y.; Ishikawa, I. *J. Cryst. Growth* **1993**, *128*, 1137-1142.
(18) Beaglehole, D.; Nason, D. *Surf. Sci.* **1980**, *96*, 357-363.
(19) Doeppenschmidt, A.; Butt, H.-J. *Langmuir* **2000**, *16*, 6709-6714.
(20) Dosch, H.; Lied, A.; Bilgram, J. H. *Surf. Sci.* **1996**, *366*, 43-50.
(21) Sadtchenko, V.; Ewing, G. E. *J. Chem. Phys.* **2002**, *116*, 4686-4697.
(22) Golecki, I.; Jaccard, C. *J. Phys. C* **1978**, *11*, 4229-4237.
(23) Kahan, T. F.; Reid, J. P.; Donaldson, D. J. *J. Phys. Chem. A* **2007**, *111*, 11006-11012.
(24) Kaverin, A.; Tsionsky, V.; Zagidulin, D.; Daikhin, L.; Alengoz, E.; Gileadi, E. *J. Phys. Chem. B* **2004**, *108*, 8759-8762.
(25) Guettinger, H.; Bilgram, J. H.; Kaenzig, W. *J. Phys. Chem. Solids* **1979**, *40*, 55-66.
(26) Brown, R. A.; Keizer, J.; Steiger, U.; Yeh, Y. *J. Phys. Chem.* **1983**, *87*, 4135-4138.
(27) Bilgram, J. H. *Phys. Rep.* **1987**, *153*, 1-89.
(28) Bluhm, H.; Ogletree, D. F.; Fadley, C. S.; Hussain, Z.; Salmeron, M. *J. Phys. Condens. Matter* **2002**, *14*, L227-L233.
(29) Beaglehole, D.; Wilson, P. *J. Phys. Chem.* **1993**, *97*, 11053-11055.
(30) Beaglehole, D.; Wilson, P. *J. Phys. Chem.* **1994**, *98*, 8096-8100.
(31) Elbaum, M.; Lipson, S. G.; Dash, J. G. *J. Cryst. Growth* **1993**, *129*, 491-505.
(32) Gilpin, R. R. *J. Colloid Interface Sci.* **1980**, *77*, 435-448.
(33) Karim, O. A.; Kay, P. A.; Haymet, A. D. J. *J. Chem. Phys.* **1990**, *92*, 4634-4635.
(34) Halter, P. U.; Bilgram, J. H.; Kaenzig, W. *J. Chem. Phys.* **1988**, *89*, 2622-2629.
(35) Bilgram, J. H. *Prog. Cryst. Growth Charact. Mater.* **1993**, *26*, 99-119.
(36) Gleiter, H. *Acta Met.* **1969**, *17*, 565-573.

(37) Knight, C. A. *J. Appl. Phys.* **1966**, *37*, 568-574.
(38) Knight, C. A.; Wen, D.; Laursen, R. A. *Cryobiology* **1995**, *32*, 23-34.
(39) Alley, R. B.; Perepezko, J. H.; Bentley, C. R. *Journal of Glaciol.* **1986**, *32*, 415-424.
(40) Alley, R. B.; Perepezko, J. H.; Bentley, C. R. *Journal of Glaciol.* **1986**, *32*, 425-433.
(41) Sutton, R. L.; Lips, A.; Piccirillo, G.; Sztehlo, A. *J. Food Sci.* **1996**, *61*, 741-745.
(42) Hagiwara, T.; Hartel, R.; Matsukawa, S. *Food Biophysics* **2006**, *1*, 74-82.
(43) Budke, C.; Heggemann, C.; Koch, M.; Sewald, N.; Koop, T. *J. Phys. Chem. B* **2009**, *113*, 2865-2873.
(44) Goff, H. D. *Food Res. Int.* **1994**, *27*, 187-189.
(45) Petzold, G.; Aguilera, J. *Food Biophysics* **2009**, *4*, 378-396.
(46) Baust, J. M.; Van, B.; Baust, J. G. *In Vitro Cell Dev. Biol. Anim.* **2000**, *36*, 262-270.
(47) Baust, J. M. *Cell Preserv. Technol.* **2002**, *1*, 17-31.
(48) Balcerzak, A. K.; Capicciotti, C. J.; Briard, J. G.; Ben, R. N. *RSC Adv.* **2014**, *4*, 42682-42696.
(49) DeVries, A. L.; Wohlschlag, D. E. *Science* **1969**, *163*, 1073-1075.
(50) Komatsu, S. K.; DeVries, A. L.; Feeney, R. E. *J. Biol. Chem.* **1970**, *245*, 2909-2913.
(51) DeVries, A. L. *Science* **1971**, *172*, 1152-1155.
(52) Scholander, P. F.; Maggert, J. E. *Cryobiology* **1971**, *8*, 371-374.
(53) Feeney, R. E.; Burcham, T. S.; Yeh, Y. *Annu. Rev. Biophys. Biophys. Chem.* **1986**, *15*, 59-78.
(54) Fletcher, G. L.; Hew, C. L.; Davies, P. L. *Annu. Rev. Physiol.* **2001**, *63*, 359-390.
(55) Yeh, Y.; Feeney, R. E. *Chemical Reviews* **1996**, *96*, 601-618.
(56) Chao, H.; Davies, P. L.; Carpenter, J. F. *J. Exp. Biol.* **1996**, *199*, 2071-2076.
(57) Mazur, P. *Science* **1970**, *168*, 939-949.
(58) Mazur, P. *Am. J. Physiol.* **1984**, *247*, C125-C142.
(59) Fowler, A.; Toner, M. *Ann. N. Y. Acad. Sci.* **2006**, *1066*, 119-135.
(60) Knight, C. A.; Hallett, J.; DeVries, A. L. *Cryobiology* **1988**, *25*, 55-60.
(61) Tomczak, M. M.; Marshall, C. B.; Gilbert, J. A.; Davies, P. L. *Biochem. Biophys. Res. Commun.* **2003**, *311*, 1041-1046.
(62) Yu, S. O.; Brown, A.; Middleton, A. J.; Tomczak, M. M.; Walker, V. K.; Davies, P. L. *Cryobiology* **2010**, *61*, 327-334.
(63) Yagci, Y. E.; Antonietti, M.; Börner, H. G. *Macromol. Rapid Commun.* **2006**, *27*, 1660-1664.
(64) Baruch, E.; Mastai, Y. *Macromol. Rapid Commun.* **2007**, *28*, 2256-2261.
(65) Mastai, Y.; Rudloff, J.; Cölfen, H.; Antonietti, M. *ChemPhysChem* **2002**, *3*, 119-123.
(66) Jackman, J.; Noestheden, M.; Moffat, D.; Pezacki, J. P.; Findlay, S.; Ben, R. N. *Biochem. Biophys. Res. Commun.* **2007**, *354*, 340-344.
(67) Smallwood, M.; Worrall, D.; Byass, L.; Elias, L.; Ashford, D.; Doucet, C. J.; Holt, C.; Telford, J.; Lillford, P.; Bowles, D. J. *Biochem. J.* **1999**, *340*, 385-391.
(68) Gibson, M. I.; Barker, C. A.; Spain, S. G.; Albertin, L.; Cameron, N. R. *Biomacromolecules* **2009**, *10*, 328-333.
(69) Inada, T.; Lu, S.-S. *Cryst. Growth Des.* **2003**, *3*, 747-752.
(70) Horwath, K. L.; Easton, C. M.; Poggioli, G. J., Jr.; Myers, K.; Schnorr, I. L. *Eur. J. Entomol.* **1996**, *93*, 419-433.

(71) Chaytor, J. L.; Tokarew, J. M.; Wu, L. K.; Leclere, M.; Tam, R. Y.; Capicciotti, C. J.; Guolla, L.; von Moos, E.; Findlay, C. S.; Allan, D. S.; Ben, R. N. *Glycobiology* **2012**, *22*, 123-133.
(72) Hagiwara, T.; Sakiyama, T.; Watanabe, H. *Food Biophysics* **2009**, *4*, 340-346.
(73) Heggemann, C.; Budke, C.; Schomburg, B.; Majer, Z.; Wissbrock, M.; Koop, T.; Sewald, N. *Amino Acids* **2010**, *38*, 213-222.
(74) Nagel, L.; Plattner, C.; Budke, C.; Majer, Z.; DeVries, A. L.; Berkemeier, T.; Koop, T.; Sewald, N. *Amino Acids* **2011**, *41*, 719-732.
(75) Nagel, L.; Budke, C.; Erdmann, R. S.; Dreyer, A.; Wennemers, H.; Koop, T.; Sewald, N. *Chem. - Eur. J.* **2012**, *18*, 12783-12793.
(76) Peltier, R.; Evans, C. W.; DeVries, A. L.; Brimble, M. A.; Dingley, A. J.; Williams, D. E. *Cryst. Growth Des.* **2010**, *10*, 5066-5077.
(77) Lifshitz, I. M.; Slyozov, V. V. *J. Phys. Chem. Solids* **1961**, *19*, 35-50.
(78) Wagner, C. *Z. Elektrochem. Angew. Phys. Chem.* **1961**, *65*, 581-591.
(79) Pudney, P. D. A.; Buckley, S. L.; Sidebottom, C. M.; Twigg, S. N.; Sevilla, M. P.; Holt, C. B.; Roper, D.; Telford, J. H.; McArthur, A. J.; Lillford, P. J. *Arch. Biochem. Biophys.* **2003**, *410*, 238-245.
(80) Budke, C.; Dreyer, A.; Jaeger, J.; Gimpel, K.; Berkemeier, T.; Bonin, A. S.; Nagel, L.; Plattner, C.; DeVries, A. L.; Sewald, N.; Koop, T. *Cryst. Growth Des.* **2014**, *14*, 4285-4294.
(81) Capicciotti, C. J.; Leclere, M.; Perras, F. A.; Bryce, D. L.; Paulin, H.; Harden, J.; Liu, Y.; Ben, R. N. *Chem. Sci.* **2012**, *3*, 1408-1416.
(82) Tam, R. Y.; Ferreira, S. S.; Czechura, P.; Chaytor, J. L.; Ben, R. N. *J. Am. Chem. Soc.* **2008**, *130*, 17494-17501.
(83) Galema, S. A.; Hoeiland, H. *J. Phys. Chem.* **1991**, *95*, 5321-5326.
(84) Galema, S. A.; Engberts, J. B. F. N.; Hoeiland, H.; Foerland, G. M. *J. Phys. Chem.* **1993**, *97*, 6885-6889.
(85) Galema, S. A.; Howard, E.; Engberts, J. B. F. N.; Raul Grigera, J. *Carbohydr. Res.* **1994**, *265*, 215-225.
(86) Capicciotti, C.J., Ph.D Dissertation, University of Ottawa, 2014.

Chapter 2: Goals and Objectives

2.1 Introduction

Ice recrystallization is a significant cause of cellular injury and death during cryopreservation.[1,2] As such, compounds displaying ice recrystallization inhibition (IRI) activity have unrealized potential as cryoprotectants. The goal of our laboratory is to design small-molecule ice recrystallization inhibitors.[3-11]

While we have previously reported novel small-molecule IRI active compounds, the mechanism by which these compounds inhibit ice recrystallization is unknown. Furthermore, there currently exists no universal standard method for quantifying IRI activity, and there are limitations within the various different assay methods currently employed.[12-17] As such, the overall goal of this thesis is to develop a method to better quantify IRI activity to aid in identifying compounds that have potential use as cryoprotectants. This may also provide further insight into the mechanism by which our compounds are inhibiting ice recrystallization. Therefore, the main objectives for this thesis are as follows:

1. To improve the accuracy of the IRI assay and quantification of IRI activity through kinetic profiling of ice recrystallization inhibitors.
2. To use the kinetic profiles of our inhibitors to develop an improved IRI screening assay for new compounds.

2.2 Objective 1: Improving the accuracy of the IRI assay

To date, the most effective method for quantifying IRI activity was developed by Koop *et al*. as described in Section 1.7.[18-20] However, this kinetic analysis is not compatible with the assay employed by our laboratory as ours results in high ice volume fractions and the diffusional growth model with LSW theory cannot properly represent IRI kinetics within a sample that is mostly ice.[18,21-24] As mentioned in Section 1.7, it seems likely that constant high volume ice fractions would be a closer representation of a cryopreserved sample which we could assume to be completely frozen. As a result, our assay with a PBS solution is an effective model to assess IRI activity for use in the field of cryopreservation rather than a dilute sucrose slurry as utilized in the Koop method (see Figure 2.1). As such, it is important to develop a kinetic analysis method better suited for high ice volume fractions found in our laboratory's assay.

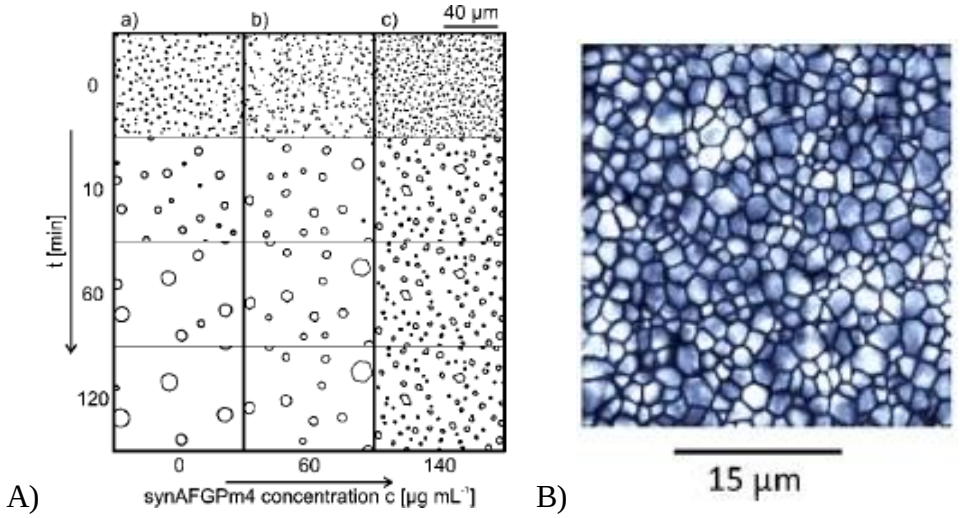

Figure 2.1 Photographs of ice crystals from a splat-cooling IRI assay in A) a sucrose slurry solution, where there is a very small ice volume fraction within the sample as used in the Koop method[18], and B) a PBS solution which results in a high ice volume fraction within the sample as used by our laboratory[9].

An advantage to the Koop method is that it provides recrystallization data across a given period of time. However, our current assay analyzes one concentration of inhibitor at one time

point only, which does not provide a proper measure of a compound's overall ability to inhibit ice recrystallization.[25] As demonstrated by previous studies in our laboratory, IRI is a dynamic process where ice crystal size changes drastically over time.[26] These studies have shown that some inhibitors inhibit ice recrystallization relative to a PBS control initially, but that the "endpoint" crystal size matches that of PBS. Alternatively, other inhibitors essentially halt ice crystal growth after a brief period of time, and average crystal size remains constant. Thus, by taking one picture after 30 minutes of annealing and only analyzing 12 random crystals in a sample, it is impossible to know whether or not an endpoint of crystal growth has been reached, and begs the possibility that two different inhibitors displaying the same relative activity could actually possess completely different efficiencies.

Consequently, we sought to obtain a full kinetic profile of some of our small-molecule inhibitors by studying changes in ice crystal growth in all crystals in a field of view as a function of time and concentration. This would constitute a full kinetic analysis in which all crystals in each image are circled, rather than a small sample size of 12. This would provide a better understanding of the distribution and growth patterns of ice crystal area throughout recrystallization. The first goal of this project was therefore to determine an appropriate set of parameters through which to quantify IRI activity, as we cannot use the same ones as utilized in the Koop method.[18] Koop *et al*. were able to quantify IRI activity of AF(G)Ps through the use of LSW theory, where rate constants could be obtained as a function of mean ice crystal radius.[18] However, as previously stated, LSW theory may not apply in samples containing high ice volume factions, and thus we need to determine a different inhibition model from which to obtain rate constants. From there, the concentration dependence of the rate constants could be assessed. This method would be tested both with known effective and ineffective small-

molecule ice recrystallization inhibitors, with the expectation that the former will fit the concentration dependence model and the latter will not.

2.3 Objective 2: Development of a simplified time-efficient IRI screening assay based on the kinetic profiling of ice recrystallization inhibitors

As mentioned previously, the current IRI assay employed by our laboratory looks at our compounds at a single concentration and time point, neglecting many factors influencing IRI activity. Ice recrystallization and inhibition is a dynamic process that changes drastically over time. As a result, collecting data across various time points provides a more complete picture of the changes that occur during ice recrystallization. Furthermore, by testing at numerous concentrations, we can determine which concentrations are most effective at inhibiting ice recrystallization. As such, the full kinetic profile provides much more information as well as a much more quantitative assessment of a compound's IRI activity. However, obtaining this profile is a highly time-consuming process in which assays must be run in triplicate at each different concentration for a period of 60 minutes. Furthermore, pictures of ice crystals are taken at 5-minute intervals and all ice crystals are analyzed rather than just a random sample of 12. As such, this greatly increases assay time as well as the amount of analysis to be performed. Therefore, the goal of this project is to develop a streamlined assay that generates useful kinetic data that is statistically consistent with the full profile. Ideally, this method would be simplified enough such that it does not consume more time than the original assay, but provides enough quantitative data that the compound in question's potential as an effective inhibitor of ice recrystallization can be evaluated. This method, as with the full kinetic profile, will be tested

with positive and negative controls for ice recrystallization inhibitors, and the results obtained should be consistent with those obtained in Objective 1.

2.4 Summary of Goals and Objectives

With the goal of using kinetics of ice recrystallization inhibition to quantify IRI activity, the overall objectives are as follows:

1. To develop a method for obtaining a full kinetic profile for our small-molecule ice recrystallization inhibitors and to use this profile to properly quantify IRI activity. We will extrapolate from the previous IRI kinetics studies done by our laboratory and look at the distribution of ice crystal size as a function of time. From there, we will study the disappearance of the smallest crystals over time and fit it to an appropriate inhibition model to obtain a rate constant. Concentration dependence of the rate constant will then be assessed, and IC_{50} values will be obtained. These results will be discussed in Chapter 3.
2. To condense the full kinetic profile from the previous objective to a simplified screen for initial assaying of a compound's potential as an inhibitor of ice recrystallization. This will involve a concentration scan but at a singular, early time point, from which initial rates of recrystallization can be determined. Ideally, the concentration dependence of these rates should give statistically similar results to those of the full kinetic profile, thus providing an accurate representation of a compound's IRI activity in a much more time-efficient process. These results will be discussed in chapter 4.

2.5 References

(1) Baust, J. M.; Van, B.; Baust, J. G. *In Vitro Cell Dev. Biol. Anim.* **2000**, *36*, 262-270.
(2) Baust, J. M. *Cell Preserv. Technol.* **2002**, *1*, 17-31.
(3) Wu, L. K.; Tokarew, J. M.; Chaytor, J. L.; von Moos, E.; Li, Y.; Palii, C.; Ben, R. N.; Allan, D. S. *Carbohydr. Res.* **2011**, *346*, 86-93.
(4) Balcerzak, A. K.; Ferreira, S. S.; Trant, J. F.; Ben, R. N. *Bioorg. Med. Chem. Lett.* **2012**, *22*, 1719-1721.
(5) Capicciotti, C. J.; Leclere, M.; Perras, F. A.; Bryce, D. L.; Paulin, H.; Harden, J.; Liu, Y.; Ben, R. N. *Chem. Sci.* **2012**, *3*, 1408-1416.
(6) Chaytor, J. L.; Tokarew, J. M.; Wu, L. K.; Leclere, M.; Tam, R. Y.; Capicciotti, C. J.; Guolla, L.; von Moos, E.; Findlay, C. S.; Allan, D. S.; Ben, R. N. *Glycobiology* **2012**, *22*, 123-133.
(7) Ben, R.; Capicciotti, C. J.; (The University of Ottawa, Can.). Application: WO, 2013, p 81pp.
(8) Capicciotti, C. J.; Doshi, M.; Ben, R. N. Ice Recrystallization Inhibitors: From Biological Antifreezes to Small Molecules. In: P. Wilson, editor. Recent Developments in the Study of Recrystallization. New York: InTech; 2013. p177-224.
(9) Balcerzak, A. K.; Capicciotti, C. J.; Briard, J. G.; Ben, R. N. *RSC Adv.* **2014**, *4*, 42682-42696.
(10) Capicciotti Chantelle, J.; Mancini Ross, S.; Ben Robert, N.; Kurach Jayme, D. R.; Turner Tracey, R.; Acker Jason, P. *Sci. Rep.* **2015**, *5*, 9692.
(11) Capicciotti, C. J.; Poisson, J. S.; Boddy, C. N.; Ben, R. N. *Cryobiology* **2015**, *70*, 79-89.
(12) Knight, C. A.; Hallett, J.; DeVries, A. L. *Cryobiology* **1988**, *25*, 55-60.
(13) Tomczak, M. M.; Marshall, C. B.; Gilbert, J. A.; Davies, P. L. *Biochem. Biophys. Res. Commun.* **2003**, *311*, 1041-1046.
(14) Yu, S. O.; Brown, A.; Middleton, A. J.; Tomczak, M. M.; Walker, V. K.; Davies, P. L. *Cryobiology* **2010**, *61*, 327-334.
(15) Yagci, Y. E.; Antonietti, M.; Börner, H. G. *Macromol. Rapid Commun.* **2006**, *27*, 1660-1664.
(16) Baruch, E.; Mastai, Y. *Macromol. Rapid Commun.* **2007**, *28*, 2256-2261.
(17) Mastai, Y.; Rudloff, J.; Cölfen, H.; Antonietti, M. *ChemPhysChem* **2002**, *3*, 119-123.
(18) Budke, C.; Heggemann, C.; Koch, M.; Sewald, N.; Koop, T. *J. Phys. Chem. B* **2009**, *113*, 2865-2873.
(19) Nagel, L.; Budke, C.; Erdmann, R. S.; Dreyer, A.; Wennemers, H.; Koop, T.; Sewald, N. *Chem. - Eur. J.* **2012**, *18*, 12783-12793.
(20) Budke, C.; Dreyer, A.; Jaeger, J.; Gimpel, K.; Berkemeier, T.; Bonin, A. S.; Nagel, L.; Plattner, C.; DeVries, A. L.; Sewald, N.; Koop, T. *Cryst. Growth Des.* **2014**, *14*, 4285-4294.
(21) Sutton, R. L.; Lips, A.; Piccirillo, G.; Sztehlo, A. *J. Food Sci.* **1996**, *61*, 741-745.
(22) Smallwood, M.; Worrall, D.; Byass, L.; Elias, L.; Ashford, D.; Doucet, C. J.; Holt, C.; Telford, J.; Lillford, P.; Bowles, D. J. *Biochem. J.* **1999**, *340*, 385-391.
(23) Hagiwara, T.; Sakiyama, T.; Watanabe, H. *Food Biophysics* **2009**, *4*, 340-346.

(24) Pudney, P. D. A.; Buckley, S. L.; Sidebottom, C. M.; Twigg, S. N.; Sevilla, M. P.; Holt, C. B.; Roper, D.; Telford, J. H.; McArthur, A. J.; Lillford, P. J. *Arch. Biochem. Biophys.* **2003**, *410*, 238-245.
(25) Jackman, J.; Noestheden, M.; Moffat, D.; Pezacki, J. P.; Findlay, S.; Ben, R. N. *Biochem. Biophys. Res. Commun.* **2007**, *354*, 340-344.
(26) Capicciotti C.J., Ph.D Dissertation, University of Ottawa, 2014.

Chapter 3: Kinetic Profiling of Small Molecule Ice Recrystallization Inhibitors

3.1 Introduction

Currently, there is no widely accepted quantifiable method for assessing IRI activity. Furthermore, each of the commonly utilized assays has drawbacks.[1-6] Detailed studies of the ice recrystallization process were lacking until recent work by Koop *et al*, who applied the Lifshitz Slyozov Wagner (LSW) theory of Ostwald ripening to obtain rate constants from sucrose solutions with inhibitors present over a wide range of concentrations.[7-9] Dose-response curves were constructed, resulting in IC_{50} values. This was significant as it allowed for direct comparison between inhibitors. This method, however, relied on the theory of diffusional growth, which was thought to only hold true for large liquid volume fractions such as those found in their assay, and it is unknown as to whether or not the same can be applied to the high ice volume fractions found in our laboratory's assay.[7,10-13] Previously, our laboratory attempted to study the kinetics of ice recrystallization with carbohydrate-based small molecule inhibitors (see Section 1.7). These studies revealed three major issues specific to any IRI assay that relies on a "snapshot" of ice crystal growth after a predetermined time. First, there is a concentration dependence on IRI activity that cannot be determined by simply testing a compound at one arbitrarily chosen concentration. Second, the "endpoint" ice crystal size at the end of a 60-minute kinetic profiling experiment varies depending on the nature and concentration of the inhibitor used. Thirdly, the rate at which an inhibitor reaches this endpoint varies. As such, this underscores the need for a concentration scan with time dependence studies.

With these in mind, we sought to develop a kinetic profile for our small molecule inhibitors of ice recrystallization based on the Koop method, but that could be applied to high ice

volume fractions such as those found in our assay. This would be done by first determining which features in a high ice volume fraction assay adhere to Ostwald ripening theory and which should be considered in a kinetic profile. This would be followed by studying the distribution of ice crystal sizes in order to determine the most appropriate parameter to study kinetically. From there, this parameter can be fit to a time-dependent equation that results in the acquisition of rate constants. These rate constants can then be used to construct dose-response curves in order to determine an IC_{50} value, permitting the successful application of the Koop method to our compounds. The goals and objectives of this chapter are therefore as follows:

1. As discussed in Section 2.2, the currently accepted assay results in a snapshot of ice crystals at a single time and concentration. Furthermore, only 12 randomly selected crystals are analyzed to calculate the average crystal area.[14] As such, we repeated the kinetic profiling experiment (described in Section 1.7) for PBS and 22 mM PMP-Glc in order to determine the differences in analyzing 12 crystals versus the entire sample. Furthermore, other important geometrical features such as surface area and volume were studied throughout these samples in order to determine whether or not high ice volume fraction samples adhere to Ostwald ripening theory. These results are discussed in Section 3.2.
2. Following studies on average ice crystal area, we sought to determine how this affected the distribution of ice crystal sizes, noting that even at late time points where larger crystals dominate the field of view, there are still some smaller crystals that remain. We therefore sorted the crystals into bins based on their individual areas and studied the distribution of the relative population of these bins over time-dependence experiments. These results are shown in Section 3.3.

3. Following the binning experiment, it was determined that the disappearance of bin 1 over time could be fit to a mono-exponential decay equation, resulting in the acquisition of rate constants. This method was applied to two previously determined effective inhibitors (PMP-Glc and pBrPh-Glc)[15] and one ineffective inhibitor (Glc)[16]. The results are presented in Section 3.4.
4. We sought to apply the results obtained in our kinetic profiling experiments to the method for quantifying IRI activity employed by Koop *et al*. As such, dose-response curves were constructed using the rate constants obtained in Section 3.4 and IC_{50} values were obtained. These results are discussed in Section 3.5.

3.2 Initial studies: method comparison, ice volume fraction and adherence to Ostwald ripening theory

As mentioned previously (Section 1.7), previous methods of IRI analysis in our laboratory involved the use of Domain Recognition Software (DOMAN) to determine the area of 12 randomly selected crystals.[14] In order to carry out a full kinetic analysis, however, it would be important to include all ice crystals within an image for the analysis. As such, the images used in our laboratory's previous kinetics studies were analyzed using ImageJ software instead of DOMAN. With this software, all crystals whose areas were completely visible and not cut off by the edges of the camera were circled. This was carried out with PBS and 22 mM PMP-Glc at time points of 0, 5, 10, 15, 20, 25, 30, 45, 60, and 120 minutes. The switch to ImageJ was made purely for practical reasons, as the program ran smoother and quicker than DOMAN while still yielding the same results.

Determining the area of each ice crystal in every image proved to be a highly labour-intensive analysis. For example, for PBS at time 0, the original method would involve circling 12 random crystals; we now had to circle 434 crystals. At a time of 120 min, however, that number had decreased down to 16 crystals, despite the camera magnification having been zoomed out in order to capture more crystals within the field of view (FOV). This demonstrates the remarkable difference in the total number of crystals as ice recrystallization takes place. Furthermore, it was noted that the average ice crystal area was consistently smaller when performing the full analysis than when only 12 crystals were analyzed. At time of 30 min, the standard time point utilized by our laboratory for our IRI assays, PBS resulted in an average crystal size of $5.73 \pm 0.28 \times 10^{-3}$ mm^2 when circling 12 random crystals, while the full analysis resulted in an average crystal size of $2.83 \pm 0.35 \times 10^{-3}$ mm^2. This is a staggering difference between mean ice crystal size – in fact, the actual average area of the entire sample is essentially half that of the estimate from the initial screen with 12 random crystals. Furthermore, this difference held true even when inhibitors such as 22 mM PMP-Glc were present at 30 min. Analysis of 12 crystals yielded an average ice crystal area of $9.84 \pm 0.06 \times 10^{-3}$ mm^2, but analysis of all crystals in the FOV gave an average ice crystal area of $6.83 \pm 0.03 \times 10^{-3}$ mm^2. With this in mind, we then sought to compare % MGS (mean grain size) from both methods, as this is the standard measurement for IRI activity utilized by our laboratory. Previous studies have assessed 22 mM PMP-Glc of having a % MGS consistently around 22-23%, that is to say, the average ice crystal area of the sample is less than a quarter that of PBS.[15] With the full analysis of every ice crystal within the FOV, 22 mM PMP-Glc was found to have a % MGS of 24%. This demonstrates that the 12-crystal sample size does not, in fact, affect the overall result when determining IRI activity as a percentage of ice crystal size relative to PBS. However, this

also introduces a systematic bias into the crystal size analysis. Even though crystals are chosen randomly by DOMAN, there is nevertheless a user bias present as it is dependent on the human eye to determine which crystals have been marked for circling. Furthermore, in samples with larger crystals, these crystals take up more of the overall area of the FOV and therefore have a higher statistical probability of being chosen. Finally, the disparity in average ice crystal size between the 12-crystal sample and the full analysis suggests that % MGS may not be providing an accurate indication of a compound's ability to inhibit ice recrystallization, and that there are more factors to consider when quantifying IRI activity. Ice crystal size and distribution thereof will be further discussed in Section 3.3.

We also looked at several geometrical parameters of ice crystals obtained by using a splat-cooling assay with PBS with the goal of finding the best parameter to approximate the changes in ice during recrystallization. For example, using the data obtained from the time studies of the PBS standard, where all ice crystals are circled rather than a sample of 12, we calculated the mean crystal area, volume, surface area, and surface area to volume ratios at each time point. These were then plotted to determine their relationships, as shown in Figure 3.1.

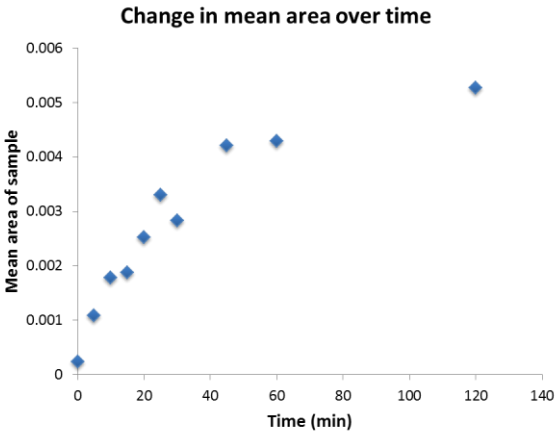

A)

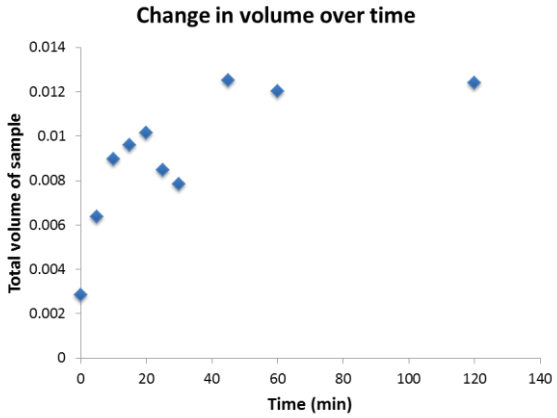

B)

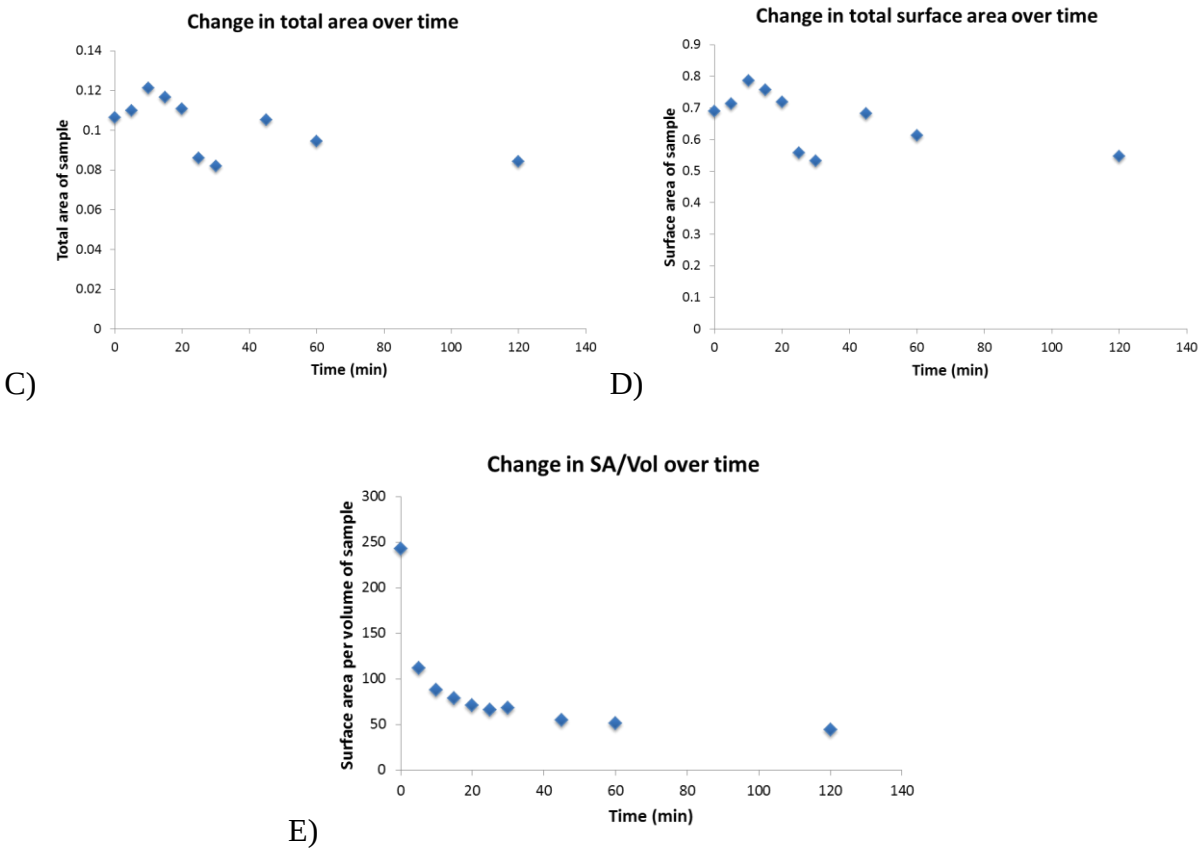

Figure 3.1 Time dependence plots of various properties when all ice crystals within the image are analyzed: A) mean crystal size, B) total ice crystal volume, C) total area of the sample, D) total surface area of the sample, and E) surface area to volume ratio of the sample.

As predicted, the mean ice crystal area increases exponentially and thus becomes constant as a function of time. This also held true for total volume of the sample. The volumes obtained were based on the radius derived from the area, corrected under the assumption that all ice crystals can be considered spherical (even though it is evident from ice crystal images that they are much more complex polygons).

Total area of the sample and total surface area of the sample both remained more or less constant over time. There was, however, a slight decrease in the higher time points that can be explained by the fact that only crystals whose entire outlines could be seen within the image were analyzed. At higher time points, the ice crystals are larger in size, and so there is a larger

total area of ice that is not circled for analysis since there is more ice cut off by the edges of the field of view. This also provides evidence that our assay results in a high ice volume fraction that remains constant over the recrystallization process.

Perhaps the most interesting and important observation is the time dependence of surface area to volume ratio. As shown in the plot, we observe a mono-exponential decrease over time. Smaller crystals are known to have a higher surface area to volume ratio and this ratio decreases in larger crystals, which we see more of at higher time points when ice recrystallization occurs. These results are in agreement with Ostwald ripening theory, as crystals with a higher surface area to volume ratio contain more surface energy than crystals with smaller ratios. As such, the decrease in surface area to volume ratio is indicative of the decrease in total surface energy of the system, which is the driving force for ice recrystallization.[7,10,17]

From these results we conclude that our methodology adheres to the principles of Ostwald ripening theory while maintaining constant high ice volume fractions across all time points. Furthermore, we have shown that % MGS, while remaining constant for a sample relative to PBS whether only 12 crystals are circled or the entire image is analyzed, is not a proper quantitative representation of ice recrystallization as there are still many smaller crystals within a sample that are overlooked during an approximate MGS calculation.

3.3 Ice crystal size and distribution analysis

Following the results in section 3.2, we can see that the MGS approximation when using a sample size of 12 crystals does not provide accurate data with respect to the entire sample. In fact, the MGS when circling all visible crystals in the image rather than just 12 is drastically smaller, indicating there are many smaller crystals within a sample that are not taken into

account. As such, we can conclude that MGS is not an accurate representation of a non-homogeneous system as seen with our assays. Furthermore, previous research in our laboratory has suggested that our ice recrystallization inhibitors may affect not only the rate of crystal growth, but also the average ice crystal size at the end point (see Section 1.7).

In order to get a better picture of what our non-homogeneous systems of ice crystals look like during recrystallization, we sought to look at the distribution of ice crystal sizes throughout the various time points. This was accomplished by grouping ice crystals from each image into equally sized bins, where incremental bin size was determined by the smallest area in which all ice crystals could fit at time 0. The summed area of the crystals in each bin was converted to a proportion of the total area measured in the sample, thus providing an indication of the relative importance of each bin at each time point.

After analyzing images of PBS and various concentrations of PMP-Glc at time 0, it was determined that this bin size would be 0.001 mm^2, as none of the crystals circled in these images ever surpassed this value. Using data from the time-dependence studies of the PBS control solution, the binning analysis was carried out and the results are shown in Figure 3.2.

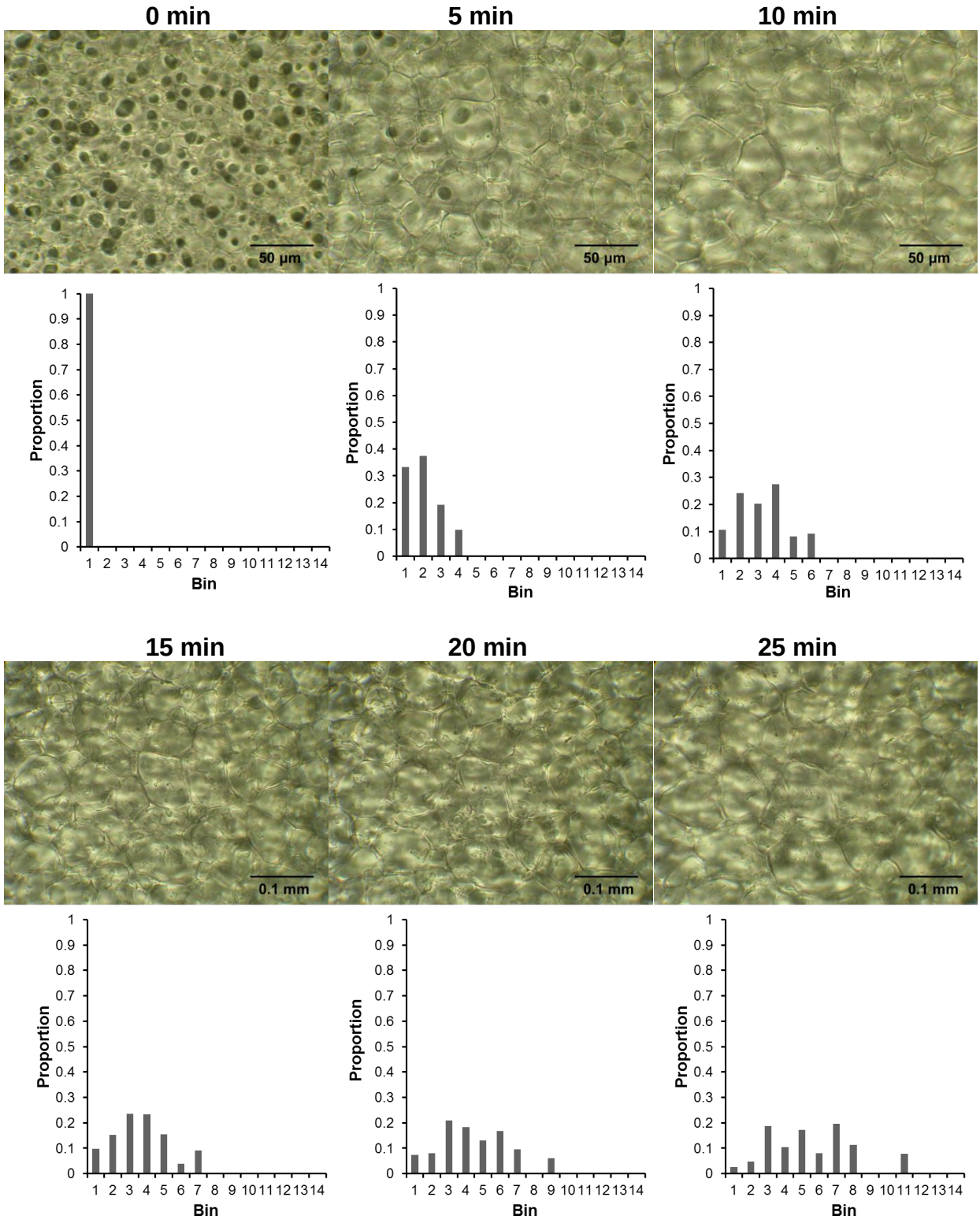
0 min
5 min
10 min
50 µm
50 µm
50 µm
Proportion
Bin
15 min
20 min
25 min
0.1 mm
0.1 mm
0.1 mm
Proportion
Bin

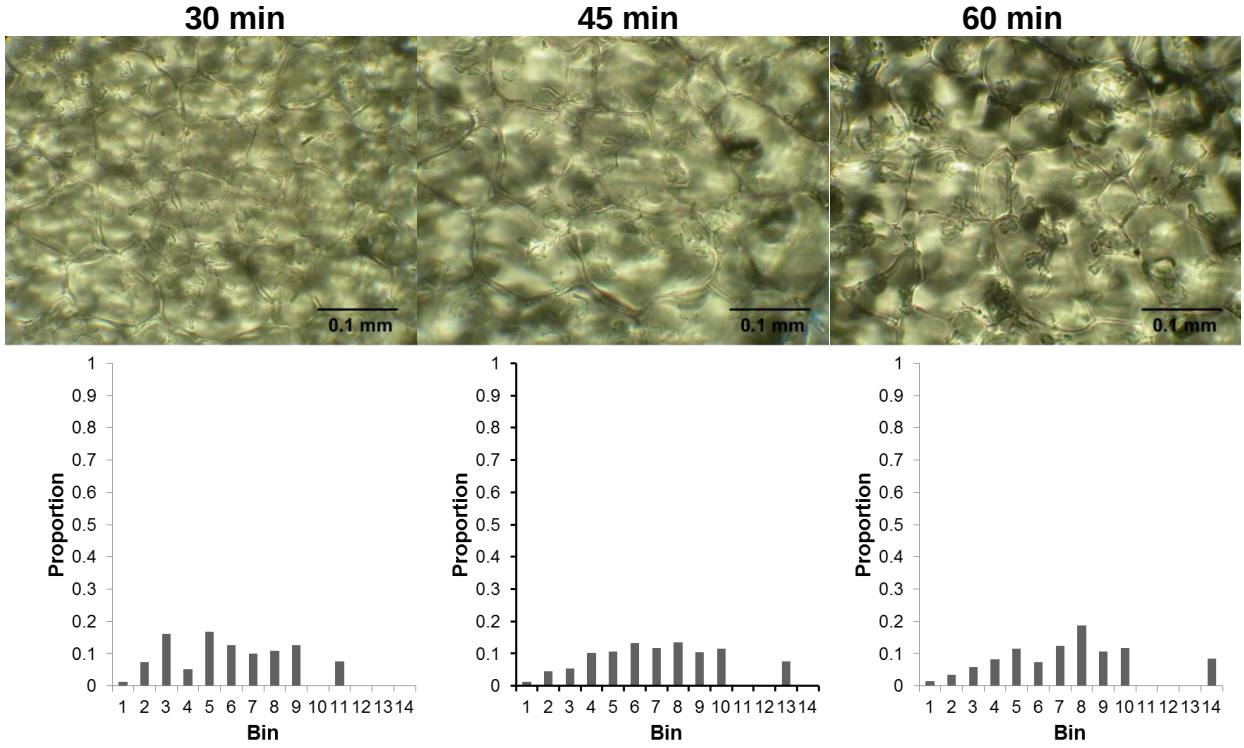

Figure 3.2 Time-dependent distribution of crystal sizes in a PBS control carried out at times 0, 5, 10, 15, 20, 25, 30, 45, and 60 min. Images obtained at each time point are shown, with the corresponding histograms of the crystal size distributions located directly underneath the images of ice crystals. It is important to note that pictures at times 0, 5, and 10 were taken at maximum camera magnification; 15, 20, 25, and 30 were taken at a different camera magnification; 45 and 60 were taken at yet another magnification. All images have been adjusted and scaled accordingly, with the appropriate correction factors applied during analysis to obtain accurate crystal area data.

As shown in Figure 3.2, at time 0, all crystals were small enough that they were located in bin 1 only as all ice crystal areas were found to be less than 0.001 mm^2. This amounted to 254 total crystals and was consistent with the set parameters such that all crystals should be located in bin 1 at time 0. At 5 min, the number of crystals decreased significantly to 72, and bin 1 was no longer the most populated bin (having dropped to 33%). Bin 2 represented the greatest proportion of total area of the sample at 38%. Bins 3 and 4 had also become populated. At 10 min, crystals had grown even larger, cutting the total number of crystals within the field of view by half, to 35. The crystals occupying bin 1 now took up only 11% of the total area, and the population of bin 2 decreased. Furthermore, crystals grew large enough to populate up to bin 6.

Past 10 min, crystals had grown so large that it was impossible to obtain a proper sample size at the camera's maximum magnification, and so the zoom factor was decreased at 15 min, resulting in 68 visible crystals in the FOV. The number of visible crystals in the FOV would continue to decrease over time as recrystallization took place. The population of bin 1 saw a slight decrease at 15 min, and population increased into the 7^{th} bin as the distribution began to broaden. The broadening continued as time increased, resulting in more bins being populated at each time point. At 30 min, the population of bin 1 had decreased to 1% of the total area of the sample, the smallest fraction of all occupied bins. From this point onwards, the population of bin 1 did not change, and most other bins experienced slight fluctuations in proportionate area. The distribution continued to broaden such that by 60 min, crystals could be found in up to 14 bins.

From this distribution analysis, we see that bin 1 remains populated throughout the ice recrystallization process. By the 30 minute time point, it has reached a more or less constant population of 1%, indicating that while most of the small crystals have grown, they do not completely disappear. By 60 min, even bins 2-4 are sparsely populated (less than 10% each), but there are still small ice crystals present in the sample even as the distribution broadens to include up to 14 bins. Furthermore, the recrystallization process is quick without inhibitors present, as the population of bin 1 decreases drastically in the first 5 min of annealing time from 100% to 33%. Bin 1 is the only bin that continually decreases across time, until its decrease eventually flattens out. All other bins start out unpopulated, but once they become populated, the proportion fluctuates as other bins similarly become more or less populated and the distribution broadens. The distribution broadens quickly, moving from 1 to 4 bins in the first 5 minutes, and then to 6 bins in the first 10 minutes, where the distribution steadily increases for the remainder of the experiment until it reaches a 14^{th} bin at 60 min. We can therefore conclude from this

binning analysis that there is a wide distribution of ice crystal sizes during the ice recrystallization process, resulting in a non-homogeneous mixture, and that the smaller ice crystals never completely disappear from the sample.

Following this binning analysis, a time dependent study with 22 mM PMP-Glc was performed in order to compare and contrast the ice crystal size distribution with and without the presence of an active inhibitor. The data obtained from this analysis is shown in Figure 3.3.

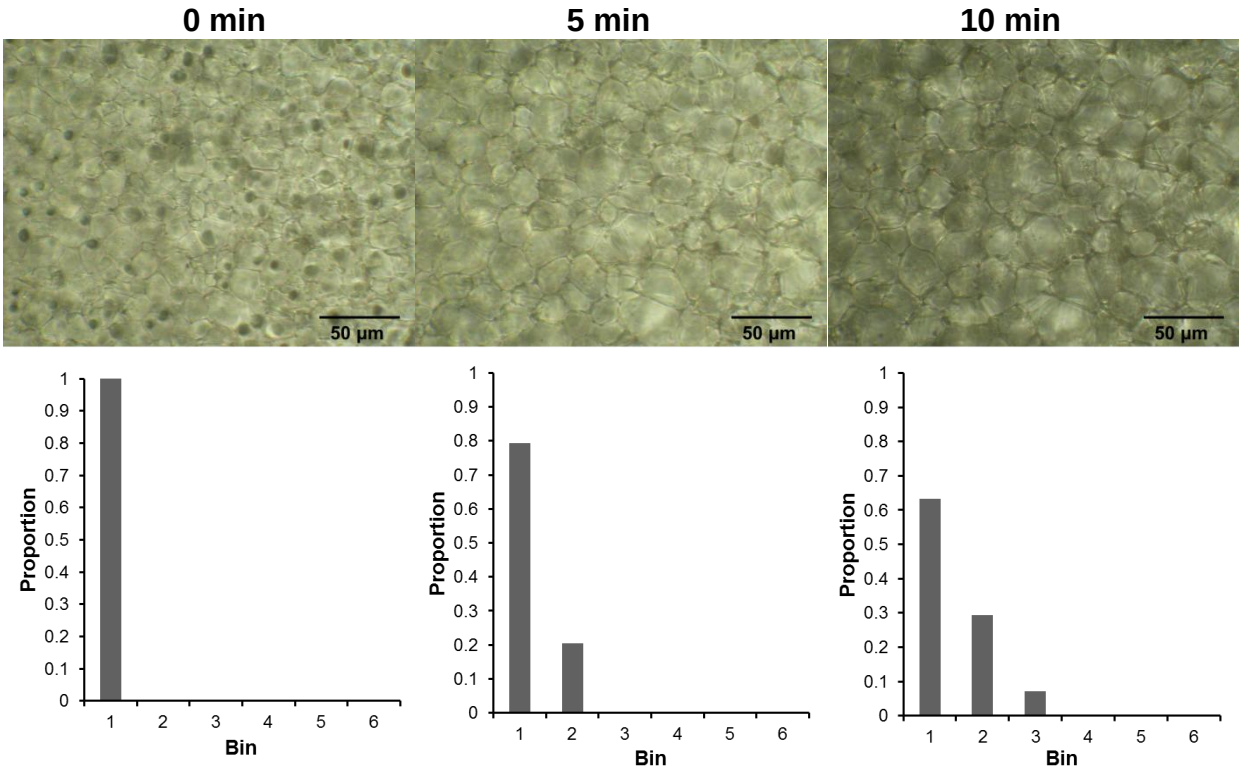

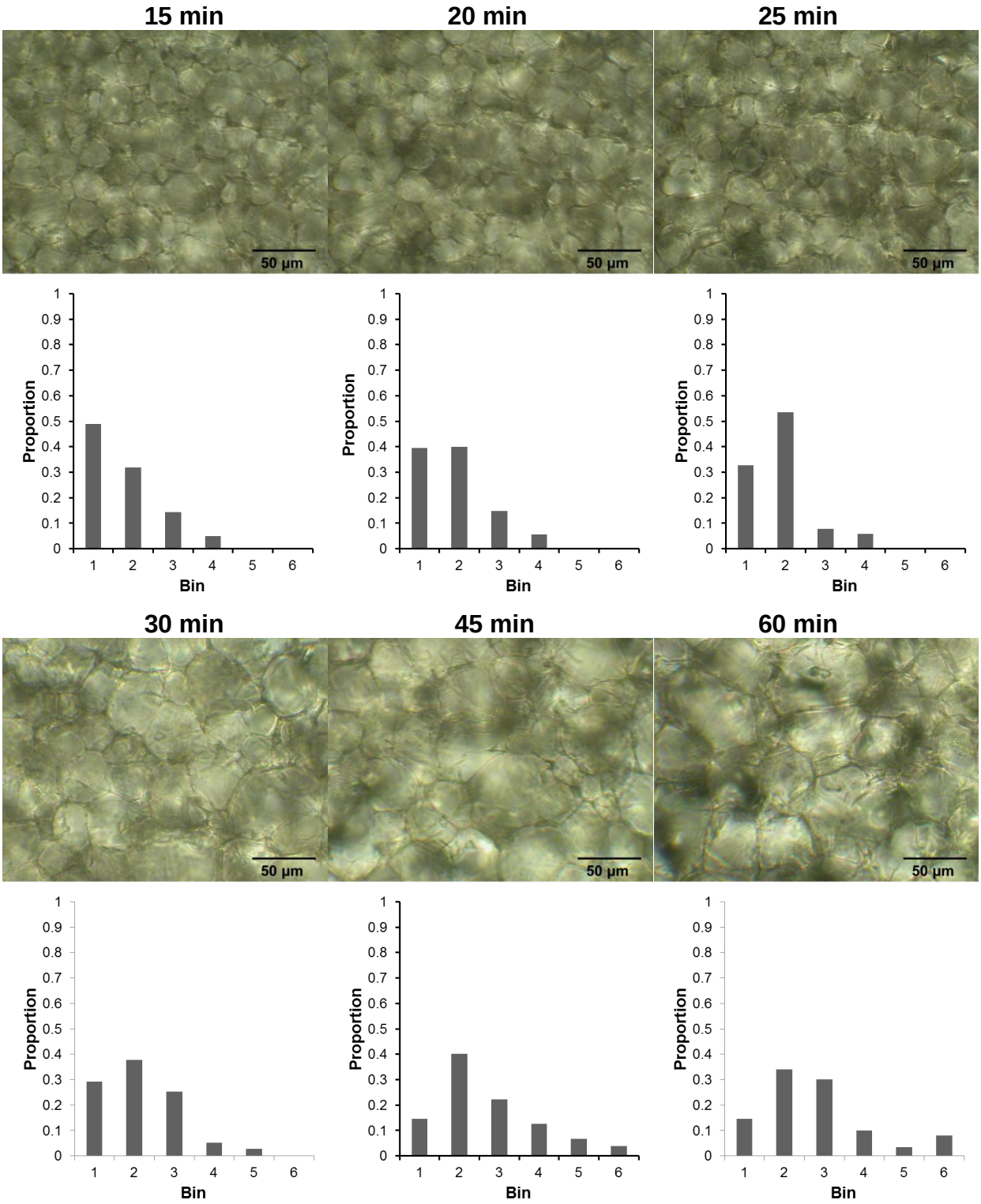

Figure 3.3 Time-dependent distribution of crystal sizes with 22 mM PMP-Glc carried out at times 0, 5, 10, 15, 20, 25, 30, 45, and 60 min. Images obtained at each time point are shown, with the corresponding histograms of the crystal size distributions located directly underneath the images of ice crystals. It is important to note that pictures at times 0, 5, 10, 15, 20, and 25 were taken at a different camera magnification than times 30, 45, and 60, but the images have been adjusted and scaled accordingly.

As shown in Figure 3.3, all crystals at 0 min resulted in areas under 0.001 mm^2 as expected. These crystals were thus placed in bin 1, corresponding to a total of 277 crystals in the FOV. At 5 min, the total number of crystals was cut in half at 135 and 80% of the total area of these crystals remained in bin 1. The remaining 20%, however, consisted of crystals located in bin 2. This demonstrates that while crystals are still small, they are beginning to grow. The trend continues at 10 min, where once again, fewer crystals are found in the sample image. Here, we see that there is a small population of crystals beginning to occupy the 3rd bin. The population of bin 2 has increased to 30%, and the population of bin 1 continues to slowly decrease, now at 63%. At 15 min, crystal sizes began to occupy the 4th bin. At this point, only half of the total crystal area of the sample was now located in the 1st bin as its population continued to slowly decrease. Over the next 10 min, the population of bin 1 decreased while the other three bins saw slight fluctuations. At 30 min, the magnification of the camera used to take these pictures was changed. For the first 6 time points, the magnification was set to the highest possible zoom to facilitate visualization and analysis the small ice crystals. At this time, the crystals were too large to obtain the desired sample size, and thus the magnification was decreased. It is important to note that there is an appropriate correction factor applied for each magnification to ensure all crystals are accurately measured. While at 25 min the population of bin 1 once again decreased, the distribution broadened slightly to 5 bins. This showed the continuing increase in crystal size over time, though there was still a large population of small crystals. At 45 min, crystal distribution expanded to 6 bins with only 15% of the total area located in bin 1. This distribution remained constant through the final 15 min of annealing time, while all other populations showed minor fluctuations, indicating that recrystallization was tailing off.

From this distribution analysis, we see that bin 1 is the only bin that continuously decreases with time, ultimately reaching a relatively constant population across the final 15 minutes. All other bins start off empty, but slowly grow in population as recrystallization occurs. The biggest growth occurs in bin 2, whose population surpasses 50%, at which point it slowly decreases as crystals continue to grow. Bin 3 also experiences significant growth, notably in the final 30 minutes of the assay. Bin 4 only becomes populated after the first 15 minutes, and bins 5-6 are only populated after half an hour, demonstrating a much slower recrystallization process than what was seen with PBS.

Comparing the binning analysis of PBS with 22 mM PMP-Glc, we are able to note that during ice recrystallization, small crystals are still present throughout all time points even though large crystals eventually take up more of the sample. This could be due to the fact that in recrystallization, large ice crystals grow at the expense of smaller ones, meaning some crystals shrink as others grow. This further indicates that not all ice crystals grow large when recrystallization occurs. It is also interesting to note that the summed area of all ice crystals does not significantly vary from one time point to the next. This further demonstrates the constant high ice volume fractions that result from the use of our splat-cooling assay with PBS solution as a standard.

While these similarities exist between the binning analyses of the two samples, there are also notable differences. Primarily, it is evident that there is a much wider distribution of ice crystal sizes when there is no inhibitor present. Through the entire 60 min of annealing time, the distribution of crystal sizes expands to 14 bins in PBS but only to 6 in 22 mM PMP-Glc. Furthermore, the time it takes to occupy more bins is notably longer in 22 mM PMP-Glc than it is in PBS. For example, the PBS distribution reaches 6 bins after only 10 minutes, whereas the

22 mM PMP-Glc distribution takes 30 minutes before crystals grow large enough to populate the 6th bin. In addition, the spread of the distribution varies greatly between the two solutions. In 22 mM PMP-Glc, even after 60 min, 50% of the total area of the sample is found in the first 2 bins; for PBS, that 50% is spread across the first 8 bins, with only 5% occupying the first 2 bins. The differences in distribution are further validated when looking at the change in population of bin 1. In PBS, the population of bin 1 drops to 33% after 5 min, whereas in 22 mM PMP-Glc, the population remains high at 80% and does not reach 33% until 25 min of annealing time.

From this analysis, we can conclude that there is a clear difference in the distribution of ice crystal sizes with and without the presence of inhibitor, demonstrating the effect of inhibitors not only on average ice crystal size, but on distribution as well. While it can be said that the system is always heterogeneous in terms of crystal sizes, it is still evident that there is a narrower distribution more geared towards smaller sized crystals when an ice recrystallization inhibitor is present. Finally, when looking at the populations of the earlier bins, we can see that the proportions remain high in the presence of inhibitor. Conversely, in the absence of an inhibitor, the wider distribution of ice crystal sizes is a result of a reduced amount of smaller ice crystals and an increased amount of larger ones.

3.4 Determining rate constants for the mono-exponential decay of the relative proportion of "ice crystal area in Bin 1"

3.4.1 Applying the binning results to a mono-exponential decay curve and obtaining a rate constant for inhibition

Koop *et al*. have already shown that the kinetic analysis of ice recrystallization over an extended period of time is a more reliable measure of IRI activity than mean crystal size at a single time point.[9] However, their approach focuses on the change in ice crystal radius over

time. As demonstrated by the binning analysis in Section 3.3, the ice crystal sizes within a completely frozen sample are not homogenous, especially at later time points, where there is a much broader distribution. This serves as an indication that mean crystal area (or any parameter derived from crystal radius) is not the most reliable attribute to measure for our kinetic analysis. We therefore sought a different attribute that could be followed kinetically, and thus decided to look at the population distribution resulting from the binning analysis. As mentioned in Section 3.3, some bins may increase and then decrease in population over time, while others continue to fluctuate up and down. The only bin that continually decreases over time is bin 1, the bin containing the smallest ice crystals and which at time 0 contains 100% of the sample area. By plotting the proportion of sample area located in bin 1 over time, we found that this decrease in population fit that of a mono-exponential decay (see Figure 3.4 on p.44). We therefore fit the decrease of the relative area of bin 1 to a mono-exponential curve using non-linear least squares analysis according to Equation 3.1.

$$A_t^{rel} = A_0^{rel}(e^{-k_{obs}t}) + A_\infty^{rel}$$

Equation 3.1 Mono-exponential decay equation for the disappearance of bin 1 over time.

In this equation, A_t^{rel} is the measured relative area of Bin 1 at time t, A_0^{rel} is the fitted relative area at time zero, k_{obs} is the fitted rate constant for the decrease of the relative area of bin 1 and A_∞^{rel} is the fitted final end point. The fitted value for A_0^{rel} was designed such that it would nearly always be 1.0, since 100% of the crystal areas at time 0 should theoretically be found under bin 1. The final end point A_∞^{rel} was nearly always zero, though this could sometimes change depending on the nature and concentration of inhibitor used.

The above-mentioned analysis was applied to the proportion data obtained from the binning experiments carried out in a PBS control (0 mM) as well as 22 mM PMP-Glc from Section 3.3. The binning experiment was repeated two additional times on top of the initial experiments at each concentration in order to obtain triplicate data for standard error measurements. From there, the average proportion of bin 1 was plotted over time (see Figure 3.4) and fit to the mono-exponential equation shown above (Equation 3.1). Both curves displayed excellent fits to the model equation, with R^2 values of 0.998 and 0.993 respectively. These fits corresponded to between 3-21 half-lives of monophasic, mono-exponential decrease, with tight standard error intervals at 95% confidence (4% and 7% respectively). The k_{obs} values for PBS and 22 mM PMP-Glc were calculated to be 0.213 ± 0.009 min^{-1} and 0.041 ± 0.003 min^{-1} respectively. Therefore, at a concentration of 22 mM, it can be concluded that PMP-Glc slows crystal growth out of bin 1 at a rate that is 19% of that of the PBS control, that is to say, with no inhibitor present. This marks a significant step forward in the quantitative measurement of IRI activity. Previously, 22 mM PMP-Glc was said to have a % MGS of approximately 22% that of PBS.[15] However, due to the heterogeneity of ice crystal areas, this relative proportion cannot necessarily correspond to the same k_{obs} value for other effective inhibitors with the same % MGS. That is to say, another inhibitor with an activity of 22% may not necessarily produce the same rate constant. This relative measure was therefore unable to provide a concise indication of "potent" IRI activity. However, an observed rate constant could potentially fill the need for a more quantitative measurement of IRI activity.

3.4.2 Obtaining rate constants across a concentration scan for PMP-Glc

As mentioned in Section 1.7, there is a pronounced concentration effect on inhibition of ice recrystallization, and thus a concentration scan is necessary to determine an inhibitor's full

capabilities. We therefore repeated the binning experiment in Section 3.3 with PMP-Glc at concentrations of 1, 10, 15, 44, and 100 mM and subjected them to the same mono-exponential curve fitting as with 0 mM (PBS) and 22 mM (Section 3.4.1). The mono-exponential decay curves are shown in Figure 3.4 and the resulting rate constant data is tabulated in Table 3.1.

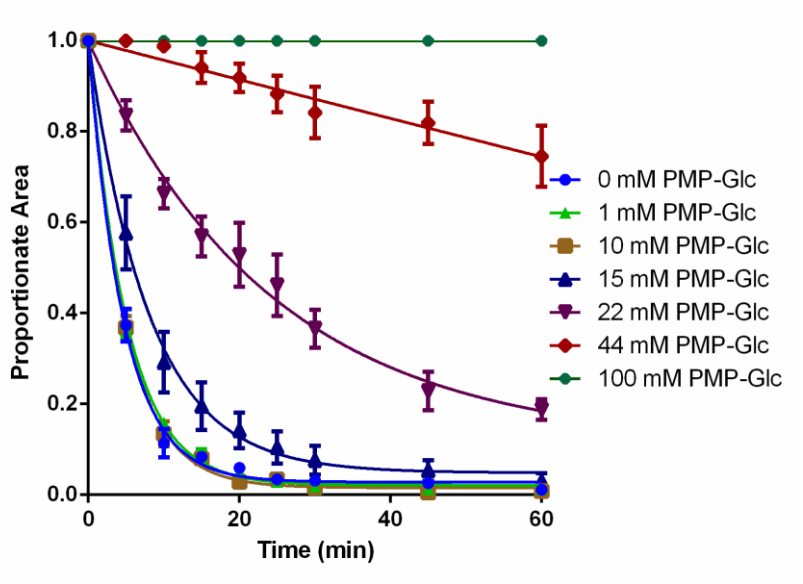

Figure 3.4 Mono-exponential decay curves of the proportionate area of bin 1 for 0, 1, 10, 15, 22, 44, and 100 mM PMP-Glc using non-linear least squares analysis.

Concentration (mM)	k_{obs} (min^{-1})	R^2	Half-life (min)
0	0.213 ± 0.009	0.9977	3.25
1	0.197 ± 0.005	0.9992	3.52
10	0.204 ± 0.005	0.9991	3.40
15	0.124 ± 0.005	0.9975	5.59
22	0.041 ± 0.003	0.9928	16.9
44	0.0003 ± 0.007	0.9596	2.31×10^3
100	0	1	N/A

Table 3.1. Summary of data obtained from the concentration scan of PMP-Glc fit to a mono-exponential decay curve, displaying the observed rate constant k_{obs} with standard error intervals at 95% confidence, R^2, and half-life for each concentration tested.

As shown in Figure 3.4, the most notable differences are the initial rates of decay. For 0, 1, and 10 mM PMP-Glc, the proportion of crystals that are found in bin 1 has already dropped to 37% after the first 5 minutes. At this same time point, the proportion for 15 mM PMP-Glc is 58%, and for 22 mM PMP-Glc it is 84%. PMP-Glc at 44 and 100 mM are so effective that after the first 5 minutes, the entire crystal population remains small enough to be located in bin 1. PMP-Glc at 100 mM is a strong enough inhibitor that ice crystals remain small throughout the entire 60 minute assay time, resulting in a flat line with all crystal areas fitting in bin 1 at all times. PMP-Glc at 44 mM is also strongly inhibiting ice crystal growth, as all crystals remain located in bin 1 for the first 10 minutes of assay time before the population finally begins to decrease. However, even at 60 minutes the proportion of crystal area found in bin 1 remains high at 75%. PMP-Glc at 0, 1, 10, 15, and 22 mM all clearly follow mono-exponential decay curves, with R^2 values above 0.99 (as shown in Table 3.1), half-lives ranging from 3-21, and less than 10% error on all rate constants. However, while 1 and 10 mM PMP-Glc appear to have the

same effect as a solution with no inhibitor present, there are notable differences with 15 and 22 mM PMP-Glc. Not only do 0, 1, and 10 mM PMP-Glc see a much steeper decay rate, but a lower endpoint as well, resulting in approximately 1% of the proportion of total area corresponding to crystals in bin 1 after 60 minutes annealing time. PMP-Glc at 15 mM reaches an endpoint of 3% at 60 minutes, and it is worth noting that it took 0, 1, and 10 mM PMP-Glc only 25 minutes to reach 3% proportion. At 22 mM, PMP-Glc is a stronger inhibitor and has a much shallower curve, taking 30 minutes for the proportion to decrease below 40%, whereas this decrease happened in 5 minutes with 0, 1, and 10 mM PMP-Glc. Furthermore, at 60 minutes, 22 mM PMP-Glc still contains 18% of the total area of crystals in bin 1, a much higher proportion than those at the lower concentrations, indicating much more effective inhibition. This can be confirmed by looking at the k_{obs} values generated by the mono-exponential decay plots tabulated in Table 3.1. The rate constants for 0 mM (0.213 ± 0.009 min^{-1}), 1 mM (0.197 ± 0.005 min^{-1}), and 10 mM (0.204 ± 0.005 min^{-1}) do not differ significantly from one another, indicating that PMP-Glc is ineffective as an inhibitor at concentrations of 10 mM or less. At 15 mM PMP-Glc, the rate constant of 0.124 ± 0.005 min^{-1} is almost half of that measured at 10 mM, a substantial difference in effectiveness achieved from a slight increase in concentration. As mentioned previously, 22 mM PMP-Glc has a rate constant of 0.041 ± 0.003 min^{-1}, while 44 mM PMP-Glc has a rate constant of 0.0003 ± 0.007 min^{-1}. The wide margin of error in the latter can be partly explained by the poorer fit ($R^2 = 0.9596$), especially since there is no decay present within the first three data points, as the proportion remains at 100% within the first 10 minutes of annealing time. As a result, 44 mM PMP-Glc displayed the worst fit to a mono-exponential decay curve of all concentrations tested (not counting 100 mM PMP-Glc, which resulted in a straight line). It is still worth noting, however, since it is obvious from the plot that this is a highly effective

inhibitor concentration. At 100 mM, PMP-Glc is an even more effective inhibitor and does not fit a standard mono-exponential curve as there is no actual rate of decrease of the proportionate area of crystals found in bin 1, since it remains at 100% throughout the experiment. As such, the rate constant at this concentration can be considered to be 0 min^{-1}. As expected, these results demonstrate a pronounced concentration effect on inhibitor, and once again prove that testing at one concentration is not enough to determine the capability of a compound as an ice recrystallization inhibitor. As shown by the rate constants obtained at 10 and 15 mM PMP-Glc, just a slight increase in concentration can be the difference between no inhibition and effective inhibition. Therefore, in the past, compounds tested and deemed "inactive" could have actually had missed potential as inhibitors, which could have been discovered simply by increasing the testing solution's concentration. Furthermore, we can also deduce that there is an effective inhibition end point, such as at 100 mM PMP-Glc, where there is effectively no change in proportionate area of bin 1. We can therefore say that this concentration completely inhibits crystal growth. However, this may not necessarily be true, as the ice crystals at time 0 appear to be much smaller than those produced at lower concentrations. To demonstrate this difference, crystal sizes at various concentrations were compared and graphed in Figure 3.5.

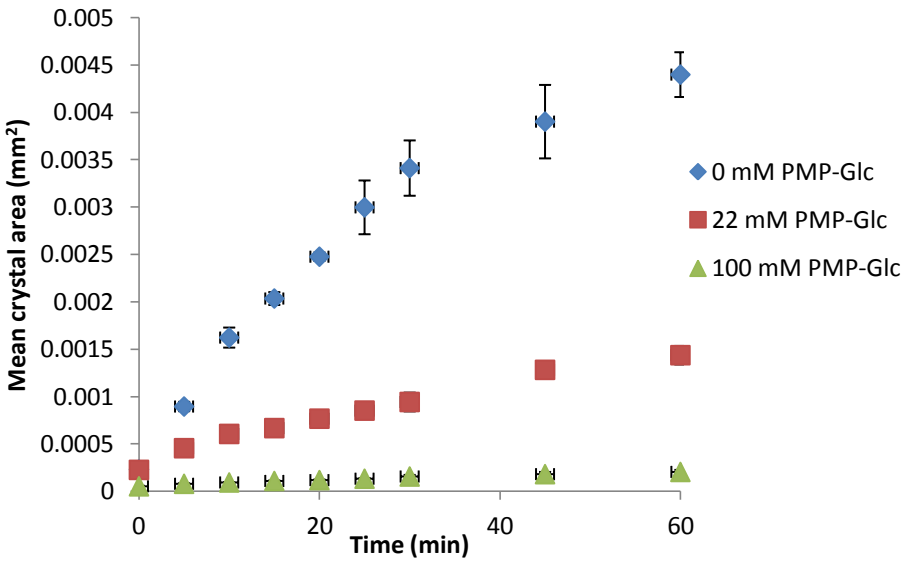

Figure 3.5 Average ice crystal area of 0, 22, and 100 mM PMP-Glc as a function of time.

As established previously, mean crystal area is not an appropriate measure for a non-homogeneous system such as those found with large ice crystals, particularly at higher time points with high amounts of ice recrystallization. This can be seen by the large error bars of 0 mM PMP-Glc from 25 min onwards. However, when looking at effective inhibitors, the distribution of crystal sizes is much less broad, though it still exists with 22 mM PMP-Glc (see the binning analysis in Section 3.3). With 100 mM PMP-Glc, however, there is no distribution across different time points as the proportionate area of crystals in bin 1 remains at 100% throughout the set assay time. The average crystal area at 60 min for 100 mM PMP-Glc is still less than that of 22 mM PMP-Glc at time 0, and the initial crystal size for 100 mM PMP-Glc is only a quarter that of 22 mM PMP-Glc. From this graph, we can see that there is a definite increase in crystal size over time for 100 mM PMP-Glc, but relative to 0 and 22 mM PMP-Glc these changes are so small that they can be considered negligible. As such, we can loosely use the term "complete inhibition" to describe 100 mM PMP-Glc in the context of our assay with the

bin sizes we have determined. We can therefore conclude that our new method of kinetic profiling appears to be effective at determining the rates of crystal growth over various concentrations of inhibitor, as well as assigning quantitative measurements rather than a relative proportion of mean grain size, as was the case with our previous assay.

3.4.3 Obtaining rate constants across a concentration scan for Glc

Following the results obtained with the kinetic profiling of PMP-Glc, it was decided that this method should be tested with other inhibitors in order to verify the scope of this method. Ideally, other active inhibitors would result in similar kinetic profiles to PMP-Glc, and inactive compounds would be expected to show little to no change in rate constant over a concentration scan. As such, we chose to repeat this kinetic profiling experiment with D-glucose (Glc), a simple carbohydrate with little to no inhibition effects.[16] By subjecting an "inactive" compound to the same experiment, we can hypothesize that the rate constants obtained across various concentrations of Glc will differ only slightly if at all from that with no inhibitor present. The utility of the kinetic profile in separating active inhibitors (with pronounced concentration effects on rate constant) from inactive ones (little to no change in rate constant) could therefore be proven. The binning analysis was repeated for Glc concentrations of 0, 1, 10, 22, 44, and 100 mM, and mono-exponential decay curves of bin 1 were constructed for each. The plots are displayed in Figure 3.6 and the k_{obs} values are tabulated in Table 3.2.

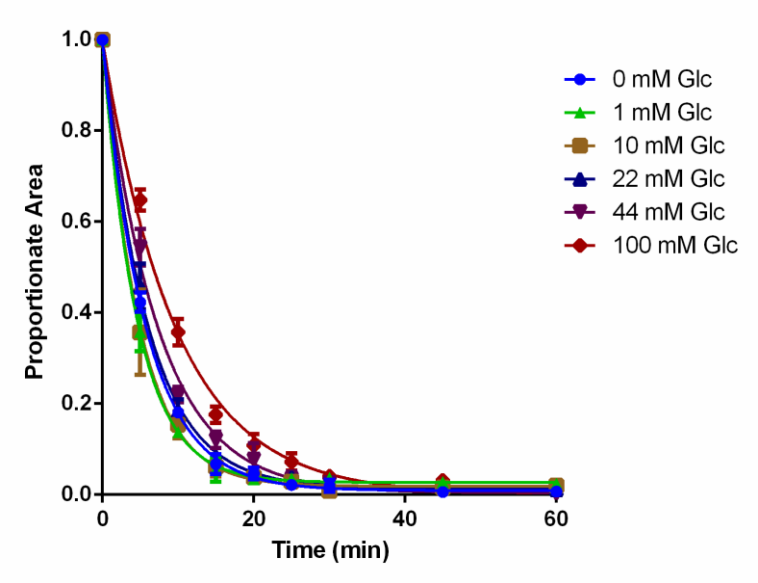

Figure 3.6 Mono-exponential decay curves of the proportionate area of bin 1 for 0, 1, 10, 22, 44, and 100 mM Glc using non-linear least squares analysis.

Concentration (mM)	**k_{obs} (min^{-1})**	**R^2**	**Half-life**
0	0.176 ± 0.003	0.9997	3.806 to 4.088
1	0.218 ± 0.003	0.9997	3.080 to 3.303
10	0.208 ± 0.004	0.9995	3.188 to 3.506
22	0.168 ± 0.004	0.9991	3.886 to 4.393
44	0.137 ± 0.006	0.9967	4.545 to 5.684
100	0.104 ± 0.006	0.9948	5.879 to 7.751

Table 3.2. Summary of data obtained from the concentration scan of Glc fit to a mono-exponential decay curve, displaying the observed rate constant k_{obs} with standard error intervals at 95% confidence, R^2, and half-life for each concentration tested.

As per Table 3.2, all curves strongly fit the mono-exponential decay model, with R^2 values of 0.9948 or higher, half-lives ranging from 3-8, and with less than 6% errors on the rate constants. Looking at Figure 3.6, there is much less discrepancy between the mono-exponential

decay curves at various Glc concentrations than there is with PMP-Glc (Figure 3.4). At 5 min, 0, 1, 10, and 22 mM Glc all show proportionate areas of crystals in bin 1 at around 40%, with no significant differences between one another. Even 44 mM Glc, with a proportionate area of 54% at 5 min, does not differ significantly from 22 mM Glc when error margins are considered. The only concentration that shows a significant difference when no inhibitor is used is 100 mM Glc, with a proportionate area of 65% at 5 min. At first glance, this is on par with 22 mM PMP-Glc. Therefore, if looking only at proportionate area at 5 min as an indication of IRI activity, we can deduce that 100 mM Glc is equivalent to 22 mM PMP-Glc. Furthermore, no matter the concentration of Glc tested, all curves reach the same endpoint of approximately 1-2%. This is where 100 mM Glc strongly differs from 22 mM PMP-Glc, as 22 mM PMP-Glc still retains 18% proportionate area of crystals in bin 1 at 60 min, whereas 100 mM Glc is reduced to a meager 1%. This result once again proves that it is not sufficient to assess a compound's affinity for IRI at a single time point only, as two compounds that appear to inhibit ice recrystallization in the same way might actually differ greatly in endpoint and also the rate at which they reach that endpoint. This is further proven when we look at the k_{obs} values obtained for the various Glc concentrations. The rate constants for 1 mM (0.218 ± 0.003 min^{-1}) and 10 mM (0.208 ± 0.004 min^{-1}) are not significantly different from that of 0 mM PMP-Glc (0.213 ± 0.009 min^{-1}). However, the rate constant for 0 mM Glc is actually lower than these values, at 0.176 ± 0.003 min^{-1}. It is unknown as to why there is this discrepancy, though this does not greatly alter the results and can thus be ignored. Glc at 22 mM (0.168 ± 0.004) does not differ greatly from 0 mM Glc (0.176 ± 0.003 min^{-1}). It is only at 44 mM Glc (0.137 ± 0.006 min^{-1}) and 100 mM Glc (0.104 ± 0.006 min^{-1}) that we begin to see greater differences in the k_{obs} values obtained. However, as mentioned earlier, despite the proportionate area at 5 min for 22 mM PMP-Glc and

100 mM Glc being almost identical, there remains a large difference in their k_{obs} values, with 22 mM PMP-Glc at 0.041 ± 0.003 min^{-1} and 100 mM Glc at 0.104 ± 0.006 min^{-1}. Overall, this demonstrates that 22 mM PMP-Glc slows the rate of crystal growth out of bin 1 by over twice as much as 100 mM Glc. Therefore, we can conclude from these rate constants that 22 mM PMP-Glc is a much better inhibitor than 100 mM Glc. While Glc does show that increasing concentration increases IRI, even at 100 mM Glc cannot be considered an effective ice recrystallization inhibitor. Thus, with this method, we are able to distinguish between effective and ineffective inhibitors.

3.4.4 Obtaining rate constants across a concentration scan for pBrPh-Glc

Next, we tested this method with another known IRI-active compound, *p*-bromophenyl-β-D-glucoside (pBrPh-Glc), which has actually proven to be more effective than PMP-Glc using the previously accepted assay.[15] This was done firstly to verify that the kinetic profiling method continues to work for other active inhibitors, but also to compare the results obtained for these two compounds between the two methods. Once again, pBrPh-Glc was subjected to the binning analysis method at concentrations of 0, 1, 5, 10, 15, 22, 40, and 60 mM, and the decrease in the proportionate area of bin 1 over time was fitted to the same mono-exponential curve as done previously. The plots are shown in Figure 3.7 and the rate constants are tabulated in Table 3.3.

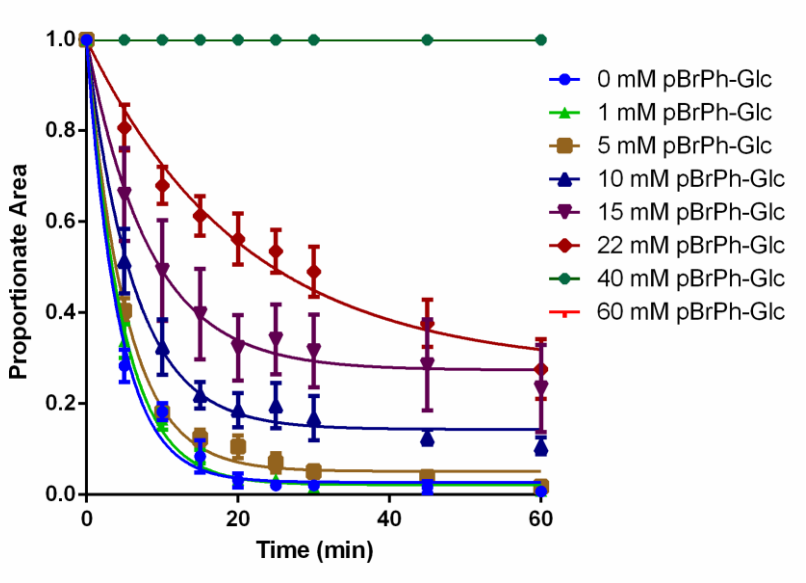

Figure 3.7 Mono-exponential decay curves of the proportionate area of bin 1 for 0, 1, 5, 10, 15, 22, 44, and 100 mM pBrPh-Glc using non-linear least squares analysis.

Concentration (mM)	**k_{obs} (min^{-1})**	**R^2**	**Half-life**
0	0.234 ± 0.021	0.9911	2.446 to 3.739
1	0.211 ± 0.009	0.9976	2.975 to 3.667
5	0.192 ± 0.010	0.9961	3.197 to 4.141
10	0.159 ± 0.010	0.9943	3.791 to 5.101
15	0.120 ± 0.008	0.9923	4.956 to 6.915
22	0.048 ± 0.007	0.9759	10.91 to 21.46
40	0	1	N/A
60	0	1	N/A

Table 3.3 Summary of data obtained from the concentration scan of pBrPh-Glc fit to a mono-exponential decay curve, displaying the observed rate constant k_{obs} with standard error intervals at 95% confidence, R^2, and half-life for each concentration tested.

As displayed in Table 3.3, all curves demonstrated an excellent fit (R^2 above 0.99) resulting in rate constants with under 10% error with a few minor exceptions: 22 mM pBrPh-Glc with an R^2 of 0.9759 and 15% error for k_{obs}, and 40 and 60 mM pBrPh-Glc resulted in straight lines, therefore showing no signs of decay. Looking at the curves in Figure 3.7, we can see already that there is a much wider range of effectiveness than what was seen with PMP-Glc and Glc, but at a smaller range of concentrations, as pBrPh-Glc was insoluble in PBS past 60 mM and therefore could not be tested at 100 mM like the others. Firstly, looking at the decrease in proportionate area of bin 1 from 0 to 5 min, there is a broad range of distributions present among the various pBrPh-Glc concentrations. The proportionate area of bin 1 for 0 and 1 mM pBrPh-Glc is around 30%, 5 mM pBrPh-Glc is at 40%, 10 mM pBrPh-Glc is at 51%, 15 mM pBrPh-Glc is at 66%, 22 mM pBrPh-Glc is at 80%, and 40 and 60 mM pBrPh-Glc remain at 100%. 15 and 22 mM pBrPh-Glc are statistically similar to 15 and 22 mM PMP-Glc respectively, while 10 mM pBrPh-Glc is about 10% higher than 10 mM PMP-Glc. Furthermore, 40 mM pBrPh-Glc remains at 100% throughout the 60 min assay, whereas 44 mM PMP-Glc only remains at 100% for the first 10 minutes. This demonstrates that pBrPh-Glc has a much tighter separation of IRI activities over a concentration scan than does PMP-Glc, information that could not have been obtained with the traditional single concentration 30-minute annealing assay. Furthermore, there is a broader range of endpoints for the various concentrations of pBrPh-Glc, once again demonstrating the difference between a good inhibitor and a poor one such as Glc, which resulted in the same endpoint over all concentrations tested. While 0, 1, and 5 mM pBrPh-Glc resulted in endpoints of proportionate area around 1%, 10 mM pBrPh-Glc resulted in an endpoint of 11%, 15 mM pBrPh-Glc had an endpoint of 23%, and 22 mM pBrPh-Glc has an endpoint of 28%. 40 and 60 mM pBrPh-Glc remained at 100%. 15 and 22 mM pBrPh-Glc are therefore

both better than 22 mM PMP-Glc, which had an endpoint of 19%. This is interesting because 22 mM PMP-Glc contains a slightly greater proportion of smaller crystals than 22 mM pBrPh-Glc at 5 min (though the two are statistically similar), but the opposite occurs at 60 min. Additionally, 44 mM PMP-Glc has an endpoint of 75% at 60 min, whereas 40 mM pBrPh-Glc remains at 100%. This indicates that pBrPh-Glc can achieve complete inhibition at a lower concentration than PMP-Glc. Finally, when looking at the rate constants obtained (Table 3.3), we see that 0, 1, and 5 mM pBrPh-Glc do not differ significantly from one another (0.234 ± 0.021 min^{-1}, 0.211 ± 0.009 min^{-1}, and 0.192 ± 0.010 min^{-1} respectively), indicating that essentially no inhibition takes place at these concentrations. These results are consistent with 0, 1, and 10 mM PMP-Glc. Unlike 10 mM PMP-Glc, however, 10 mM pBrPh-Glc displays some activity with a k_{obs} of 0.159 ± 0.010 min^{-1}. 15 mM pBrPh-Glc resulted in a k_{obs} of 0.120 ± 0.008 min^{-1}, which is on par with that of 15 mM PMP-Glc (0.124 ± 0.005 min^{-1}). There is also a statistical similarity between 22 mM pBrPh-Glc (0.048 ± 0.007 min^{-1}) and 22 mM PMP-Glc (0.041 ± 0.003 min^{-1}).

3.4.5 Summary and conclusions for the extrapolation of rate constants from mono-exponential decay curves of PMP-Glc, Glc, and pBrPh-Glc

With the fitting of the decrease of the relative proportionate area of bin 1 to mono-exponential decay curves, we have obtained rate constants across a concentration scan that are indicative of a compound's ability to inhibit ice recrystallization. There is a pronounced concentration effect on rate constant for two well-known inhibitors, PMP-Glc and pBrPh-Glc, while this effect is negligible in Glc, a known poor inhibitor. Therefore, this method can be used to distinguish between effective and ineffective inhibitors.

The kinetic profiling results thus far have not demonstrated significant differences between the effectiveness of the two active inhibitors. As such, we can no longer state that

pBrPh-Glc is a more potent inhibitor than PMP-Glc, despite differences in the IRI activities of these compounds using the traditional method. This is due to the fact that we have shown that average crystal size is not an appropriate measure for IRI activity, and that there is more than one singular factor affecting it: initial rate, endpoint, the rate at which the endpoint is reached, and concentration dependence. All of these factors must be considered when attempting to fully quantify a compound's IRI activity, none of which are taken into account using the previously accepted assay. As such, this new method of kinetic profiling considers these factors and assigns quantifiable values for activity (k_{obs}) by monitoring the distribution of ice crystal sizes, which is a much more appropriate parameter to consider than mean grain size.

3.5 Constructing dose-response curves as a method of quantifying IRI activity

As mentioned in Section 3.1, one of the objectives for this project was to apply Koop's methodology for quantifying IRI activity in low ice volume fraction samples to high ice volume fraction samples.[7] Koop's method resulted in dose-response curves, commonly used in the field of medicinal chemistry, constructed from rate constants obtained through monitoring the change in average ice crystal radius over time. We have shown, however, that in high ice volume fractions, a sample wafer is heterogeneous during the recrystallization process, especially without the presence of inhibitor. Therefore, we applied the binning analysis from Section 3.3 and plotted mono-exponential decay curves for the disappearance of the smallest bin as a function of time (Section 3.4), which resulted in our rate constants, k_{obs}. These were the rate constants applied to Koop's method of dose-response curves. We noted that when plotting our rate constants against concentration, it yielded a sigmoidal curve. As such, we sought to obtain IC_{50} values by fitting our data into such a curve. In order to do so, we normalized our rate

constants (k_{obs}) by dividing them by the average PBS (0 mM) rate constant, resulting in a set of normalized rate constants (k_{norm}) for each inhibitor. We were able to construct these normalized rate constants due to the observation that at low inhibitor concentrations, the k_{obs} values obtained were indistinguishable from that of PBS (see Section 3.4). From there, we fit each data set to a four-parameter sigmoidal equation (Equation 3.2):

$$k_{\text{norm}} = \frac{k_0 - k_f}{\left(1 + n \times 10^{(\log IC_{50} - \log[I])} + k_f\right)}$$

Equation 3.2 Four-parameter sigmoidal dose-response curve used for the quantification of IRI activity.

In this equation, k_{norm} is the normalized rate constant mentioned above, measured in triplicate using the data from the mono-exponential decay curves; k_0 is the top plateau (blank value); k_f is the bottom plateau (efficacy); n is the Hill slope, where values above 1 indicate some degree of cooperativity; IC_{50} is the concentration at which k_{norm} is 50, essentially giving a k_{obs} value half that of PBS, and thus a measure of the inhibitor's potency; and [I] is the concentration of inhibitor and must be greater than 0. The four parameters of the equation were thus k_0, k_f, n, and IC_{50}. However, we chose to simplify the equation by reducing it to two parameters: n and IC_{50} only. As mentioned above, rate constants obtained at low inhibitor concentrations were essentially equal to that of PBS, thus resulting in an initial k_{norm} value of 100. We therefore set the top plateau k_0 to 100. Furthermore, as discussed in Section 3.4, we observed complete suppression of the depletion of bin 1 at high inhibitor concentrations, resulting in a rate constant of 0. It was therefore clear that our strong inhibitors demonstrate excellent efficacy and allowed us to set the bottom plateau k_f to 0. The two remaining parameters could then be determined by non-linear regression to Equation 3.2. The dose-response curves were therefore constructed for

all three compounds examined in Section 3.4: PMP-Glc, Glc, and pBrPh-Glc, and are displayed in Figure 3.8.

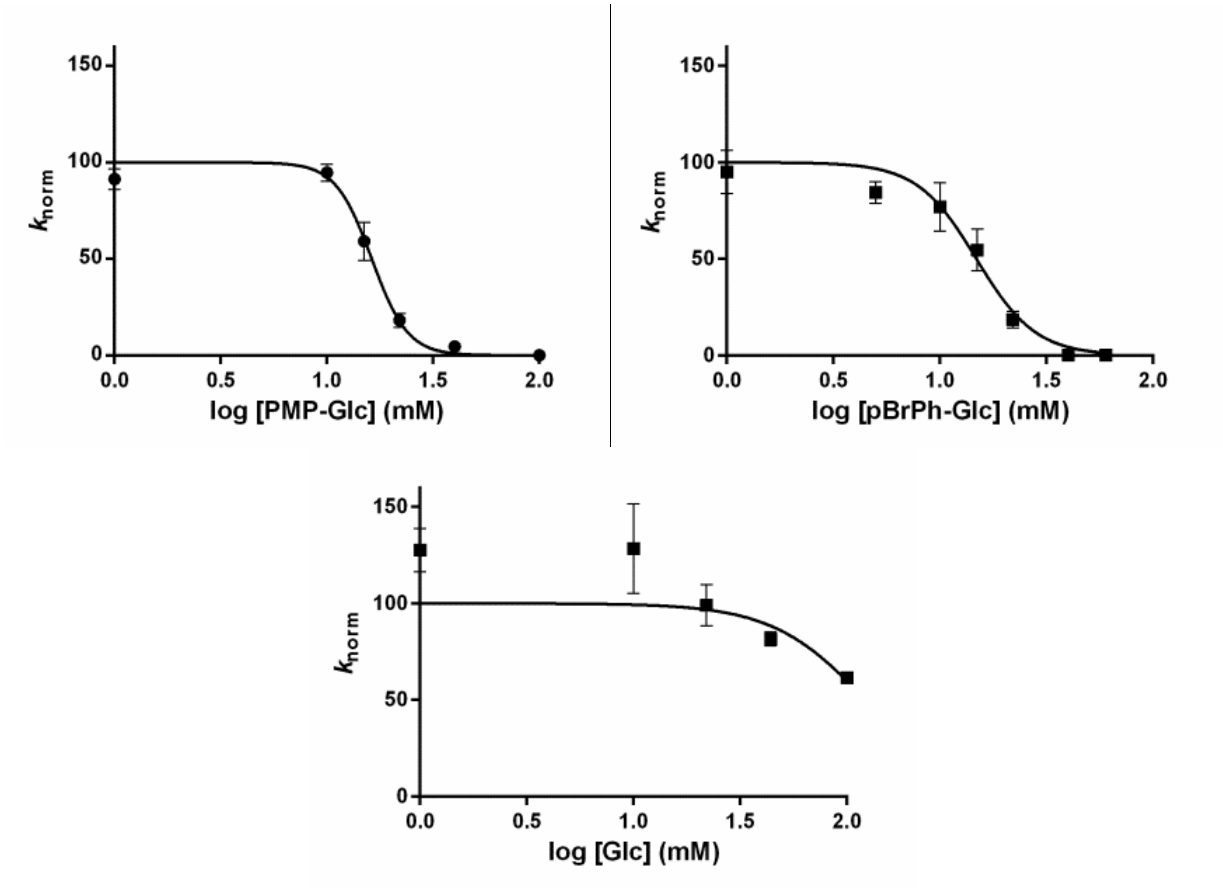

Figure 3.8 Dose-response curves where the normalized rate constant k_{norm} is plotted against log[I] and fitted to a two-parameter sigmoidal equation (Equation 3.2).

PMP-Glc gave an IC_{50} value of 16.3 ± 1.4 mM and a Hill slope of 5.12 ± 0.81, pBrPh-Glc showed an IC_{50} value of 14.8 ± 2.2 mM and a Hill slope of 3.12 ± 0.62, and Glc displayed an IC_{50} value of 122.1 mM with very poor error intervals at 95% confidence and a Hill slope of 1.98 ± 2.60. It is important to note that the error on Glc is so large in part due to the fact that a full sigmoidal curve could not be constructed from the concentration range tested, as we tested only up to 100 mM, yet the IC_{50} value obtained is greater than 100 mM. It is certainly possible that,

in repeating the binning analysis with increasing concentrations of Glc, a proper curve could be constructed in which both the top and bottom plateaus are visible; however, in terms of practicality, this would not be advisable as the IC_{50} would correspond to a concentration that is much higher than desired for what we would consider an effective inhibitor. As such, the fact that the Glc dose-response curve did not fit the sigmoidal curve properly is an indication of the compound's poor IRI activity. PMP-Glc and pBrPh-Glc, on the other hand, reveal excellent IC_{50} values that are actually lower in concentration than the 22 mM originally tested in the traditional assay. Though pBrPh-Glc has a lower value (14.8 mM) than PMP-Glc (16.3 mM), they remain statistically similar to one another, thus making it impossible to truly determine if one inhibitor is better than the other in terms of pure ice recrystallization inhibition effects (this does not, for example, take into account performance in a practical application such as cryopreservation). To the best of our knowledge, PMP-Glc and pBrPh-Glc are the best carbohydrate-based small molecule ice recrystallization inhibitors currently known. As such, these IC_{50} values mark a threshold value for new inhibitors to reach in order to be considered effective inhibitors of ice recrystallization.

As mentioned previously, the sigmoidal dose-response curves were obtained using a simplified version of Equation 3.2. It was therefore important to determine whether or not there were any significant differences between the actual and simplified versions of the sigmoidal fit. Consequently, dose-response curves were constructed four times, each with a different number of parameters. The values obtained are shown in Table 3.4:

Setting	4 parameters				3 parameters			2 parameters	
Parameter	k_0	k_f	n	IC_{50}	k_0	n	IC_{50}	n	IC_{50}
PMP-Glc	94.8	2.6	5.9	16.4	94.8	5.9	16.4	5.1	16.3
pBrPh-Glc	89.8	-1.9	4.0	16.5	89.5	4.2	16.3	3.1	14.8
Glc	130.3	58.6	2.2	27.9	133.0	1.0	77.9	2.0	122.1

Table 3.4. Comparison of the values obtained from the sigmoidal dose-response fit with 4, 3, and 2 parameters.

The final test, which involved setting the Hill slope to 1, was not considered as it produced a sigmoidal curve with an extremely poor fit, thus skewing the IC_{50} value obtained as well as resulting in a much wider margin of error. These plots are depicted in Figure 3.9 below:

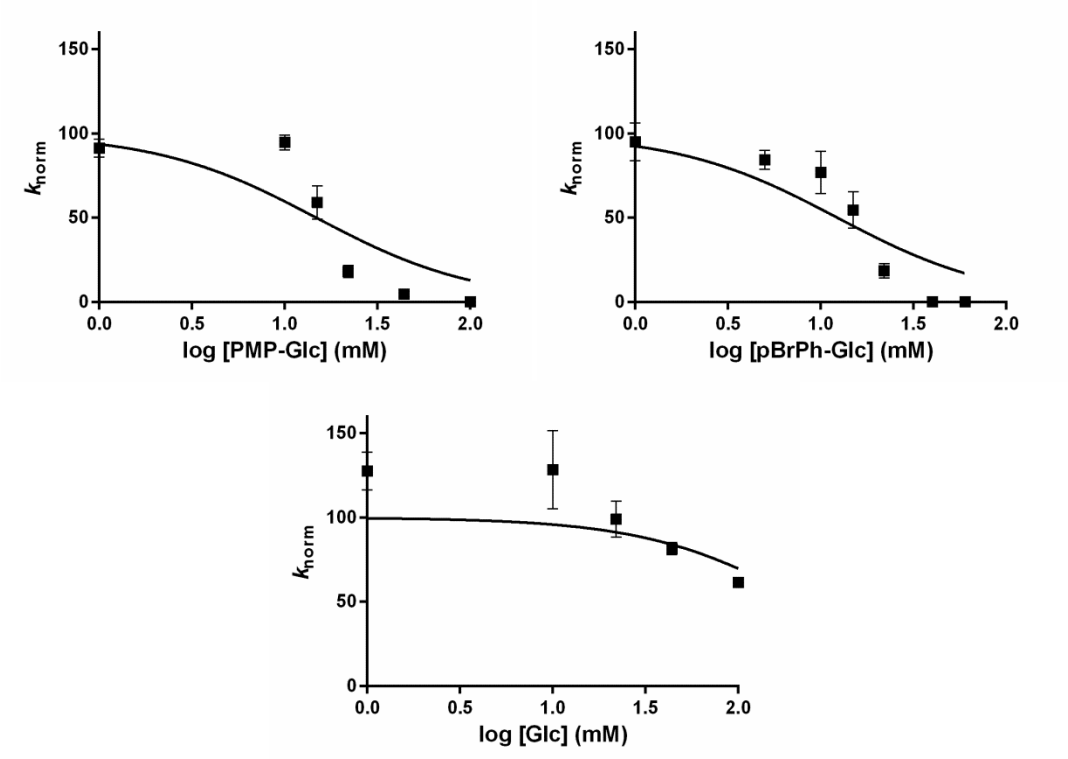

Figure 3.9 Dose-response curves where the normalized rate constant k_{norm} is plotted against log[I] and fitted to a sigmoidal equation where the Hill slope is set to 1.

This demonstrates the importance of solving for *n* in the sigmoidal equation, as well as that of the Hill slope itself. The fact that the Hill slope cannot be set to 1 and will result in a much greater number when solved for proves that there is definitely some cooperativity involved in the inhibition mechanism. As shown in Table 3.4, it is actually very important to restrict the parameters from four to two, as the fit could otherwise lead to false conclusions of IRI activity, such as was the case with Glc. When all four parameters were solved for, the bottom plateau k_f was 58.6, resulting in an IC_{50} of 27.9 mM. This is a huge difference from the 122.1 mM obtained when restricting the parameters. This is similarly an issue with pBrPh-Glc, which solves for a negative k_f at -1.9. Due to the nature of the experiment, negative numbers simply cannot exist, which therefore causes a slight discrepancy in the *n* and IC_{50} values. Furthermore, when low enough inhibitor concentrations are tested, the k_{obs} values obtained should be equal to those of PBS, therefore allowing us to set k_0 to 100. Finally, for the more active compounds, PMP-Glc and pBrPh-Glc, there is no significant change in the IC_{50} or *n* values obtained when changing the number of parameters to solve for in the sigmoidal equation. As such, reducing to two parameters does not detriment the results for effective inhibitors and also helps eliminate the appearance of "false positives" such as was seen with Glc, which is actually a poor inhibitor that does not fit a proper sigmoidal equation within a concentration scan of up to 100 mM.

Furthermore, as mentioned above, our compounds resulted in high Hill slopes. This parameter *n* is the resultant slope between the two plateaus and is an indication of cooperativity within an inhibition mechanism. The Hill slopes for PMP-Glc and pBrPh-Glc were obtained with good precision and were also both significantly greater than 1, thus suggesting a high degree of cooperativity. It is important to note that the error on the Glc Hill slope was large due to the inability to fit the data to a full dose-response curve under the concentrations tested. There

was, however, a visible difference in the shape of the curve when *n* was set to 1, thus suggesting that cooperativity is still a factor for this compound. This provides some insight into the potential mechanism by which our compounds inhibit ice recrystallization. It has been previously shown that our small molecule carbohydrate based inhibitors do not bind to ice as they do not display properties of thermal hysteresis or dynamic ice shaping, so there has to be some other phenomenon at work with regards to the inhibition process.[15,18,19] However, our laboratory has previously shown a direct correlation between the hydration index of a carbohydrate and its impact on IRI.[16,19] Since our compounds are not part of the ice lattice, it is most likely that our inhibitors would reside in the bulk water that exists between the quasi-liquid layers (QLL) of adjacent ice crystals (see Section 1.2). The more highly hydrated a carbohydrate, the more it disrupts the ordered bulk water around it. Furthermore, we have previously demonstrated that many of our small molecule inhibitors can form hydrogels or other assembled structures in solution.[18] If cooperativity was to be a factor, we can speculate that our inhibitors rely on some sort of assembly process within bulk water. We have previously proposed that our inhibitors limit the diffusion of water from shrinking crystals to growing crystals by increasing the order of bulk water.[16,19,20] Recrystallization is a thermodynamically driven process through which the dissociation of an ordered crystal to a less ordered solvent is favored; therefore, the relative ordering of bulk solvent via cooperativity between small molecules would result in the diffusion process being less favoured overall. We can therefore hypothesize that our inhibitors function by forming a network of small molecules associated through non-bonding interactions such as hydrogen bonding, dipole-dipole interactions or π-stacking. These speculations lead to the potential for future projects with the goal of elucidating the exact nature of the mechanism behind IRI.

3.6 Summary and conclusions for the kinetic profiling of small molecule ice recrystallization inhibitors

To date, there has been no proof that Ostwald ripening theory of ice recrystallization holds true in large ice volume fractions. We have studied the changes in the following factors of the ice recrystallization in a PBS solution over time using the standard splat-cooling assay: mean area, total area, total volume, total surface area, and surface area to volume ratio. The most important result obtained in this study was the mono-exponential decrease of surface area to volume ratio over time. Ostwald ripening is the growth of large crystals at the expense of smaller ones in order to decrease the total energy of the system.[7,10,17] Since smaller crystals have a higher surface area to volume ratio, they are higher in energy, and thus the formation of larger crystals results in a net decrease of total energy of the system. Thus, we have shown that recrystallization within large ice volume fractions does apply to Ostwald ripening theory.

We have also demonstrated that there are issues to be addressed with the previously accepted method for characterizing the IRI activity of inhibitors. Mean ice crystal areas in PBS and 22 mM PMP-Glc varied greatly when measuring a sample of 12 randomly selected crystals versus all crystals found in the sample. Furthermore, it was proven that MGS is not an appropriate parameter for measuring IRI activity due the wide distribution of crystal sizes. Time-dependence studies and binning analyses of PBS and PMP-Glc determined that even with an inhibitor present, there is still a wide range of crystal sizes within a sample.

From the binning analysis, it was found that bin 1, the bin containing the smallest ice crystals, was the only bin to continually decrease over time. The depletion of bin 1 was found to follow a mono-exponential decay. As such, this analysis was repeated over a concentration scan of PMP-Glc and mono-exponential decay curves were constructed, resulting in observed rate

constants k_{obs} for each concentration. This was further tested with another known inhibitor, pBrPh-Glc[15], and a poor inhibitor, Glc[16], to determine the effectiveness of this method in distinguishing inhibitors based on their IRI ability. From these kinetic traces, it was clear that there was a greater variance in rate constants for the different concentrations of PMP-Glc and pBrPh-Glc than there was for Glc.

The observed rate constants could then be fit to a sigmoidal two-parameter dose-response curve similar to that used in Koop's method for quantifying IRI activity via kinetics.[7] From these dose-response curves, IC_{50} values and Hill slopes were obtained. PMP-Glc resulted in an IC_{50} value of 16.3 mM, pBrPh-Glc resulted in an IC_{50} value of 14.8 mM, and Glc resulted in an IC_{50} value of 122.1 mM. As the most effective carbohydrate-based small molecule ice recrystallization inhibitors produced by our laboratory to date, PMP-Glc and pBrPh-Glc have thus set a threshold value for improved IRI-active compounds to follow. All compounds tested resulted in Hill slopes with values much greater than 1, therefore indicating a high degree of cooperativity within the ice recrystallization inhibition mechanism. While this mechanism remains unknown, this knowledge nevertheless provides further insight that can aid in elucidating this mechanism in the future.

In conclusion, we have determined a method to assess the full kinetic profile of our ice recrystallization inhibitors which allows us to quantify IRI activity based on rate constants rather than mean grain size. These rate constants address the wide distribution of ice crystal sizes, the differences in endpoint with various inhibitors, and the concentration dependence on IRI. From these results, the next step is to modify the standard screening assay utilized by our laboratory to reflect the kinetics of ice recrystallization inhibition, while still maintaining the simplification of the assay serving as a screen for active compounds. This project will be discussed in Chapter 4.

3.7 References

(1) Knight, C. A.; Hallett, J.; DeVries, A. L. *Cryobiology* **1988**, *25*, 55-60.
(2) Tomczak, M. M.; Marshall, C. B.; Gilbert, J. A.; Davies, P. L. *Biochem. Biophys. Res. Commun.* **2003**, *311*, 1041-1046.
(3) Yu, S. O.; Brown, A.; Middleton, A. J.; Tomczak, M. M.; Walker, V. K.; Davies, P. L. *Cryobiology* **2010**, *61*, 327-334.
(4) Yagci, Y. E.; Antonietti, M.; Börner, H. G. *Macromol. Rapid Commun.* **2006**, *27*, 1660-1664.
(5) Baruch, E.; Mastai, Y. *Macromol. Rapid Commun.* **2007**, *28*, 2256-2261.
(6) Mastai, Y.; Rudloff, J.; Cölfen, H.; Antonietti, M. *ChemPhysChem* **2002**, *3*, 119-123.
(7) Budke, C.; Heggemann, C.; Koch, M.; Sewald, N.; Koop, T. *J. Phys. Chem. B* **2009**, *113*, 2865-2873.
(8) Nagel, L.; Budke, C.; Erdmann, R. S.; Dreyer, A.; Wennemers, H.; Koop, T.; Sewald, N. *Chem. - Eur. J.* **2012**, *18*, 12783-12793, S12783/12781-S12783/12721.
(9) Budke, C.; Dreyer, A.; Jaeger, J.; Gimpel, K.; Berkemeier, T.; Bonin, A. S.; Nagel, L.; Plattner, C.; DeVries, A. L.; Sewald, N.; Koop, T. *Cryst. Growth Des.* **2014**, *14*, 4285-4294.
(10) Sutton, R. L.; Lips, A.; Piccirillo, G.; Sztehlo, A. *J. Food Sci.* **1996**, *61*, 741-745.
(11) Smallwood, M.; Worrall, D.; Byass, L.; Elias, L.; Ashford, D.; Doucet, C. J.; Holt, C.; Telford, J.; Lillford, P.; Bowles, D. J. *Biochem. J.* **1999**, *340*, 385-391.
(12) Hagiwara, T.; Sakiyama, T.; Watanabe, H. *Food Biophysics* **2009**, *4*, 340-346.
(13) Pudney, P. D. A.; Buckley, S. L.; Sidebottom, C. M.; Twigg, S. N.; Sevilla, M. P.; Holt, C. B.; Roper, D.; Telford, J. H.; McArthur, A. J.; Lillford, P. J. *Arch. Biochem. Biophys.* **2003**, *410*, 238-245.
(14) Jackman, J.; Noestheden, M.; Moffat, D.; Pezacki, J. P.; Findlay, S.; Ben, R. N. *Biochem. Biophys. Res. Commun.* **2007**, *354*, 340-344.
(15) Capicciotti Chantelle, J.; Mancini Ross, S.; Ben Robert, N.; Kurach Jayme, D. R.; Turner Tracey, R.; Acker Jason, P. *Sci. Rep.* **2015**, *5*, 9692.
(16) Czechura, P.; Tam, R. Y.; Dimitrijevic, E.; Murphy, A. V.; Ben, R. N. *J. Am. Chem. Soc.* **2008**, *130*, 2928-2929.
(17) Hagiwara, T.; Hartel, R.; Matsukawa, S. *Food Biophysics* **2006**, *1*, 74-82.
(18) Capicciotti, C. J.; Leclere, M.; Perras, F. A.; Bryce, D. L.; Paulin, H.; Harden, J.; Liu, Y.; Ben, R. N. *Chem. Sci.* **2012**, *3*, 1408-1416.
(19) Tam, R. Y.; Ferreira, S. S.; Czechura, P.; Chaytor, J. L.; Ben, R. N. *J. Am. Chem. Soc.* **2008**, *130*, 17494-17501.
(20) Tam, R. Y.; Rowley, C. N.; Petrov, I.; Zhang, T.; Afagh, N. A.; Woo, T. K.; Ben, R. N. *J. Am. Chem. Soc.* **2009**, *131*, 15745-15753.

Chapter 4: Development of a Simplified Time-Efficient IRI Screening Assay

4.1 Introduction

In Chapter 3, we reported a novel method for quantifying IRI in high ice volume fractions by modifying a kinetics-based approach published by Koop et al.[1-3] Rather than use the change in mean crystal area as a measure of activity, which does not accurately represent a non-homogeneous sample as seen in our high ice volume fraction assays, each ice crystal in a sample was sorted into bins where bin size was based on ice crystal area. From this, rates were obtained by monitoring the depletion of bin 1, the bin containing the smallest crystals. Dose-response curves were constructed with these rates, normalized to a PBS standard, and IC_{50} values were obtained.

Following the development of this method, which is a time-consuming, labour-intensive process, a need has arisen to condense this analysis into a more simplified screen that can be used as a preliminary assessment for a new compound's IRI activity in order to replace the traditional screen currently employed by our laboratory. This traditional method utilizes the well-known splat-cooling assay where samples are annealed for 30 minutes, at which point pictures of the ice crystals are taken and analyzed using Domain Recognition Software (DOMAN) to determine their mean grain size.[4-6]

Considering the drawbacks to the traditional assay (see Section 1.7) as well as the improvements presented in the full kinetic analysis, this therefore leads to a set of parameters that a condensed simplified screen should adhere to. First, there must be a concentration scan conducted in triplicate for each concentration in order to provide sufficient statistical data as well as to determine a compound's concentration effect on inhibition. Second, the condensed screen

should somehow follow a similar structure to the full kinetic profile, in which binning analysis leads to the calculation of rate constants, from which dose-response curves can be constructed. Finally, this screening method must be time-efficient and less labour-intensive than the full kinetic method and should preferably be comparable in time and labor to the traditional method. With these factors in mind, the goals and objectives for this chapter are as follows:

1. As described in Section 3.4, mono-exponential decay curves for the depletion of the proportionate area of bin 1 were constructed and fit to Equation 3.1 in order to obtain observed rate constants. This, however, relies on the acquisition of data over many time points over an extended period of time. In order to save time, we sought to gauge whether we could determine the initial *rates* of depletion, at one time point only, which would result in a shorter assay time. These results are described in Section 4.2.
2. Following the calculation of initial rates, the next step is to use them to construct dose-response curves such as those in Section 3.5 for the full kinetic analysis. Ideally, these plots should provide IC_{50} values and Hill slopes that are statistically equivalent between the initial rates method and the rate constants method. These results are presented in Section 4.3.
3. Once dose-response curves using the initial rates are successfully obtained in good agreement with the full kinetic analysis, comparisons can be drawn between the two methods, as well as with the traditional assay. Time, labour, and ease-of-use factors are considered in order to successfully design a new kinetics-based IRI screen. These results are discussed in Section 4.4.

4.2 Analyzing the initial rates of depletion of the proportionate area of bin 1

Instead of performing a full 60-minute kinetic analysis, we sought to look at the initial rate of depletion of bin 1, since the greatest decreases in proportionate area are largely found within the first 15-20 minutes of annealing time (see Section 3.4). For example, within the first 5 minutes of annealing time, the proportionate area of bin 1 has dropped to 37% in PBS but remains high at 84% in 22 mM PMP-Glc (see Figure 3.4). At 10 minutes, PBS is down to 11% proportionate area in bin 1, whereas 22 mM PMP-Glc sits at 66%. From there, PBS decreases by small increments of a few percent at a time until the mono-exponential decay curve flattens out. As the least effective inhibitor by virtue of being a blank with no inhibitor actually present, PBS therefore represents the steepest possible decrease in the proportionate area of bin 1, and thus we can deduce that the bulk of the recrystallization process occurs within the first 10 minutes. While previous studies have indicated that rates and endpoints between inhibitors may differ and thus affect the efficiency of inhibition (see Section 1.7), it was unknown by what degree these factors may affect our results.[7] Furthermore, analyzing the initial rates of decay rather than performing a full 60-minute kinetic analysis would provide a drastic improvement in time- and labour-efficiency. As such, we sought to determine these initial rates of depletion from the mono-exponential decay. With these initial rates, rather than rate constants, dose-response curves could be constructed and the resulting IC_{50} values could be compared to those from the full kinetic analysis. If there are no resulting significant differences, we would then be able to conclude that analyzing the initial rates alone is an accurate method for quantifying IRI, and thus can be applied to a condensed screen for IRI activity of novel compounds.

Based on previous studies in which incremental bin size was determined from the smallest area to which all ice crystals fit in at time 0 (see Section 3.3), we can conclude that our arbitrarily chosen bins result in the proportionate area of bin 1 remaining at 100% at time 0 no

matter the compound tested. As such, the initial rate could easily be determined by simple calculation of the slope from time 0 to the time chosen to measure (either 5 or 10 min), as shown by Equation 4.1:

$$v_t = \frac{A_0^{rel} - A_t^{rel}}{t - t_0} = \frac{1 - A_t^{rel}}{t}$$

Equation 4.1 Initial rate of decrease for the proportionate area of bin 1

where v_t is the initial rate at time t (either 5 or 10 min); A_0^{rel} is the initial relative area of bin 1, which we can set to 1; A_t^{rel} is the relative area at time t; and t_0 is the initial time, set to 0. Using the same binning analysis as described in Section 3.3, we can determine the proportionate area of bin 1 at any given time point and simply enter it into Equation 4.1 to determine the initial rate.

This analysis was thus performed on PMP-Glc, pBrPh-Glc, and Glc in order to determine the initial rates of depletion of the proportionate area of bin 1, and was carried out at two time points, 5 and 10 min. The combined results are shown in Table 4.1 below:

	PMP-Glc		pBrPh-Glc		Glc	
Conc (mM)	**v_5 (min^{-1})**	**v_{10} (min^{-1})**	**v_5 (min^{-1})**	**v_{10} (min^{-1})**	**v_5 (min^{-1})**	**v_{10} (min^{-1})**
0 (PBS)	0.125 ± 0.007	0.089 ± 0.003	0.143 ± 0.007	0.082 ± 0.002	0.112 ± 0.007	0.081 ± 0.001
1	0.122 ± 0.009	0.082 ± 0.002	0.132 ± 0.007	0.088 ± 0.006	0.130 ± 0.010	0.086 ± 0.001
5			0.119 ± 0.005	0.086 ± 0.006		
10	0.126 ± 0.005	0.089 ± 0.005	0.097 ± 0.014	0.076 ± 0.009	0.129 ± 0.019	0.078 ± 0.009
15	0.085 ± 0.016	0.071 ± 0.007	0.067 ± 0.019	0.067 ± 0.007		
22	0.049 ± 0.009	0.046 ± 0.009	0.039 ± 0.010	0.050 ± 0.015	0.108 ± 0.010	0.072 ± 0.012
40			0	0		
44	0	0			0.091 ± 0.008	0.078 ± 0.002
60			0	0		
100	0	0			0.070 ± 0.005	0.047 ± 0.019

Table 4.1. Initial rates *k* for the depletion of proportionate area of bin 1 after 5 and 10 min of annealing time for PMP-Glc, pBrPh-Glc, and Glc. Blank boxes indicate inhibitor untested at the indicated concentration.

It is important to remember that these values are initial rates, and thus are not comparable to the rate constants such as those calculated in Section 3.4. However, it is interesting to compare the rates of depletion of the proportionate area of bin 1 for the same inhibitor but using different time points. For example, v_{10} for 1 mM PMP-Glc is two-thirds the size of its respective v_5 value. There exists a similar discrepancy between to v_5 and v_{10} values for all low concentrations of inhibitor, notably concentrations at which there is little inhibitory effect taking place. This is indicative of the steepness of the initial slope as well. There is a higher rate of depletion at 5 min than at 10 min due to the fact that the steepest drop in proportionate area of bin 1 must occur within the first 5 minutes of annealing time. Following this, the mono-exponential decay curve already begins to flatten out, and thus v_{10} becomes an inaccurate measure of initial rate. This, however, is not always the case. While it does hold true for high Glc concentrations, as we approach higher concentrations of PMP-Glc and pBrPh-Glc we begin to see similar results. For example, 15 mM pBrPh-Glc has the exact same initial rate at 5 min as it does at 10 min (0.067 min^{-1} with slightly different error margins). The initial rates for 22 mM PMP-Glc are near-identical as well (0.049 ± 0.009 min^{-1} at 5 min and 0.046 ± 0.009 min^{-1} at 10 min). It can even be said that v_5 and v_{10} for 10 mM pBrPh-Glc are statistically similar within 95% confidence intervals, at 0.097 ± 0.014 min^{-1} and 0.076 ± 0.009 min^{-1}, respectively. This is also the case with 15 mM PMP-Glc (0.085 ± 0.016 min^{-1} at 5 min and 0.071 ± 0.007 min^{-1} at 10 min). As such, these results indicate that the rate of depletion within the first 5 minutes of annealing time is approximately the same as the rate of depletion between 5 and 10 minutes. Furthermore, since these rates are lower than those at lower concentrations of inhibitor, we can once again confirm that there is a significant inhibitory effect taking place. This is consistent with the calculated IC_{50} values in Section 3.5, which sees the IC_{50} values of PMP-Glc and

pBrPh-Glc within the 15 mM range. Another interesting observation is the difference in initial rates for 22 mM pBrPh-Glc. Though once again statistically similar at 95% confidence intervals, v_{10} is actually greater than v_5 (0.050 ± 0.015 min^{-1} and 0.039 ± 0.010 min^{-1}, respectively). This indicates the possibility that the rate of depletion between 5-10 minutes is actually steeper than the rate during the initial 5 min of annealing time. This could be explained by inhibition occurring more strongly within the first 5 min of annealing time, followed by the effect wearing off slightly. However, the differences between these two rates are not significant enough to hold much weight, so it would be more appropriate to assume inhibition is slowing the rate of depletion equally over the first 10 min of annealing time. At the highest concentrations of PMP-Glc and pBrPh-Glc, there is no disappearance of the population of bin 1 within the first 10 minutes, and as such the rates are listed as 0, since there is essentially full inhibition occurring, at least initially. On the other hand, Glc, as a poor inhibitor, does not see as great a difference in the initial rates over the course of a concentration scan. Even at 100 mM, the initial rates are not even half of those calculated at 0 mM (0.070 ± 0.005 min^{-1} versus 0.112 ± 0.007 min^{-1} at 5 min, and 0.047 ± 0.019 min^{-1} versus 0.081 ± 0.001 min^{-1} at 10 min). These results are consistent with the IC_{50} value obtained for Glc using the full kinetic analysis (122.1 mM, see Section 3.5). Since the IC_{50} was found to be above the concentrations tested, the fact that the initial rates at 100 mM Glc do not reach as low as 50% of the initial rates at 0 mM indicates a good correlation between the initial rates and the full kinetic profile thus far. Furthermore, it is interesting to note the comparison between the v_{10} values of 100 mM Glc (0.047 ± 0.019 min^{-1}) and 22 mM PMP-Glc (0.046 ± 0.009 min^{-1}) and 22 mM pBrPh-Glc (0.050 ± 0.015 min^{-1}). These values are all statistically similar to one another, indicating that it would take 5 times the amount of Glc in a sample to achieve the same level of inhibition as PMP-Glc and pBrPh-Glc. Conversely, there is

no statistical similarity when comparing the v_5 values for these concentrations (0.070 ± 0.005 min^{-1} for Glc compared with 0.049 ± 0.009 min^{-1} for PMP-Glc and 0.039 ± 0.010 min^{-1} for pBrPh-Glc). In fact, it would be more appropriate to say that at 5 min, 100 mM Glc has an initial rate comparable to 15 mM PMP-Glc (0.085 ± 0.016 min^{-1}) and 15 mM pBrPh-Glc (0.067 ± 0.019 min^{-1}). As such, it could be said that 100 mM Glc shows more of an inhibitory effect over the first 10 minutes than it does over the first 5 minutes, with a much slower rate of depletion of bin 1 after the first 5 minutes. This can also be explained by 100 mM Glc reaching its endpoint faster than 15-22 mM PMP-Glc and pBrPh-Glc, which would result in a much slower rate at earlier time points, since there is less depletion occurring after the initial decrease. However, there is still a greater initial decrease over the first 5 minutes, thus indicating Glc is not as strong of an inhibitor as PMP-Glc and pBrPh-Glc. Of course, it bears repeating that the Glc concentration used to obtain this level of inhibition is 5 times higher than those of PMP-Glc and pBrPh-Glc, further confirming that Glc is a poor inhibitor and that PMP-Glc and pBrPh-Glc are strong inhibitors of ice recrystallization. These results provide preliminary confirmation that initial rates could prove to be an acceptable alternative to obtaining rate constants after a detailed kinetic analysis of an inhibitor.

4.3. Constructing dose-response curves using the initial rates and comparing them to those obtained from the full kinetic analysis

Having obtained initial rates v_5 and v_{10} from binning analysis at a single time point in the previous section, these can be further analyzed to verify their agreement with the full kinetic analysis. This was done by constructing dose-response curves in the same manner as in Section 3.5. This was performed with the aim of comparing the IC_{50} values obtained with those

described in Section 3.5. Should the IC_{50} values prove statistically similar, it could then be confirmed that the initial rates method is a valid and simplified method to assess a compound's IRI ability. As such, the initial rates v_5 and v_{10} were normalized by dividing by the average initial rate at 0 mM (PBS), resulting in a new set of normalized initial rates, v_{5norm} and v_{10norm}. Once again, these were fit to a four-parameter sigmoidal equation (see Equation 3.2) with the same constraints as applied in Section 3.5. Non-linear regression was applied to afford the IC_{50} and Hill slope for each curve. The dose-response curves for PMP-Glc, pBrPh-Glc, and Glc from the 5-minute and 10-minute analyses are displayed in Figure 4.1 and the IC_{50}s and Hill slopes are compared in Table 4.2.

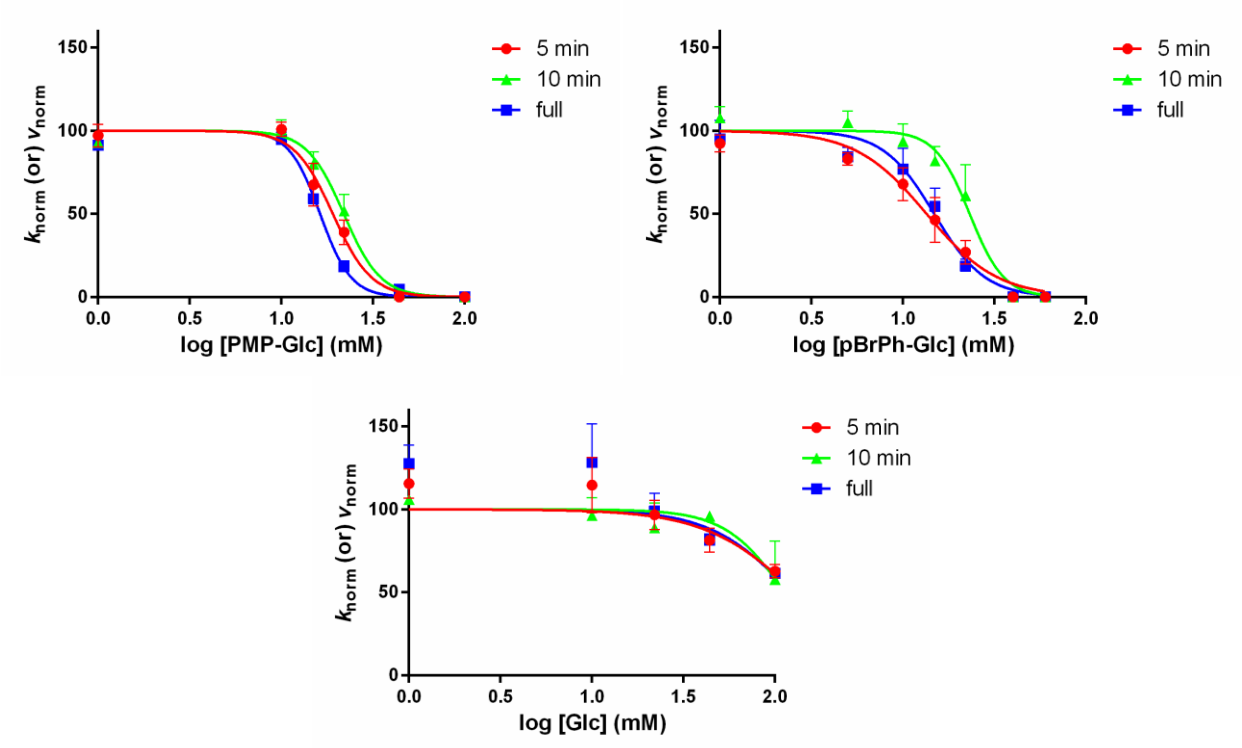

Figure 4.1 Dose-response curves for PMP-Glc, pBrPh-Glc, and Glc comparing the normalized initial rates from the 5-minute and 10-minute analyses with the normalized rate constants from the full kinetic analysis. These were plotted against log[I] and were fitted to a two-parameter sigmoidal equation as described in Section 3.5.

	PMP-Glc		pBrPh-Glc		Glc	
	IC_{50} (mM)	**Hill slope**	**IC_{50} (mM)**	**Hill slope**	**IC_{50} (mM)**	**Hill slope**
5 min	19.1 ± 2.4	4.13 ± 0.73	13.5 ± 2.2	2.24 ± 0.36	130*	1.73 ± 1.26
10 min	21.9 ± 2.4	4.33 ± 0.79	23.2 ± 3.1	4.63 ± 1.12	113.5*	2.64 ± 1.24
full	16.3 ± 1.4	5.12 ± 0.81	14.8 ± 2.2	3.12 ± 0.62	122.1*	1.98 ± 2.60

*indicates very large error intervals at 95% confidence

Table 4.2. Comparison of the IC_{50} values and Hill slopes obtained using the initial rates method for 5 and 10 min, along with the results from the full kinetic analysis (as described in Section 3.5).

As shown in Figure 4.1, in both cases of the 5-minute and 10-minute initial rates, PMP-Glc and pBrPh-Glc display very similar curves. They are nearly identical in b) while in a) pBrPh-Glc clearly has a shallower curve, but they still follow a sigmoidal pattern. Conversely, in both graphs, Glc is a poor fit to a full sigmoidal curve, as demonstrated by R^2 values ranging from 0.51 to 0.88. This could be due to the fact that the concentrations tested do not result in high enough inhibition to reach an inflection point on the curve. At first glance, these results appear to be consistent with those obtained from the full kinetic analysis in Section 3.5. Looking at Table 4.2, this observation is further validated. In all three methods, an IC_{50} value of over 100 mM is obtained for Glc; however, the error margins at 95% confidence are so high that these results hold no true meaning. Nevertheless, as explained in Section 3.5, this is mostly due to the fact that within the concentrations tested, the resulting data was not sufficient to fit a proper sigmoidal curve, only landing on the upper half. This also uses the assumption that should the Glc concentration be increased sufficiently, a similar pattern to the effective inhibitors will follow, albeit over a larger range of concentrations. It is equally plausible that "complete" inhibition in which the rates drop so low that they are effectively zero simply cannot occur no matter the Glc concentration tested, as it simply is not an effective enough inhibitor. No matter

the case, it is clear that the Glc fits obtained demonstrate its ineffectiveness as an ice recrystallization inhibitor, no matter the method used to determine the rates. The Hill slopes obtained for Glc in all three methods, similar to the IC_{50} values, have error margins so large that they cannot truly be considered statistically similar. PMP-Glc results in excellent fits, with R^2 values of 0.99 in all three cases. The IC_{50} errors at 95% confidence range around 10%, which are acceptable margins. Considering these, the IC_{50} values for the 5 min (19.1 ± 2.4 mM) and 10 min (21.9 ± 2.4 mM) method are statistically similar to one another, which would lead to the assumption that there is no distinct advantage to either method. However, only the IC_{50} obtained with the 5 min method is statistically similar at 95% confidence to that obtained using the full kinetic analysis (16.3 ± 1.4 mM). All Hill slopes are statistically similar to one another, confirming that cooperativity is a factor no matter the method used. The results differ slightly with pBrPh-Glc. As with PMP-Glc, the IC_{50} values at 5 min and the full analysis are comparable, at 13.5 ± 2.2 mM and 14.8 ± 2.2 mM respectively. At 10 min, on the other hand, the IC_{50} is statistically different at 23.2 ± 3.1 mM. The same pattern can be found for their Hill slopes. Furthermore, with all three methods, the IC_{50} values for PMP-Glc and pBrPh-Glc remain similar to one another, though generally pBrPh-Glc has a lower value than PMP-Glc. As such, the dose-response curves obtained with the normalized initial rates provide results that are essentially the same as when constructing a full kinetic profile, demonstrating that there is great potential to develop a simplified method using only one time point. Furthermore, despite the apparent discrepancies with the 10 min method, the overall results nevertheless coincide with those obtained from the full kinetic profile. This illustrates the great difference between effective and ineffective inhibitors when constructing a dose-response curve, with not so great of a difference between the results obtained from one method to another. In addition, the goal of

this project is to develop a simplified screening method to assess IRI activity. This resulted in the emergence of a 5 min or 10 min method in which the initial rates can be used to determine an inhibitor's potency. Section 4.4 will detail the advantages and disadvantages between these two initial rate methods in order to determine the most appropriate choice for the simplified assay. Nevertheless, there are great implications with these results. To the best of our knowledge, this is the first instance where initial rates of inhibition can be used to assess IRI. The discovery that initial rates can provide an accurate indication of a compound's full kinetic profile and thus its IRI activity is ground-breaking and has the potential to completely change the current IRI protocols. With these results, we can now use them to further the development of a simplified screening assay.

4.4. Assessing the advantages and disadvantages of a new simplified IRI screen

4.4.1 Determining the appropriate parameters to adjust for the simplified assay

Concluding that analysis of initial rates of depletion of the proportionate area of bin 1 can provide enough information to assess a compound's effectiveness at inhibiting ice recrystallization, a condensed IRI screening assay could be constructed around this result. Thus far, we have determined that a concentration scan can be performed, taking pictures of ice crystals at one earlier time point only using the splat-cooling assay, and binning analysis can lead to the calculation of initial rates which can then be normalized and fit to a sigmoidal dose-response curve. From here, an IC_{50} value can be obtained and this will provide a quantifiable measure of IRI activity. As such, there remain two main aspects of developing the condensed screen to consider: choice of time point for annealing and choice of concentrations.

Regarding the choice of time point, based on the results in Section 4.3 there are two considerations: 5 min and 10 min. Essentially, when performing the splat-cooling assay, it must be decided whether to let the sample anneal for 5 min or 10 min. As determined in Section 4.3, there is no clear advantage to using one time point over the other regarding the accuracy of the results obtained. As such, time efficiency becomes the major deciding factor. Annealing for 5 min instead of 10 min cuts the time of the splat-cooling assay in half; at first glance, it would appear that the 5 min annealing time is the logical choice. However, assuming that ice crystals grow in size over the course of these 5 extra minutes, as binning analysis has shown that they do, there will be less ice crystals in the field of view at 10 min than at 5 min. As described in Section 3.3, all visible ice crystals in the field of view must be circled using the ImageJ program, from which ice crystal area can be calculated and then sorted into bins. As such, annealing for 10 min would result in an overall lower ice crystal count than at 5 min, cutting down the amount of analysis time. In order to determine the time difference, the average number of total crystals at 5 and 10 min for PBS (0 mM) and 22 mM PMP-Glc were looked at. In PBS, where there is no inhibitor present to promote the inhibition of ice recrystallization, there are on average 40 more crystals to circle at 5 min than at 10 min. In 22 mM PMP-Glc, which is known to substantially inhibit ice recrystallization, there are approximately 28 more crystals to circle at 5 min than at 10 min. Using the ImageJ software to circle individual ice crystals, the extra ice crystals at the 5-minute time point could easily be circled within 5 minutes. As such, there is no real gain to using one time point over the other as there is no change in total time spent. However, it must also be considered that initial rates should theoretically be within the first 10% of the reaction conversion. When applied to the 60-minute annealing time used in the full kinetic profile, this indicates that the initial rate should reflect the proportionate area's decrease to 90%. In cases

with PBS or low inhibitor concentrations, this easily occurs within the first few minutes of annealing time (see Section 3.4). Thus, 5-minute time point fits the definition of an initial rate the most closely. By choosing to anneal for 5 minutes, this theoretically provides more accurate results without increasing the time spent on the assay, and is also a reasonable time point to use in terms of preserving the practicality of the assay.

The second aspect of designing the condensed screening assay to be determined is the set of concentrations to be tested in a 5-minute splat-cooling assay. As with the full kinetic profile, all concentrations should be run in triplicate. PBS (0 mM) should be tested as the blank for all compounds tested, providing an initial rate without inhibitor which is used to normalize the initial rates in samples with inhibitor present. Ideally, five data points would be desired to fit to a sigmoidal curve: one at the top plateau, one at the bottom plateau, one at the inflection point, and one each at the upper and lower ends of the inflection point. The latter three concentrations are difficult to arbitrarily choose, given that it is impossible to predict where a new compound's IC_{50} will lie on a curve. The first two concentrations can be set to 1 mM (which results in a log[I] of zero) and 100 mM (in order to have two orders of magnitude across the concentration scan). An adjustment could be made to 100 mM should this concentration surpass an inhibitor's solubility maximum. Based on the results obtained by assessing these two concentrations, an educated decision can be made on what concentration to test next. Ideally, the five chosen concentrations will fill out a sigmoidal curve, but the possibility exists that more concentrations may be necessary to test.

With these aspects decided, a preliminary protocol can be established for the screening of new compounds to test for their IRI activity. Five concentrations plus PBS will be run in triplicate in a splat-cooling assay lasting five minutes. Using ImageJ, ice crystals will be circled

in one image from each trial, and binning analysis will be performed and initial rates will be determined. These rates will be normalized with the PBS values and a dose-response curve will be constructed. From there, IC_{50} values will be obtained which will provide a measure of a compound's IRI activity that is both quantifiable and directly comparable amongst other inhibitors. All analysis from the binning onwards will be carried out using the same method as described in Chapter 3.

4.4.2 Comparative assessment of the different IRI protocols

It is important to consider this new method's advantages and disadvantages in comparison with the traditional IRI assay in order to determine its effectiveness; furthermore, comparing the condensed kinetic screen to the full kinetic profile is also of value. There are seven main factors that therefore need to be considered: assay time, the amount of time spent on the splat-cooling assay; crystal count, the number of crystals needed to circle; image size, regarding adjustments made to the FOV via camera zoom; crystal circling software, the program used to complete the crystal circling analysis; crystal circling time, the time it takes to circle the ice crystals; data analysis, the method of taking the crystal areas and analyzing them; and data analysis time, the time it takes to perform the data analysis following crystal circling. The advantages and disadvantages of each method are summarized and compiled in Table 4.3 below.

	Traditional assay	Condensed kinetic analysis	Full kinetic analysis
Assay time	6 trials 3 hours	18 trials 1.5 hours	18 trials 18 hours
Crystal count	216 crystals	~2100 crystals (active compound) ~1500 crystals (inactive compound)	~16000 crystals (active compound) ~12000 crystals (inactive compound)
Image size	Generally no zoom needed	Zoom required, occasional image crop	Zoom required, occasional image crop
Circling time	1 hour	A few hours	~1 week
Software	Domain Recognition Software	ImageJ	ImageJ
Data analysis	Previously designed spreadsheets	Previously designed spreadsheets	Previously designed spreadsheets
Analysis time	Very quick	Very quick	Relatively quick

Table 4.3. A summary of the main factors to consider when comparing the efficiency of the three methods for assessing IRI activity: the traditional method as utilized by our laboratory to date, the simplified kinetic screen as discussed in this chapter, and the full kinetic analysis from which the condensed screen was inspired.

Immediately, there are notable differences in assay time. The condensed analysis requires half the time as does the traditional assay, and both are immensely faster than the full kinetic analysis. This is due to the fact that the full kinetic analysis employs an annealing time of one hour per trial, with six concentrations run in triplicate (PBS and five varying inhibitor concentrations) for a total of 18 trials. Similarly, the condensed analysis uses 18 trials but with only 5 minutes of annealing time each. The traditional assay, on the other hand, tests triplicate runs of PBS plus one concentration only (typically 22 mM) over a 30-minute annealing time. The kinetic analyses are thus immediately advantageous in that they test for inhibition over a range of concentrations, taking into account the fact that there is a clear concentration effect on

inhibition, as previously determined.[7] The incredible assay time for a full kinetic analysis clearly renders the method completely impractical when conducting a preliminary screen for IRI activity. However, the condensed kinetic analysis has proven to mimic the results of the full analysis while taking up only a small fraction of the assay time. As mentioned previously, more than five inhibitor concentrations could potentially be tested; each extra concentration adds 15 minutes of assay time. Even with a potential increase in assay time, this time should theoretically remain smaller than that of the traditional assay, thus not only providing an advantage in time-efficiency, but in scope, since multiple concentrations are tested in this span rather than just one.

The biggest advantage to the traditional method over the kinetic ones is the image size, the amount of crystals to be circled, and the amount of time it takes to circle them. In the traditional assay, there is rarely a need to utilize the camera's zoom factor unless there is an extremely potent inhibitor. With the kinetic analyses, crystals are so small through at least the first 10 minutes that the zoom factor is necessary in order to better see and analyze them, as well as reduce the total number of crystals in the image to a manageable amount. In the old method, a sample of 12 randomly selected crystals are circled for each image, with three images selected for each trial for a total of 18 images resulting in 216 total crystals circled. For the kinetic analyses, these numbers become much more variable due to the great difference in crystal sizes among samples with active and inactive inhibitors as well as the image FOV. As such, the PMP-Glc and Glc crystal counts were used for comparison in the above table, listed as active and inactive inhibitors respectively. As shown above, there are drastic differences in the number of ice crystals to be circled, and consequently the amount of time spent circling them. With both active and inactive inhibitors, the amount of crystals to be circled for the full kinetic analysis is

approximately 8 times greater than with the condensed analysis, thus increasing the time spent from a range of several hours to approximately a week. This increased labour, combined with the splat-cooling assay time, renders the full kinetic analysis an impractical method for assessing IRI when it has now been clearly demonstrated that the condensed kinetic screen can provide the same results. Within the condensed kinetic analysis, however, there is already a discrepancy between the number of crystals circled for an active compound compared to an inactive one. When working under the earlier assumption that 40 crystals can be circled within 5 minutes, an active compound will take roughly an hour longer to circle crystals than an inactive compound. Furthermore, these high crystal counts ranging from 8-10 times more crystals than the traditional assay result in a much longer time spent circling crystals with the kinetic analysis, whereas the traditional method only takes about an hour. This is the largest disadvantage held by the new kinetic approach, as it requires several more hours of crystal circling. Despite the splat-cooling assay time being shorter, the total amount of time does not balance out and the kinetics method is therefore more labour-intensive. However, the argument can be made that the extra labour is worth the more quantitative results and is thus more meaningful.

While not as outstanding a factor as the assay or crystal circling time, it has been determined that ImageJ is a more reliable crystal circling software than DOMAN. This is due to the fact that the DOMAN software cannot run on all computer platforms, requires very specific criteria for image quality, and is an older program with a tendency for glitches when circling large numbers of crystals. ImageJ, on the other hand, is compatible with all platforms and image file types, and is extremely easy to use. Furthermore, it has the potential to be adapted to an iPad platform with a pen, or even to become a fully automated process in which the program automatically recognizes and registers all crystals without user input. Research on these

adjustments are currently being investigated in order to make the process even more user-friendly and accessible.

The data analysis for all methods is carried out using previously designed Excel spreadsheets, in which it is simply sufficient to enter the crystal area data obtained from either DOMAN or ImageJ and then the rest of the analysis is performed automatically in the pre-programmed spreadsheets. These are very quick and simple processes which result in no real advantages or disadvantages to any of the methods. The full kinetic analysis will result in slightly longer analysis times simply due to the increased amount of data to enter into the spreadsheet, but otherwise has no other effect on ease of use.

Overall, the condensed kinetic analysis boasts vast improvements on the full kinetic profile, notably in total time spent, while still yielding relatively equal results. When compared to the traditional method, however, there is an overall increase in labour between this and the condensed kinetic screen, resulting in a more time-consuming process. However, it can be argued that the slight increase (2-3 hours) in overall time is worth the benefit of the quality of the results obtained. In addition to including a concentration scan where the traditional method does not, the condensed kinetic method also provides proper quantification of a compound's IRI efficacy which further allows for the direct comparison between inhibitors. It can therefore be said that the advantages outweigh the disadvantages and thus the condensed kinetic method should be adopted over the traditional assay.

4.5 Summary and conclusions for the development of a simplified time-efficient IRI screening assay

Following the quantification of IRI activity in assays with high ice volume fractions via kinetics established in Chapter 3, a detailed and time-consuming process, the need to develop a simplified screening assay emerged. This was accomplished through calculating the initial rates of depletion of the proportionate area of bin 1 at 5 and 10 min of annealing, rather than constructing a mono-exponential decay curve over the course of a 60-minute annealing process and obtaining an observed rate constant. These initial rates, v_5 and v_{10}, provided preliminary evidence that initial rates could follow the same concentration dependence pattern as with the observed rate constants k_{obs} as shown in Chapter 3.

With these initial rates, dose-response curves were constructed that resulted in IC_{50} values and Hill slopes that were statistically equivalent to those obtained using the k_{obs} values from the full kinetic analysis in Section 3.5. This data showed that dose-response curves using initial rates alone can provide the same quantification of IRI activity as compared to a full kinetic profile and as such presented the opportunity to employ the initial rates analysis in a condensed screen.

In order to approach a theoretical rate in the most practical fashion for this kind of assay, the 5-minute annealing time was selected over 10 min. From here, comparisons were drawn between the traditional assay, the proposed condensed kinetic screen, and the full kinetic analysis as described in Chapter 3. The condensed screen provided a much more realistic workload than the labour-intensive full profile, resulting in the same quality of data produced. Furthermore, while slightly more labor-intensive than the traditional method, the condensed kinetic screen provided much more complete and quantitative data with regards to IRI activity as it tests over a range of concentrations and relies on kinetics as a means of quantification, which is a much more appropriate measurement of efficiency than mean crystal size.

In conclusion, following the kinetic analysis of IRI activity in Chapter 3, a simplified screening assay using initial rates was designed and found to produce the same results as with the full kinetic profile. The development of this condensed kinetic screen provides the first instance of a kinetics-based protocol for assessing IRI in high ice volume fraction samples that our laboratory can employ in order to provide improved quantitative data for our compounds while also allowing for better comparison between inhibitors.

4.6 References

(1) Budke, C.; Heggemann, C.; Koch, M.; Sewald, N.; Koop, T. *J. Phys. Chem. B* **2009**, *113*, 2865-2873.

(2) Nagel, L.; Budke, C.; Erdmann, R. S.; Dreyer, A.; Wennemers, H.; Koop, T.; Sewald, N. *Chem. - Eur. J.* **2012**, *18*, 12783-12793.

(3) Budke, C.; Dreyer, A.; Jaeger, J.; Gimpel, K.; Berkemeier, T.; Bonin, A. S.; Nagel, L.; Plattner, C.; DeVries, A. L.; Sewald, N.; Koop, T. *Cryst. Growth Des.* **2014**, *14*, 4285-4294.

(4) Knight, C. A.; Hallett, J.; DeVries, A. L. *Cryobiology* **1988**, *25*, 55-60.

(5) Jackman, J.; Noestheden, M.; Moffat, D.; Pezacki, J. P.; Findlay, S.; Ben, R. N. *Biochem. Biophys. Res. Commun.* **2007**, *354*, 340-344.

(6) Czechura, P.; Tam, R. Y.; Dimitrijevic, E.; Murphy, A. V.; Ben, R. N. *J. Am. Chem. Soc.* **2008**, *130*, 2928-2929.

(7) Capicciotti C.J., Ph.D Dissertation, University of Ottawa, 2014.

Chapter 5: Conclusions and Future Outlook

5.1 Conclusions

The overall goal of this work was to develop a method to properly quantify ice recrystallization inhibition (IRI) activity that could be adapted for use in our laboratory. Until now, there has been no standard method for quantifying IRI activity in high ice volume fractions such as those present in our splat-cooling assay. Recently, Koop *et al*. presented ground-breaking work in which they were able to kinetically quantify IRI activity using Lifshitz Slyozov Wagner (LSW) theory of Ostwald ripening in a slurry-based assay with low ice volume fractions.[1-5] Thus, we endeavoured to employ a similar kinetic approach to our inhibitors. The main objectives of this work were: (1) to find an appropriate parameter to study kinetically, from which rate constants could be obtained and dose-response curves resulting in IC_{50} values could be plotted; and (2) adapt this kinetic approach to fit a standard protocol for screening new compounds.

Firstly, it was determined that mean ice crystal size was not an appropriate measure to monitor kinetically across a concentration scan. This was first established by a former Ph.D student in the Ben lab, Chantelle Capicciotti and her undergraduate student at the time, Evan Perley-Robertson.[6] This was due to the fact that our high ice volume fraction assays are a heterogeneous mixture of ice crystal sizes, and therefore mean grain size is not an accurate representation of the change in the sample as a whole. As such, binning experiments were performed where all ice crystals in a sample were grouped into bins based on crystal size, and the relative populations of these bins were monitored over time. Bin 1, the bin containing the smallest crystals, was the only population that continually decreased over time, and this was

found to fit to a mono-exponential decay equation and resulted in the calculation of a rate constant. This experiment was repeated with two known effective inhibitors of ice recrystallization, PMP-Glc and pBrPh-Glc,[7] as well as an ineffective inhibitor, Glc,[8] in order to attempt to discover quantifiable differences between them. Rate constants were obtained across a concentration scan for these three compounds and dose-response curves were then constructed. PMP-Glc and pBrPh-Glc demonstrated excellent sigmoidal fits and resulted in IC_{50} values of 16.3 mM and 14.8 mM respectively. Glc displayed a poor fit and resulted in an IC_{50} value of 122.1 mM. This correlated well with studies using the previously accepted assay in our laboratory. Furthermore, to the best of our knowledge, this was the first documented kinetic quantification of IRI activity for high ice volume fraction samples.

The second objective of this work was to adapt the kinetic analysis presented above into a condensed and simplified assay for use in our laboratory when screening new compounds. The above analysis was a highly labour-intensive and time-consuming process, and so we attempted to study the initial rates of depletion of bin 1 by calculating a rate from the initial slope of the mono-exponential decay curve. Dose-response curves were constructed from these initial rates and the corresponding IC_{50} values obtained demonstrated excellent correlation to those obtained from the full kinetic analysis, with no significant statistical differences. As such, we have proven that a full kinetic profile is not needed to assess a compound's IRI activity, and that we can obtain the same result through studying the initial rates. From these initial rates, a new protocol was developed such that we can now screen for IRI activity in a similar timeframe to the original assay but obtain a much more accurate measure of a compound's efficacy.

Combined, these results mark the first instance of the quantification of IRI activity in high ice volume fraction samples via a kinetic approach. Furthermore, the discovery that this

activity can be determined solely from the initial rates of depletion of bin 1 has led to the development of a new and vastly improved assay that allows for the simple and quantifiable screening of new compounds.

5.2 Future outlook

5.2.1 Towards the determination of the exact mechanism of ice recrystallization inhibition

The results presented in Chapter 3 upon the construction of the dose-response curves, notably the high Hill slopes, suggest a certain degree of cooperativity in the inhibition mechanism. This leads to a great deal of speculation regarding the exact mechanism by which our compounds inhibit ice recrystallization, which is still unknown. We have previously established that our compounds do not bind to ice.[7,9,10] Since our compounds are not part of the ice lattice, this suggests that they are located within the bulk water between adjacent ice crystals. We have also proposed that our compounds increase the order of bulk water, thereby limiting the diffusion of water molecules from shrinking crystals to growing ones.[8,10,11] Furthermore, some of our compounds have been shown to form hydrogels or other assembled structures in solution.[9] These observations lead to the potential for future projects with the goal of elucidating the exact nature of the IRI mechanism, which could in turn alter our rational design of inhibitors.

5.2.2 Towards the continued optimization of the IRI screening assay

The results obtained in Chapter 4 have led to the development of a condensed and simplified kinetic screening assay for IRI activity of new compounds. As such, its implementation into our standard laboratory protocols will allow for the optimization of this procedure. For example, efforts are currently in place to automate the crystal circling process. If

successful, this would greatly reduce the manual effort required and would result in the assay becoming even more time-efficient and accessible.

5.3 Publications from this work

1. Abraham, S., Keillor, K., Capicciotti, C.J., Perley-Robertson, G.E., Keillor, J.W., Ben, R.N. "Quantitative Analysis of the Efficacy and Potency of Novel Small Molecule Ice Recrystallization Inhibitors." *Crystal Growth & Design* **2015**, *15*, 5034-5039.

5.4 References

(1) Budke, C.; Heggemann, C.; Koch, M.; Sewald, N.; Koop, T. *J. Phys. Chem. B* **2009**, *113*, 2865-2873.
(2) Nagel, L.; Budke, C.; Erdmann, R. S.; Dreyer, A.; Wennemers, H.; Koop, T.; Sewald, N. *Chem. - Eur. J.* **2012**, *18*, 12783-12793.
(3) Budke, C.; Dreyer, A.; Jaeger, J.; Gimpel, K.; Berkemeier, T.; Bonin, A. S.; Nagel, L.; Plattner, C.; DeVries, A. L.; Sewald, N.; Koop, T. *Cryst. Growth Des.* **2014**, *14*, 4285-4294.
(4) Lifshitz, I. M.; Slyozov, V. V. *J. Phys. Chem. Solids* **1961**, *19*, 35-50.
(5) Wagner, C. *Z. Elektrochem. Angew. Phys. Chem.* **1961**, *65*, 581-591.
(6) Capicciotti C.J., Ph.D Disseration, University of Ottawa, 2014.
(7) Capicciotti Chantelle, J.; Mancini Ross, S.; Ben Robert, N.; Kurach Jayme, D. R.; Turner Tracey, R.; Acker Jason, P. *Sci. Rep.* **2015**, *5*, 9692.
(8) Czechura, P.; Tam, R. Y.; Dimitrijevic, E.; Murphy, A. V.; Ben, R. N. *J. Am. Chem. Soc.* **2008**, *130*, 2928-2929.
(9) Capicciotti, C. J.; Leclere, M.; Perras, F. A.; Bryce, D. L.; Paulin, H.; Harden, J.; Liu, Y.; Ben, R. N. *Chem. Sci.* **2012**, *3*, 1408-1416.
(10) Tam, R. Y.; Ferreira, S. S.; Czechura, P.; Chaytor, J. L.; Ben, R. N. *J. Am. Chem. Soc.* **2008**, *130*, 17494-17501.
(11) Tam, R. Y.; Rowley, C. N.; Petrov, I.; Zhang, T.; Afagh, N. A.; Woo, T. K.; Ben, R. N. *J. Am. Chem. Soc.* **2009**, *131*, 15745-15753.

Chapter 6: Experimental

6.1 Materials

D-Glucose was purchased from Sigma-Aldrich. *p*-Methoxyphenyl-β-D-glucopyranoside (PMP-Glc) and *p*-bromophenyl-β-D-glucopyranoside (pBrPh-Glc) were synthesized according to the literature.[1]

6.2 Ice Recrystallization Inhibition Assay and Analysis

6.2.1 Crystal measurement

Ice recrystallization was measured using phosphate-buffered saline (PBS) solution in a splat-cooling assay. A 10-μL drop of each solution was dropped from a height of 2 m through a shielding tube onto a polished aluminum block, which was pre-cooled to -80 °C on dry ice. The "splat cooling" of the solution landing on the block instantly produced an ice wafer about 20 μm in thickness and 1 cm in diameter. The wafer was then quickly moved onto a cooled microscope cover glass and transferred to a cryostage. The sample was annealed at -6 °C for a predetermined amount of time, during which a section in the middle of the wafer was photographed using a microscope equipped with an LMPlanF1 20x/0.40 objective. Cryostage temperature was maintained with a programmable Peltier unit (S3 Series 800 temperature controller, Alpha Omega Instruments).

The image recorded at each time point was analyzed using ImageJ. Specifically, all crystals within the field of view were circled, excluding those only partially visible at the image boundary. The area of each circled crystal was calculated using ImageJ and corrected for the appropriate magnification factor of the objective lens. An example is shown in Figure 6.1 below.

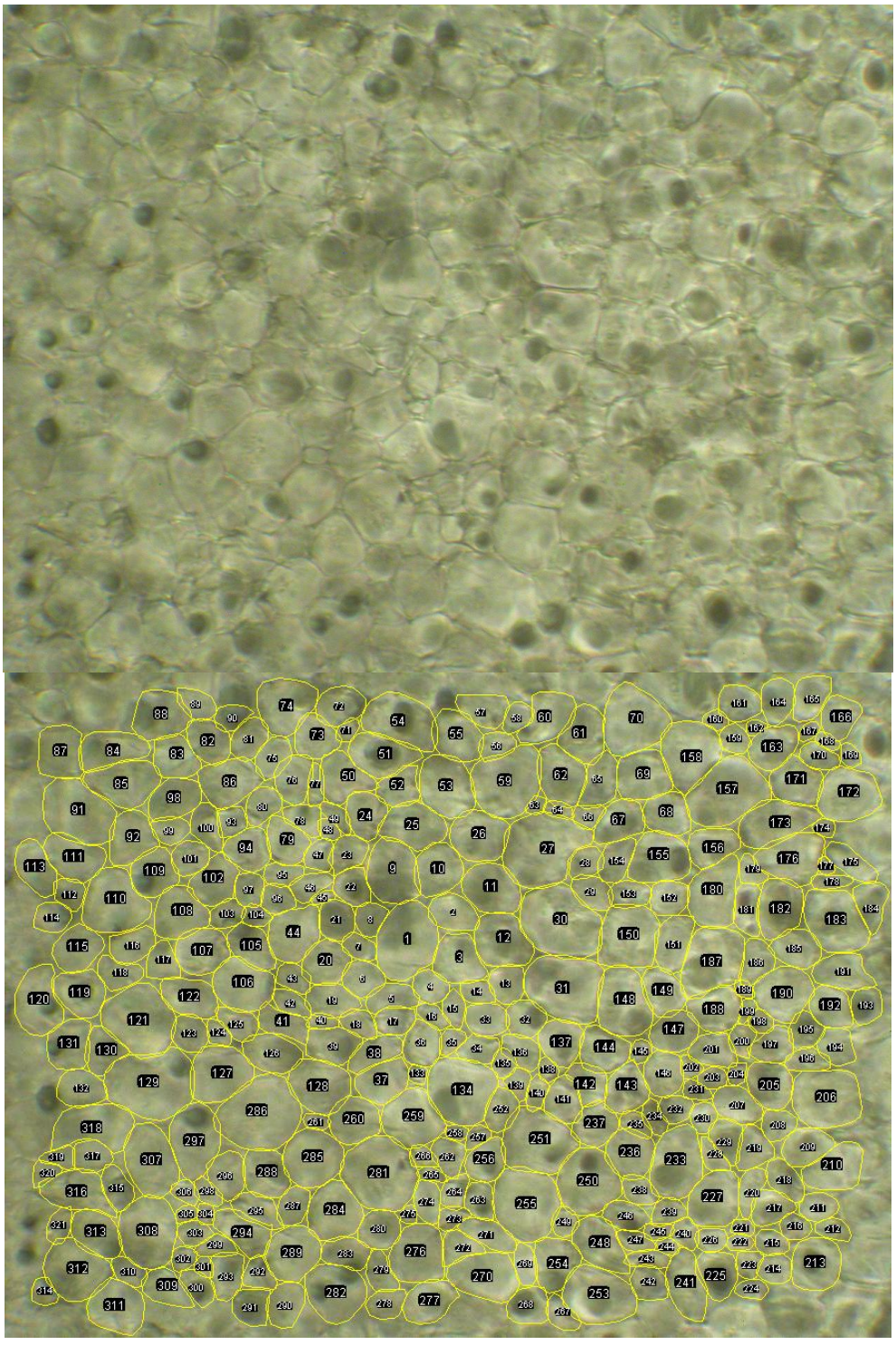

Figure 6.1 Images of 22 mM PMP-Glc at 0 min before (top) and after (bottom) being analyzed with ImageJ software.

These crystals were then sorted into discrete bins using a programmed Excel spreadsheet designed by Prof. Jeffrey Keillor (Figure 6.2). Bin sizes were assigned in increments of 0.001 mm^2, as it was observed that at time zero, all ice crystals could be just contained within this bin. In this way, subsequent crystal growth would result in larger crystals moving out of Bin 1 and into higher bins. The relative importance of each bin was determined by summing the area of each crystal within that bin, and dividing by the sum of the areas of all crystals within the field of view. In this way, the proportionate area of each bin was calculated for every sample wafer.

A)

	A	B	C	D	E	F	G	H	I	J
1					Time (min)					
2	**0**	**5**	**10**	**15**	**20**	**25**	**30**	**45**	**60**	
3	3.94569E-05	7.891E-05	8.385E-05	0.0001036	0.0001332	8.878E-05	0.0001726	0.00031	0.00021	
4	4.93211E-05	7.891E-05	9.864E-05	0.0001085	0.000148	0.0001282	0.0001726	0.00031	0.00022	
5	4.93211E-05	8.878E-05	0.0001184	0.0001134	0.0001529	0.000143	0.0001825	0.00033	0.00023	
6	5.42532E-05	9.864E-05	0.0001332	0.0001233	0.0001529	0.0001529	0.0001874	0.00038	0.00027	
7	5.42532E-05	9.864E-05	0.0001381	0.0001381	0.0001578	0.0001578	0.0001973	0.00038	0.00033	
8	5.42532E-05	0.0001085	0.0001381	0.000143	0.0001578	0.0001825	0.0002071	0.00041	0.00034	
9	5.91853E-05	0.0001184	0.0001628	0.0001578	0.0001825	0.0001874	0.0002417	0.00047	0.00045	
10	5.91853E-05	0.0001233	0.0001628	0.0001578	0.000217	0.0001924	0.0002417	0.00048	0.00047	
11	5.91853E-05	0.0001233	0.0001677	0.0001578	0.0002269	0.0001973	0.0002565	0.00052	0.00053	
12	5.91853E-05	0.0001332	0.0001825	0.0001578	0.0002269	0.0002022	0.0002565	0.00053	0.00054	
13	5.91853E-05	0.0001381	0.0001825	0.0001628	0.0002269	0.0002071	0.0002614	0.00056	0.00055	
14	6.41174E-05	0.0001381	0.0001973	0.0001726	0.0002318	0.0002121	0.0002663	0.00056	0.00056	
15	6.41174E-05	0.000148	0.0001973	0.0001825	0.0002417	0.0002121	0.0002713	0.0006	0.00059	
16	6.41174E-05	0.000148	0.0002022	0.0001924	0.0002565	0.000217	0.0002861	0.00062	0.00062	
17	6.90495E-05	0.000148	0.0002071	0.0002318	0.0002614	0.0002219	0.0002861	0.00064	0.00063	
18	7.39816E-05	0.000148	0.0002071	0.0002466	0.0002762	0.0002417	0.0003107	0.00064	0.00069	
19	7.39816E-05	0.0001578	0.0002071	0.0002466	0.0002811	0.0002466	0.0003107	0.00064	0.00071	
20	7.89137E-05	0.0001578	0.0002121	0.0002663	0.0002861	0.0002466	0.0003206	0.00066	0.00072	
21	7.89137E-05	0.0001677	0.0002121	0.0002713	0.0002861	0.0002515	0.0003305	0.00066	0.00073	
22	7.89137E-05	0.0001677	0.0002121	0.0002713	0.0002959	0.0002515	0.0003354	0.00067	0.00077	
23	7.89137E-05	0.0001677	0.000217	0.0002713	0.0002959	0.0002614	0.0003502	0.00069	0.00078	
24	8.38458E-05	0.0001677	0.000217	0.0002762	0.0003206	0.0002762	0.000365	0.0007	0.00079	
25	8.38458E-05	0.0001726	0.000217	0.0002861	0.0003305	0.0002811	0.000365	0.00073	0.0008	
26	8.38458E-05	0.0001726	0.0002367	0.000291	0.0003305	0.0002959	0.0003748	0.00074	0.00081	
27	8.38458E-05	0.0001726	0.0002367	0.000291	0.0003305	0.0003255	0.0003798	0.00075	0.00081	
28	8.87779E-05	0.0001825	0.0002417	0.0003009	0.0003403	0.0003403	0.0003946	0.00075	0.00081	
29	8.87779E-05	0.0001825	0.0002417	0.0003009	0.0003452	0.0003452	0.0003946	0.00075	0.00085	
30	8.87779E-05	0.0001874	0.0002466	0.0003107	0.0003502	0.0003452	0.0004044	0.00076	0.00087	
31	8.87779E-05	0.0001874	0.0002466	0.0003157	0.0003551	0.0003551	0.0004044	0.00078	0.00088	
32	9.371E-05	0.0001924	0.0002466	0.0003157	0.0003748	0.000365	0.0004094	0.00078	0.00089	
33	9.371E-05	0.0001973	0.0002663	0.0003157	0.0003847	0.0004044	0.0004094	0.00078	0.0009	

B)

	A	B	C	D	E	F	G	H	I	J
159	0.000266334	0.0016966								
160	0.000266334									
161	0.000266334									
162	0.000266334									
163	0.000276198									
164	0.00028113									
165	0.00028113									
166	0.000290994									
167	0.000290994									
168	0.000300859									
169	0.000300859									
170	0.000300859									
171	0.000305791									
172	0.000310723									
173	0.000330451									
174	0.000340315									
175	0.000340315									
176	0.000345247									
177	0.00035018									
178	0.00035018									
179	0.00035018									
180	0.000399501									
181	0.000419229									
182	0.000434025									
183	0.00044389									
184	0.000473482									
185	0.000508007									
186	0.000577056									
187	0.000176189	0.0004368	0.0005857	0.0006045	0.0006811	0.0007019	0.0007966	0.0012381	0.0014048	MEAN
188	9.29322E-05	0.0003131	0.0004042	0.0004092	0.0004358	0.0004908	0.0005693	0.0006192	0.0008217	STD DEV
189	3.94569E-05	7.891E-05	8.385E-05	0.0001036	0.0001332	8.878E-05	0.0001726	0.00031	0.00021	MIN
190	0.000577056	0.0016966	0.0019383	0.0018939	0.0019827	0.0022392	0.0025795	0.00284	0.00435	MAX
191	184	157	121	113	100	98	85	109	99	NUMBER

C)

	A	B	C	D	E	F	G	H	I	J	K
1		2x - 2s of t0 =	0.0002009	Mean of t0 =	0.0002678	SD of t0 =	0.0001674				
2		Max of t0 =	0.0009618	Max of t60 =	0.00548	Max # bins =	6				
3		Bin increment	0.001	lax bin size =	0.00600						
4											
5	**Bin Number**	**Bin Size**	0	5	10	15	20	25	30	45	60
6	1	0.00100	1.000	0.794	0.634	0.488	0.395	0.328	0.292	0.145	0.146
7	2	0.00200	0.000	0.206	0.294	0.319	0.400	0.535	0.377	0.401	0.340
8	3	0.00300	0.000	0.000	0.072	0.144	0.148	0.079	0.252	0.223	0.300
9	4	0.00400	0.000	0.000	0.000	0.049	0.057	0.059	0.051	0.125	0.100
10	5	0.00500	0.000	0.000	0.000	0.000	0.000	0.000	0.028	0.068	0.034
11	6	0.00600	0.000	0.000	0.000	0.000	0.000	0.000	0.000	0.038	0.080
12	7		0.000	0.000	0.000	0.000	0.000	0.000	0.000	0.000	0.000

Figure 6.2 Spreadsheets designed to sort the individual crystals from each image into bins. Shown here is a sample analysis of 22 mM PMP-Glc. The individual crystal areas from each time point as determined by ImageJ are copy-pasted into this spreadsheet (A, B) and the program then sorts them into bins based on their areas (C).

6.2.2 Determination of rate constants

Each sample wafer was allowed to develop over 60 minutes, with images recorded and analysed typically at 9 time points, namely 0, 5, 10, 15, 20, 25, 30, 45 and 60 minutes. The

proportionate area of each bin was thus followed as a function of time. The decrease of the relative area of Bin 1 was found to decrease mono-exponentially and was fit to such a curve in Excel (Figure 6.3). From this analysis, rate constants for the decrease of Bin 1 were obtained. These curves were later fit, using non-linear least squares analysis, to equation 3.1 (see Section 3.4) using the GraphPad software for better ease of analysis.

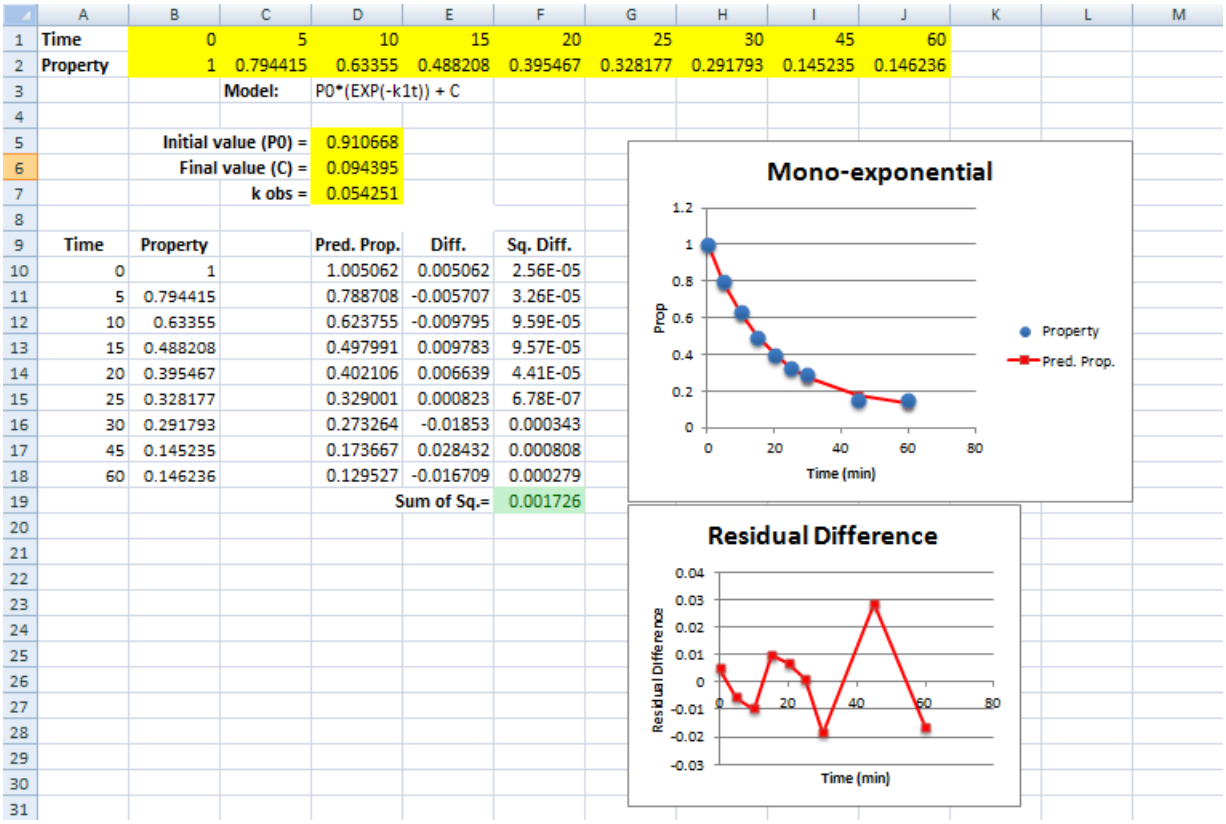

Figure 6.3 Sample spreadsheet for 22 mM PMP-Glc in which the proportionate area of bin 1 (obtained from the spreadsheet in Figure 6.2) is plotted against time to fit a mono-exponential decay, resulting in the determination of a rate constant k_{obs}.

6.2.3 Determination of initial rates

Sample wafers were annealed for a period of either 5 or 10 minutes, with images recorded and analyzed solely at the end point. The proportionate area of each bin was

determined as described above. The initial rate of decrease of the relative area of Bin 1 was calculated using equation 4.1 (see Section 4.2).

6.2.4 Dose-response curves

The rate constants / initial rates mentioned above were determined for 6-8 concentrations of ice recrystallization inhibitors in PBS buffer, ranging from 0 to 100 mM (two log units) or the highest possible concentration in the case of solubility issues. For each sample concentration, triplicate wafers were prepared and analyzed as described above. The average rate constant measured in triplicate at zero inhibitor concentration (i.e. in PBS buffer alone) was used to normalize the rate constants measured in the presence of inhibitor. This provided, for each inhibitor, a set of normalized rate constants, k_{norm}, versus inhibitor concentration, [I], whose log values were used in dose-response fitting according to equation 3.2 (see Section 3.5). This sigmoidal equation was fitted with 2-4 parameters in GraphPad. Before using GraphPad for ease of analysis, this was done in Excel (Figure 6.4).

	A	B	C	D	E	F	G
1	PBS (no inhibitor)						
2	Conc. (mM)	Rate		Model:	(v0-vf)/(1 +EXP((conc-IC50)))+vf		
3	0	0.2296065					
4	0	0.1809412		Initial rate (v0) =	93.220848		
5	0	0.2399379		Final rate (vf) =	7.5320235		
6	MEAN =	0.2168285		IC50 =	15.416074		
7	STD DEV =	0.0315057					
8							
9	Conc. (mM)	Rate	Rel. Rate		Pred. Rate	Diff.	Sq. Diff.
10	1	0.1802177	83.11529		93.220801	10.105511	102.12135
11	1	0.1945323	89.717129		93.220801	3.5036724	12.27572
12	1	0.2199931	101.45947		93.220801	-8.238666	67.87562
13	10	0.202638	93.455425		92.841684	-0.613741	0.376678
14	10	0.1905586	87.884454		92.841684	4.9572296	24.574125
15	10	0.222697	102.70648		92.841684	-9.864801	97.314295
16	15	0.1245968	57.463301		59.163253	1.6999515	2.889835
17	15	0.1669541	76.998226		59.163253	-17.83497	318.08627
18	15	0.092685	42.745751		59.163253	16.417502	269.53437
19	22	0.0347563	16.029388		7.6503171	-8.379071	70.208825
20	22	0.0542509	25.020171		7.6503171	-17.36985	301.71184
21	22	0.0290957	13.418741		7.6503171	-5.768424	33.274713
22	44	0.0130413	6.0145588		7.5320235	1.5174647	2.302699
23	44	0.0134271	6.1925086		7.5320235	1.3395149	1.7943001
24	44	0.0034674	1.5991515		7.5320235	5.932872	35.19897
25	100	0	0		7.5320235	7.5320235	56.731378
26	100	0	0		7.5320235	7.5320235	56.731378
27	100	0	0		7.5320235	7.5320235	56.731378
28							
29						Sum of Sq. =	1509.7337
30							

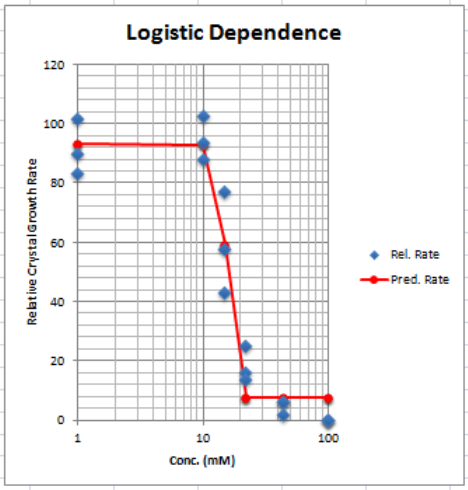

Figure 6.4 Spreadsheet initially used to plot the normalized rate constant of inhibitor (shown here: PMP-Glc) against concentration to obtain dose-response curves.

6.3 References

(1) Capicciotti Chantelle, J.; Mancini Ross, S.; Ben Robert, N.; Kurach Jayme, D. R.; Turner Tracey, R.; Acker Jason, P. *Sci. Rep.* **2015**, *5*, 9692.